Rock slope failure in the Western Alps: A first comprehensive inventory and spatial analysis

Sylvain Blondeau, Yanni Gunnell, David Jarman

Rock slope failure in the Western Alps: a first comprehensive inventory and spatial analysis

S. Blondeau[a,*], Y. Gunnell[a], D. Jarman[b]

[a,*] Sylvain Blondeau (corresponding author), Department of Geography, université Lumière Lyon 2, Environnement, Ville, Société, CNRS UMR 5600, F-69676 Bron, France

[a] Yanni Gunnell, Department of Geography, université Lumière Lyon 2, Environnement, Ville, Société, CNRS UMR 5600, F-69676 Bron, France

[b] David Jarman, Mountain Landform Research, Ross-shire, Scotland

Abstract

Rock slope failure (RSF) occurs in different contexts but is typically reported either as (i) single-category inventories or (ii) single-site geotechnical monographs. Few studies have sought to evaluate the spatial incidence of all modes of RSF conjointly, and to infer scenarios of regional landscape evolution from observed patterns of cumulative rock slope overstressing. Here we present the results of a systematic inventory of rock avalanches, rockfalls, rockslides, and gravitational rock slope deformations in the Western Alps (France, Italy, Switzerland) conducted using satellite imagery made available in Google Earth as a detection tool, and aided by preliminary ground-truth checks. The inventory totals 1446 montane RSFs, impacting 9.1% of the study area. Underpinned by GIS tools, the study further examines the spatial distribution of RSF with consideration for (i) predisposing factors (typically: lithology, geological structure), and (ii) preparatory factors (geomorphological process regimes that drives a given slope segment to the point of failure). The latter encompass slower variables (e.g., long-term crustal stress regime, cumulative residence time above equilibrium line altitudes) and faster variables (e.g., short-span glacier-related stresses, permafrost thaw, seismicity). RSF density patterns helped to define seven RSF super-hotspots (large diversity of RSF modes, up to 50% of displaced rock masses / unit area), which define the most intensely overstressed areas of the

Western Alps. These super-hotspots occur at sites where highly dynamic, thick, warm-based glaciers above the equilibrium line either intersected (middle Maurienne) or followed the strike of (middle Isère) N–S bands of highly susceptible lithologies and structures during the Quaternary. The widespread incidence of rock slope deformation (cumulative area: 1760 km^2, i.e. nearly 3 times the total of the other three RSF categories combined) appears further correlated with the low tectonic activity of the orogen and with its areas dominated by an extensional tectonic regime west of the Penninic Frontal Thrust. This contrasts with seismically active orogens, e.g. New Zealand's Southern Alps, where rock slope deformation is scarce compared to rock avalanches and shallow landslides.

Key words: rockfall; rockslide; rock avalanche; rock slope deformation; slope evolution cycle; Alps

1 Introduction

Rock slope failure (RSF) in mountain environments is the sudden or gradual release into the sediment cascade of large masses of bedrock from valley sides, plateau rims or mountain crests as a result of gravity-driven slope rupture. Sometimes referred to as 'mass movement in bedrock' (Brideau and Roberts, 2015), RSF has gained recognition as a prominent erosional process during the Quaternary (e.g. Ballantyne, 2002; Korup, 2005, 2006; McColl, 2012; Pánek and Klimeš, 2016).

The catastrophic collapse of entire mountain sides has been widely recorded also in historical times. In the Alps, Eisbacher and Clague (1984) documented 137 such events, including some debris-flow-related disasters and glacier-related mass movement not relevant to this study. Famously, the Mt. Granier mountain-side collapse in 1248 CE (Savoie, France) engulfed settlements south of Chambéry in 500 M m^3 of limestone and marl. Rock avalanches at Valpola (1987, Italy, igneous rocks) and Randa (1991, Switzerland, gneiss and schist) each involved ~30 M m^3, with major impacts on infrastructure (Sartori et al., 2003; Crosta et al., 2004). Collapses of La Suche mountain into the eastern end of Lake Geneva in 563 CE, and possibly of another during the Bronze Age, triggered destructive tsunamis (Kremer et al., 2012, 2014).

Very large deforming masses may also accelerate and collapse, as with the Sierre (Switzerland) rock avalanche (Pedrazzini et al., 2013). Monitoring of actively creeping sites is thus becoming widespread (e.g., Project Slow2Fast, Oppikofer et al., 2017; https://slow2fast.unimib.it/en/ricerca/). In the Belledonne massif (France, Fig. 1), deformation at Mt. Rognier started before 12 ka and is still active at a few mm/yr (Hippolyte et al., 2012); while Séchilienne, a 50 M m^3 mass, has been creeping for ~6 ka, with current slip rates of 20–150 mm/yr and approaching 1 m/yr in the core (Schwartz et al., 2017).

These RSF phenomena were first recognised as a distinctive class of geomorphological event in the European Alps (Heim, 1932; Abele, 1974; von Poschinger, 2002). Their slope-deforming and ridge-splitting precursors were first described in the Carpathians (Zischinsky, 1966; Nemčok, 1972), and later also in the Alps (Forcella, 1984; Mortara and Sorzana, 1987; Crosta and Zanchi, 2000). Beyond these well-known high-magnitude, low-frequency events, the existence of widespread montane RSF is only now becoming recognised as an endemic response to major system perturbations (McColl, 2012), notably erosion pulses (fluvial or glacial) induced by tectonic uplift or climate change. The present RSF stock in the Alps and cognate ranges is thus inferred to be largely inherited from a lateglacial and postglacial peak, albeit capable of reactivation (e.g. Goguel and Pachoud, 1981), including by anthropogenic disturbances (e.g., the Elm disaster; Heim, 1932). These RSF populations have gone largely unnoticed and unmapped because they are often inaccessible, invisible from below, difficult to detect and delimit when at incipient stages, and confusable with other mimicking erosional and depositional landforms. The potential of RSF spatial incidence analysis in studies of glaciation history, climate, or tectonics has scarcely been explored.

Although copious ‘landslide inventories’ are available for most European countries (e.g., van den Eeckhaut and Hervas, 2012), they are generally unsystematic, and mainly drawn from areas of threat to settlements and infrastructure. They seldom distinguish discrete RSFs—which are by definition in bedrock and above a threshold size—from abundant minor rockfalls, endemic slumping in high-plasticity rock types, and failures in regolith (Wood et al., 2020). Being more report-based than

survey-driven, they omit most metastable ('dormant') RSF sites that may undergo reactivation at some point. Area studies generally focus on landslide hazard zoning (e.g. Guzzetti et al., 2008; Bălteanu et al., 2010), but systematic identification of RSF over large areas has only recently become efficiently practicable with the advent of high-resolution, easily-interrogated satellite imagery.

Globally, comprehensive montane RSF inventories only exist as yet for a few ranges and uplands, notably Iceland (Whalley et al., 1983; Peras et al., 2016), parts of the Scandes (Braathen et al., 2004; Böhme et al., 2011), the New Zealand Alps (Korup, 2005; Allen et al., 2011), the eastern Pyrenees (Jarman et al., 2014), and the British mountains (Jarman and Harrison, 2019). In more elevated ranges, the emphasis has remained on large-scale and catastrophic RSF (e.g. Strom and Korup, 2006; Antinao and Gosse, 2009; Hewitt, 2009). Additionally, very few studies have sought to evaluate the spatial incidence of all modes of RSF in relation to possible causes and to the landscape evolution of the montane area. Within the European Alps, previous inventories (Fig. 1A) have mainly addressed smaller areas (e.g., Malatrait, 1975; Thiéry 2007; Martinotti et al., 2011; Fioraso, 2017), or local events of notable impact in historical time (Eisbacher and Clague, 1984). The groundbreaking wider study of the whole Alpine range by Crosta et al. (2013) addressed the deep-seated gravitational slope deformation (DSGSD) subset of RSF. A notably comprehensive inventory and analysis of the large Upper Rhône catchment also focused on slope deformation (Tonini et al., 2014; Pedrazzini et al., 2015).

Here presented is the first systematic database of RSF of all major modes, namely rockfall, rock avalanche, rockslide, and rock slope deformation (i.e., DSGSD) across a major sector of the European Alps (Fig. 1B). The primary aim was to map all RSFs that can be identified from remote imagery available chiefly in Google Earth, creating a database with appropriate standard parameters and using low-cost methods. It is beyond the intended scope of the study to determine the age, mode of evolution, or case by case cause of failure, let alone the current rate of slip or hazard potential for which some sites are being monitored (Fig. 1C). Readers motivated by the aforementioned list of topics may nonetheless find advantage in using the new database to conduct future studies at a

subset of locations of their choosing. Interactive Map File 1 provides a fully geolocated map of the inventory. Until much more is known about a wide sample of sites, however, the principal purpose of acquiring such a comprehensive regional dataset is aimed at understanding what might have caused RSF in the past, yielding the extant population. The data is subjected to a GIS-based spatial analysis that relates RSF location and RSF polygon size to a wide range of topographic, tectonic, and palaeoclimatic variables in a search to understand predisposing factors and causal relations over a range of geographic scales and spatial resolutions. The heuristic value of this broad-scope approach to the slope evolution cycle is tested in the final Discussion, where sharp contrasts in mountain landscape evolution between the European Alps and the Southern Alps of New Zealand are highlighted and explained in the light of the factorial analysis conducted in the Western Alps.

2 Study area: the Western Alps

2.1. Study area boundaries

The broad transect through the Western Alps presented here spans a representative gamut of Alpine geology, topography, climate, and intensity of glaciation. The study area (Fig. 1A, B) covers ~27,500 km^2 and is bounded on the north by Lake Geneva, Mont Blanc, and the Val d'Aosta, and on the south by a classic geological limit in Alpine geology (note in Fig. 1A the noticeable change in topographic elevation and relief pattern), south of which extensive outcrops of marl and shale (the 'Vocontian Basin', Fig. 2), all highly susceptible to endemic, and usually relatively shallow, landsliding, slumping, and badlands development, make for an entirely separate physiographic environment. Historically treated as such, the excluded southern region has been intensively mapped already (e.g. Thiery, 2007; El Bedoui et al., 2011), and widely monitored for active slope hazards (e.g. Malatrait and Sabatier, 1996; Palis et al., 2017). The range is almost 200 km wide, between abrupt mountain fronts of the Prealpine massifs and above the Po basin. The study area includes parts of the upper Rhône and Aosta valleys, within areas previously inventorised by Pedrazzini et al. (2015) and Martinotti et al. (2011), respectively (Fig. 1A).

2.2. Alpine landscape attributes of potential relevance to RSF

The aim of this study was to investigate the extant population of RSF in the regional landscape as a legacy and symptom of cumulative rock slope overstressing. Mapping the spatial patterns of slope overstressing could then be used as an exploratory tool for interpreting long-term landscape evolution from a perspective, and on a scale, previously unaddressed in this mountain environment. Characteristic physical features of the study area itemised below have been selected for their potential influence on RSF incidence, geographic distribution, and areal density. Hypothesis testing of these possible causal relationships through spatial analysis will be implemented in the Methods section. Given that information on the age of the RSF population in its majority is currently unobtainable, the obvious null hypothesis would postulate that RSF occurrence is entirely random, rendering any spatial associations vulnerable to a scenario of RSF having actually responded to entirely different factors over time. The Results and Discussion will show that meaningful inferences can still be made from spatial patterns without prior knowledge of individual RSF age, not least because the most widespread mode of RSF in the study area, namely slope deformation, is most often a diachronous phenomenon that has no unique 'age' (e.g. Schwartz et al., 2017).

2.2.1 Conceptual framework for investigating factors of RSF in the Alps context

McColl (2015) has provided a causal framework for analysing landslides in general that distinguishes 'preconditions', 'preparatory factors', and 'triggers'.

(i) Preconditions, or predisposing factors, are inherent attributes of the failed or failing slope: chiefly the geological variables (structure, lithology, rock mass strength), and topographic features (elevation, aspect). Brideau and Roberts (2015) and Stead and Wolter (2015) provide overviews.

(ii) Preparatory factors refer to a concatenation of circumstances and processes necessary to bring a given slope segment—in contrast to other adjacent segments—to the point of failure.

(iii) triggers are the 'on-the-day' events provoking actual failure or reactivation.

157 The main difference between triggers (e.g., the individual rainstorm) and preparatory factors is the
158 time frame of reference: triggers are instantaneous events, and for that reason mostly unknowable
159 in the context of individual RSF (particularly of slope deformation) because, unlike many smaller
160 landslides from report-based catalogues, their age is either undocumented, or documented as
161 incremental (Schwartz et al., 2017), or documented as random (Gallach, 2019) throughout the
162 Holocene period. Triggers, therefore, will not be addressed in this study. Preparatory factors, in
163 contrast, operate over a longer period before the slope failure event, building up to state changes
164 such as an increase in slope height or steepness, stress caused by glacial debuttressing, a reduction in
165 inherent rock strength (e.g., by permafrost thaw), loading of the slope, and all forms of 'slope
166 fatigue'.
167 Here we introduce an additional nuance among preparatory factors based on a distinction between
168 slower and faster variables. We thus term (i) 'stressors' the shorter-cycle and shorter-range
169 geomorphological factors acting on a slope or valleyside (e.g., glacier retreat, aspect-related
170 permafrost thaw, the seismic cycle on an active fault, increments of fluvial incision into weak
171 material, etc.); and (ii) 'drivers' the more powerful underlying changes in environmental context,
172 which have a regional and pervasive rather than local and site-specific impact on the behaviour of
173 crustal masses. Drivers would thus encompass slower processes likely to enhance overall
174 gravitational potential such as regional rock uplift (to which river channel incision into bedrock would
175 be a response), crustal stress vectors such as long-term denudation rates (quantified, e.g., by
176 thermochronology), but also radiation-driven processes such as long-term climate change and its
177 effects (e.g., glacio-isostasy, global-change related permafrost thaw). Drivers thus address long-term
178 forcing factors, and in that sense are more uniquely relevant to RSF (particularly massive rock slope
179 deformation) than to shallow landslides or to the blockfall–rockfall spectrum. In the context of a
180 regional-scale study of RSF incidence, they also broaden the scope of factor analysis because
181 variations in the relative intensity of drivers are mappable on length scales that exceed the
182 geographical scale of the RSF site or valley side.

183 Stressors are thus, at least in part, local expressions and shorter-term manifestations of drivers. In a
184 glaciated mountain range, for example, glacier-related stressors over the long term will vary
185 depending on where massifs occur in relation to the regional icefield flowline divide (which in the
186 Western Alps roughly coincides with the modern drainage divide along the Italy–France political
187 border: Fig. 1B). This should cumulatively (e.g. over the entire Quaternary) affect the residence times
188 of certain valleys in the ice accumulation zone compared to other valleys that spend longer in the
189 ablation zone or experience earlier deglaciation and overall longer periods of ice-free conditions.
190 Similarly, earthquakes trigger RSFs; but elevated seismicity over a wider area may be associated with
191 high tectonic strain, which in this instance qualifies as a stressor rather than a trigger. Both classes of
192 process, stressors and drivers, will be addressed in this study.
193
194 *2.2.2 Lithology and structure*
195 The geological structure and evolution of the Western Alps is well known (e.g., de Graciansky et al.,
196 2011; Pfiffner, 2014) and results from underthrusting of the European Plate beneath the overriding
197 Apulian (African) Plate. Although properties of rock mass fabric and strength relevant to RSF
198 incidence vary considerably within and between mapped lithological units, the region consists of
199 three broad lithological groups (Fig. 2):
200 (i) crystalline basement, mostly orthogneiss and granite displaying brittle behaviour, in two parallel
201 bands: the western, or External Crystalline Massifs of Hercynian heritage; and the eastern, or
202 Internal Crystalline Massifs, also Hercynian but with Alpine metamorphic overprints;
203 (ii) metasedimentary rocks, mainly of detrital origin, and displaying outcrop-scale ductile behaviour;
204 (iii) a sedimentary fold-and-thrust belt: Mesozoic cover rocks dominated by alternating limestone
205 and marl, chiefly confined to the Prealpine massifs and ceasing at the southern boundary of the
206 study area. Occasional overthrust klippen from the internal zones cap these series (Fig. 2).
207 The tectonic structure comprises a series of arcuate belts made up of palaeogeographic 'Domains'
208 subdivided into 'Zones' (Fig. 2). To simplify, an external Helvetic nappe system (Helvetic Domain) is

overridden from the east by an internal Penninic nappe system—itself embracing the Valais (Lower Penninic), Briançonnais (Middle Penninic), and Piemontais and Austro-alpine (Upper Penninic) domains. Metamorphic intensity increases from west to east, from the low-grade metamorphism of the Helvetic Domain to the high-pressure greenschist facies of the Briançonnais Zone, onward to the low-temperature facies of the Schistes lustrés, and lastly to the high-temperature facies of the Internal Crystalline Massifs.

The external/internal nappe systems are separated by the west-vergent Penninic Frontal Thrust (PFT). The PFT is a lithospheric-scale discontinuity offsetting the Moho, and thus one of the primary tectonic boundaries of the Alps. To its east, within the Penninic system, the east-vergent Briançonnais Backthrust (BB) separates the detrital continental rocks of the Briançonnais Domain from the overridden Piemontais and Austro-Alpine Domains, notably the oceanic flysch and ophiolites of Queyras and Mt. Viso.

Wherever the stratigraphy consists of a sedimentary sequence in which resistant caprock overlies fallible strata, typically carbonate rocks over marl or clay (a prominent situation in the Prealpine massifs), slope undermining in the weaker rocks explains a number of historic RSFs, including the Mt. Granier rock avalanche and the Moucherotte DSGSD (Vercors massif, near Grenoble; Debelmas, 1979).

2.2.3 Neotectonics

Present tectonic activity in the study area is relatively subdued because crustal convergence between Europe and Africa has substantially slackened (e.g., Calais et al., 2000; Sue et al., 2007; Nocquet et al., 2016). A tripartite stress regime has evolved since the late Neogene (Fig. 2 inset):

(i) extensional deformation within the internal (Penninic) domains, where normal faulting has been reactivating the synorogenic thrusts and backthrusts (Tricart et al., 2006; Sue et al., 2007);

(ii) transpressive stresses and strike-slip faults in broad swathes on either side (Dauphinois Zone, External Crystalline Massifs, most of the Prealps; Thouvenot et al., 2003).

(iii) compressive stress persisting only locally in the Prealpine massifs and along the Po Basin margin, as convergence continues to propagate outward along the edges of the pro-wedge, into (for example) the Jura (e.g. Sue et al., 2007).

The prevailing post-orogenic extension along the alpine spine could be attributed to gravitational spreading of the most thickened part of the crust beneath the Middle Penninic Domain (Delacou et al., 2004), and perhaps to displacement or tear of a deeper lithospheric root (Kästle et al., 2019).

Current tectonic displacement rates in all these strain modes are low (2–5 mm/yr; Nocquet et al., 2016). Rock uplift in the Alps is overall potentially attributable to tectonic shortening, lithospheric delamination, and crustal unloading caused by deglaciation and erosion (Sternai et al., 2019). Although the component of viscoelastic response to deglaciation is strongly model-dependent, reasonable estimates of contributions to total uplift rates by postglacial rebound in the Western Alps are 30–50% (Sternai et al., 2019). Overall, however, maximum surface uplift rates detected during the last 30 years do not exceed a modest 2 mm/yr, peaking along the range axis in the Beaufortain and Vanoise areas (Nocquet et al., 2016; Sternai et al., 2019) and reducing almost to zero in the southern half of the study area.

Long-term Neogene crustal uplift and erosion are quantifiable by thermochronology. Recent data compilations suggest two clear tectonic realms with contrasting exhumation histories in the Western Alps (Schildgen et al., 2018):

(i) external (Helvetic Domain), with exhumation peaking after 7 Ma for (U–Th)/He, after 10–15 Ma for apatite fission-track (AFT), and after 20 Ma for zircon fission-track (ZFT) data;

(ii) internal (Penninic Domain), with a pre-20 Ma exhumation peak for both AFT and ZFT ages.

Across the Penninic Frontal Thrust separating these two realms, a steep gradient in thermochronological ages is evident (Agliardi et al., 2013, Fig. 4 therein; Schildgen et al., 2018). In the Penninic Domain, intermediate ages imply slow, steady denudation since early Miocene time after a paroxysm during the Oligocene. In the Helvetic Domain, the younger ages imply rapid unroofing in late Miocene–early Pliocene times followed by slower denudation rates, yielding today's highest

summits. Localised younger exhumation of valley floors is attributed to Pleistocene glacial incision (Valla et al., 2012).

2.2.4 Modern seismicity

Seismicity is known to generate RSF (Jibson, 2009, 2013), particularly rock avalanches and rockfalls (Gosar, 2017; Roback et al., 2018). Modern seismicity in the Western Alps, however, is low, with no events since 1900 exceeding the M_L 6.0 threshold considered necessary to provoke substantial RSF (Tiwari and Ajmera, 2017). Only three earthquakes > M_L 5 occurred in the French sector, the largest (Vercors, 1962) registering M_L 5.3 (data from sismalp.osug.fr). Five M_S 4.5–5.5 events are reported in the Cottian Alps of Italy (Perrone et al., 2010). The importance of seismicity should nonetheless not be discounted outright because slopes at the threshold of failure could be triggered by small earthquakes.

2.2.5 Topography and glaciation

In glaciated mountains, the principal palaeoclimatic stimulant is cyclical glacial erosion, with valley deepening and hillslope steepening together compromising rock mass stability. In the Western Alps, RSF is thus expected to be predominantly paraglacial (Ballantyne, 2002), although RSF can develop widely in unglaciated mountain areas (Pánek et al., 2015). The study area is dominated by massifs of classic alpine character, with arêtes, cirques, and deep steep-sided troughs in resistant rocks, but areas of more subdued intermediate relief, with broad interfluves persisting above more open valleys, also occur. The study area also embraces the Prealps massifs and Po basin foothills, characterised by fluvially-incised plateaux or dissected terrain and where glacial impact has been more limited. Many of the highest summits lie along the main Rhône–Po drainage divide, where maximum altitudes typically exceed 3000 m. They attain >4000 m in the Mont Blanc, Ecrins, and Gran Paradiso massifs. At over 4800 m, Mont Blanc is a unique pop-up of granite and rhyolite squeezed between reverse faults (Boutoux et al., 2016; Bergemann et al., 2019).

The extent to which these valleys have been excavated fluvially or glacially over the Pleistocene is important for slope stress history. The extant RSF response to the evolution of the alpine relief may thus bear the influence of three timescales: (i) long-term decay from some original glacial resetting of slopes; (ii) propagation or perpetuation of failure at locations where previous RSF has left unstable slopes; or (iii) a fresh response to new increments of incision provoked by some change in ice dispersal or fluvial adjustment.

During the Pleistocene maxima, ice cover was predominantly constrained by the topography, only locally overtopping secondary divides to form ice domes and with the pre-existing valley system efficiently conducting ice flow away from the main watershed towards the Rhône and Po piedmonts. Thus, at the time of the Late Pleistocene most extensive glaciation (MEG), independent domes only formed in the Vanoise, Mont Blanc, and Ecrins massifs (Coutterand 2010, 2017). Consequently, local ice diffluences and transfluences shaped only a few, mid-level glaciated cols across the Alpine icefield flowline divide such as Mont Cenis and Petit Saint-Bernard. This contrasts with mountain ranges with extensive glacial breaching (e.g., Patagonian Andes; Norway; Scottish Highlands).

The thickest iceways were the Isère and Arc glaciers (Coutterand, 2010). The least glaciated massifs, skirted by the large ice streams, were the Chartreuse and Vercors, which internally possessed mainly short, east-facing cirque glaciers. Today, less than 1% of the study area is glaciated (Gardent et al., 2014).

2.2.6. Modern precipitation and permafrost

Precipitation patterns in the study area are strongly influenced by the Westerlies and conform to a gradient of decreasing rainfall from the Prealps in the west to the internal massifs in the east. This pattern, which divides the area into two climatic halves roughly coincidental with the trace of the Penninic Frontal Thrust (see Suppl. Fig. 1A), defines a wetter Helvetic Domain and a drier Penninic Domain. This conformation likely prevailed during much of the Holocene, and the inventory aims to

test whether mean annual precipitation has any control over the areal density, diversity or size of RSF.

Mountain permafrost in the Western Alps today persists at elevations above ~2700 m a.s.l. (Bodin et al., 2015; Marcer et al., 2017). In the Mont Blanc massif, for example, at 10 m depth present-day measured rock temperatures are –4.5 and –1.5 °C on north- and south-facing slopes, respectively (Bodin et al., 2015). The RSF inventory will be examined in relation to records of permafrost occurrence and behaviour, under the intuitive assumption that permafrost countervails or delays RSF.

3 Methods

3.1 Google Earth Pro and other RSF identification tools

The RSF inventory was constructed entirely from satellite imagery provided by the Earth navigation tool Google Earth Pro™. Only sites detectable on that imagery were included, with no unsystematic augmentation from field visits, geological maps, or the literature. This ensures consistency for analysis rather than selectively optimising completeness, although any inventory is likely to evolve as new sites are discovered. About 12% of the inventory has been ground-truthed, providing familiarity with RSF forms and contexts, and confirming its general validity without adjusting it for individual cases.

Satellite imagery is increasingly favoured over aerial photography and DEM imagery for large-scale RSF reconnaissance (e.g., Crosta et al., 2013; Jarman et al., 2014; Tsou et al., 2015; Pánek et al., 2016, 2018). Among its advantages, the imagery provided by Google Earth is open-access and simple to navigate, with full flexibility for angle of view and magnification down to resolutions (in the study area) of roughly 1:2000. Relief-enhancement and sharpening tools can assist in confirming RSF indicators. True-colour representation of vegetation and drainage assists detection of anomalous landforms, not available on DEM imagery. Google Earth also valuably provides a library of 'historical imagery' from earlier satellite passes, which can offer alternative sun or snow highlights, or avoid swaths affected by cloud cover or dullness. Aerial imagery resources provided by the Institut

Géographique National (IGN) data portal and the Bing Maps website were also inspected as backup, but their static nature (no navigation tools) limits their value.

Two chief difficulties have been encountered in identifying RSF from Google Earth. Firstly, where they occur or extend beneath tree cover, some under-reporting or uncertainty as to extent is likely, notably with slope deformation features. LiDAR would address this problem (Ortuño et al., 2017). Secondly, there is potential risk of mimicry between RSFs and other landforms, sometimes only resoluble by field inspection. Thus a debris cone may resemble a single-event rockslide lobe; an apparent antiscarp may be a selectively eroded bedrock rib; and rock glaciers may mimic—or grow out of—rock-avalanche deposits. Delicate deformation features may be utilised or obscured by access tracks and ski domain-moulding.

For the concept of rock slope failure to have geomorphological utility, a lower RSF threshold size has to be adopted to distinguish RSFs as discrete, infrequent, organised events from abundant minor slips and rockfalls (limiting case: the single fallen block). Most RSF studies and inventories have such a necessarily arbitrary threshold, explicit or implicit. The threshold size necessary to distinguish RSFs on that basis (typically 0.01–0.03 km^2 in other studies) was found for this study area to be ~0.02 km^2. Below this it became increasingly difficult to consistently discriminate smaller features. The impracticality of managing a dataset at lower threshold levels is evident from the high frequency of mostly small rockfalls on Mont Blanc alone, for example, with 640 events recorded in just 10 years (Ravanel et al., 2017). Although time-consuming, the procedure followed utilising Google Earth on that basis is considered to yield a comprehensive and consistent coverage of the entire study area.

General topographic variables were extracted from the 1 arcsecond (~30 m ground resolution) ALOS World 3D elevation model (DEM), with a relative vertical accuracy given as ≤ 5 m. The ALOS DEM was tested by zooming in on known RSF features: some more obvious ones, such as split ridges, could be recognised, but not in a systematically reliable way. The IGN DEM (25 m ground resolution) was also tested because of recent LiDAR-derived upgrades to 5 m resolution coverage, but only of certain valley floors and their adjacent valley footslopes. This unsystematic 5 m coverage provided an

opportunity to test for RSF indices at elevations coinciding with forest cover. A dozen features suggesting slope antiscarps were observed in total but, for consistency reasons, not included in the inventory. Their small number would indicate that RSF, in its vast majority, departs from areas situated above the modern treeline. Inspection of French geological maps, which provide standard symbols for landslides (all types, undifferentiated), came in further support of this appraisal. This preliminary observation would require to be updated in the future as 5 m DEM coverage becomes more widely available.

3.2 RSF typology adopted for this study

RSF is adopted here as an umbrella term spanning the full range of failure modes, from long-travel rockfall to in situ deformation. Classifications devised for engineering geology purposes (notably Varnes, 1978; Hungr et al., 2011) are too complex for large regional inventories. Experience shows that only a few main categories can be usefully discriminated (e.g. Jarman, 2006; McColl, 2012; Pedrazzini et al., 2015; Ortuño et al., 2017). Unfortunately, standardisation of terms and definitions is elusive. A major difficulty is whether the term RSF includes rock slope deformation (RSD), more commonly termed DSGSD. In practice, many sites display elements of both deformation and sliding, which are merely different manifestations of slope response to overstressing. The view adopted here is that failure occurs when the rock mass loses cohesion, regardless of its state or stage along a continuum towards ultimate disintegration or collapse, whether rapid or slow.

For the Alps context, this inventory adopts a four-category typology (Fig. 3), retaining rock avalanches in view of their historical prominence in the Alps despite their relative scarcity:

(i) Rock avalanche (RA): this involves the rapid displacement of large rock masses (Evans et al., 2006), with long runouts and complete fragmentation. Striking historic examples in the study area are Mt. Granier (Pachoud, 1991; Fig. 3: RA1), Madeleine (Pollet, 2004), Lauvitel (Delunel et al., 2010; Fig. 3: RA2), and Ciantiplagna (Fioraso and Baggio, 2013). RAs are recognisable from the

389 imagery as bold cavities with large masses of unsorted debris reaching the slopefoot or filling the
390 valley floor, sometimes forming landslide dams.
391 (ii) Rockfall (RF): this is on a continuum with rock avalanches but involves smaller volumes and
392 shorter travel distance (Ravanel and Deline, 2011), often because rockfall lacks the excess
393 mobility, and therefore the long runout, of RAs. RF shows up on the imagery as a discrete deposit
394 of coarse debris (Fig. 3: RF1, RF2). Difficulties may arise when distinguishing (a) single-event
395 landforms from incremental accumulations; (b) source scars, if planar shears have left no clear
396 cavities; and (c) older rockfalls blending into rugged terrain, or evolved into rock glaciers (Jarman
397 et al., 2013).
398 (iii) Rockslide (RS): this mode is characterised by a clearly defined headscarp (or rupture scars) and
399 slipped mass (Fig. 3: RS1, RS2), which commonly projects out from adjacent slope profiles. Travel
400 distance is often short, preserving rock mass coherence with only limited disintegration,
401 sometimes evolving uphill-facing scarplets during arrested descent, with a bold toe rampart and
402 bulges. A basal sliding surface is conventionally inferred, which is typically planar (translational
403 sliding) but may be curved (roto-translational) in less competent rocks (Malatrait, 1975; Hibert et
404 al., 2012).
405 (iv) Rock slope deformation (RSD). The acronym RSD is adopted here as a neutral, non-genetic (i.e.,
406 purely descriptive), and concise term of general application that befits the limitations of imagery-
407 based reconnaissance compared to the context of field identification, which would allow to more
408 fully ascertain the deep-seated and gravitational (rather than tectonic) nature of the
409 deformation. RSD entails sagging or creeping of the valleyside, without developing a clearly
410 defined and displaced failed mass. RSDs may display substantial headscarps, with open fissuring,
411 and antiscarps shaping wide trenches (extensional variant); or may have only closed fractures,
412 step-scarps and saw-toothed antiscarps (compressional variant); these variants (Jarman, 2006)
413 are not applied here as they require field discrimination. RSDs can be very large, extending for
414 tens of kilometres along valleysides. They can generate spectacular landform assemblages with

ridge rents, double or even triple crests where the source fracture daylights behind (creating a false antiscarp), and concavo-convex profiles with bulging mid- to toe-slopes (Fig. 3: RSD1, RSD2; e.g. Martinotti et al., 2011; Agliardi et al., 2012). Other key indicators include lineament swarms (Ustaszewski et al., 2008) and basal springlines (Fig. 3: RSD3, RSD4). RSDs may extend to considerable depths (~300 m: Dramis and Sorriso-Valvo, 1994; Crosta et al., 2013), but their deep structure usually lacks documentation. Although discrete basal sliding surfaces are often depicted, rock slopes more plausibly deform over a sequence of deformable layers, a mesh of joints (Jarman and Ballantyne, 2002), or zones of crush (as proven in Jettan boreholes, N. Norway; see Vick et al., 2020, and Fig. 23 therein). The lateral margins of RSD are often diffuse, but accurate boundaries can be delineated with confidence when the detection criteria listed above interrupt or fade within the search area. The imagery does not always allow high precision, but the very large size of each individual RSD unit nonetheless compensates overall for any loss of precision that might arise, and has no strong incidence on the aims and scope of this study (seeking precision greater than two decimal places for RSD surface area, in km^2, is purposeless).

The terminology around RSD is not fully settled. Although DSGSD (and its many variants) has gained currency (Crosta and Zanchi, 2000; Pànek and Klimeš, 2015) and is arguably more suitable than 'sackungen' (Němčok, 1972), 'slope tectonics', or 'rock mass creep', the binding concept of depth is commonly undefined. Terms such as 'rock instabilities' (Böhme et al., 2011) and 'unstable rock slopes', which attempt to identify sites that are 'pre-failure' in the narrow definition of Hungr et al. (2011), are unhelpful, with their implied corollary that 'failed' rockslides and rock avalanches are somehow not unstable or at least metastable. Conversely, Vick et al. (2020) adopt the term 'RSD', but then extend it to include rockslide masses translated on clear foliation surfaces, with all modes of RSF under an umbrella of 'progressive failure'.

Readers are thus invited to hold RSD in this study as synonymous with DSGSD, but only provisionally and tentatively given that the methodology relies on imagery-based reconnaissance criteria. The

441 detection of RSD really requires additional fieldwork in order to establish whether the landform truly
442 is a DSGSD or, instead, results from tectonic deformation. As documented above (Sections 2.2.3,
443 2.2.4), the chances of encountering coseismic scarplets in the Western Alps are low, but choosing to
444 label as RSD a population of DSGSD-like slope deformations on remote imagery was deemed suitably
445 neutral, objective, and prudent.
446 The simple four-category scheme employed here has the overall advantage of being on a diminishing
447 scale of (i) travel distance and (ii) degree of mass disintegration. Many compound sites display such
448 transitions (e.g. RS2' in Figure 3), progressing from incipience, via movement to partial collapse, and
449 are here categorised by their primary mode (usually RSD). As uncertainty in RSF detection remains
450 inevitable, including in the field, each site was also probability-rated. Detection uncertainty arises
451 with degradation over time and in weaker rocks, with forest concealment and anthropogenic
452 disturbance, with mimicry and equifinality in landforms of other origins, with diffuse margins, and
453 with the difficulty of distinguishing incipient RS and RSD source scarps and fractures from selectively
454 eroded lineaments. RSF probability rating was based on a relative scale from 1 to 3 (1: highly
455 probable; 2: probable; 3: less probable), and the site catalogue was independently critiqued on that
456 basis by the three co-authors.
457
458 **3.3 GIS database production and spatial analysis methods**
459 The ALOS DEM was used for computing hillslope gradients and local relief across the raster grid.
460 Altitude, slope angle and local relief values were then binned into statistical classes and plotted
461 against the topographic attributes of the RSF polygons (Pánek et al., 2018). This provides a relative
462 density distribution of RSF within a given class of elevation, slope angle or local relief values on a
463 valley side.
464 The RSFs identified in Google Earth were manually outlined as polygons in the geographical
465 information system ArcGIS™. The geographic coordinates of each RSF centroid were obtained
466 directly from the DEM layer in the GIS and checked for consistency in Google Earth. Distribution

maps were produced for each RSF category. RSF location was analysed with respect to topographic, geological, and palaeoenvironmental variables retrieved from a variety of data sources, enabling spatial patterns to be identified and possible causes inferred. Attribute tables generated in the GIS and variables obtained directly from other information sources produced the following primary data:

(i) surface area: calculated from the ALOS DEM using the WGS 1984 / UTM32N spatial reference frame. Massif areas were calculated from their boundaries depicted in Fig. 1B.

(ii) RSF aspect: obtained directly from Google Earth, thus allowing plots of RSF surface area as a function of aspect to be generated. Slope aspect maps were also produced from the DEM for the entire study area, allowing RSF aspect to additionally be compared with the total aspect distribution of hillslopes.

(iii) RSF headscarp altitudes, and centroid altitudes in the specific case of RSD. The relevance of distinguishing between the two—essentially in the case of the larger RSD—is that a number of RSF headscarps and rupture scars occur in the formerly supraglacial zone, whereas their centroids lie below valley-glacier trimlines.

(iv) Lithology: this was recorded for each RSF by headscarp or scar location, except by polygon centroid for RSDs, from BRGM 1:50,000 scale digital maps (Bureau des Recherches Géologiques et Minières), and for the Italian sector from the map by Piana et al. (2017). Consistent regional (and cross-border) overviews are provided by non-digital 1:250,000 BRGM maps that cover the entire study area, and by a simplified 1:250,000 lithological map by Gidon (1977) used as a control. The detailed BRGM maps discriminate 178 bedrock types (Suppl. Fig. 2A), some very minor. For the purpose of this study, these pre-ordained rock types were at first aggregated into 55 classes in order to approach the more tractable number of categories shown on the 1:250,000 scale maps (Suppl. Table 1). This shortlist was in turn used for further simplification measures, either into very broad types based on mass mechanical properties (such as brittle vs. ductile) or conventional rock type (4 categories: igneous, metamorphic, sedimentary/carbonate, and sedimentary/detrital) for a regional overview; or simplified to a lesser degree into 15 finer

493 taxonomic classes (Suppl. Table 1; Suppl. Fig. 2B) for closer analysis and trying to capture in
494 greater detail the influence of RSF 'preconditions' as defined in Section 2.2.1. Note that the
495 geological map taxonomies in the case of metamorphic rocks tend to emphasise protolith rather
496 than metamorphic texture, thus a mapped greywacke unit may in fact be weakly metamorphic
497 semischist.
498 (v) Structure: major tectonic lineaments were taken from the mid-range 1:250,000 scale BRGM
499 maps. This reference frame was chosen because it provides the only scale at which mapped
500 lineaments cover the entire study area in a consistent way. Given the regional scope of this
501 inventory of RSF, local alpine faults or fractures depicted in 1:50,000 scale maps were only
502 retained if also present on the 1:250,000 scale maps.
503 (vi) Variations in regional tectonic stress field: mapped after Delacou et al. (2004) and Sue et al.
504 (2007).
505 (vii) Variations in magnitudes of instrumentally measured surface uplift: after Nocquet et al. (2016).
506 (viii) Seismic activity: Thouvenot and Fréchet (2006) provides epicentre location, local magnitude,
507 focal depth and date of every earthquake exceeding M_L 2 since 1989 from the SISMALP database.
508 This very short time span is not statistically valid for higher-magnitude events with much longer
509 return periods, and can of course only be treated as a guide to variations in 'background' levels.
510 (ix) Ice thickness: this was calculated by netting the present DEM topography from the contoured
511 map of the Late Pleistocene MEG by Coutterand (2010), where ice thickness was reconstructed
512 from trimlines, moraines and nunataks. Ice thickness and iceway width provide a notional
513 understanding of relative valley-side stresses and thus the potential intensity of rock slope
514 damage revealed after deglaciation.
515 (x) Modern rainfall pattern: mapped after Gottardi (2009).
516 These various thematic layers were entered into the GIS and co-registered and georeferenced, with
517 the RSF data points likewise georeferenced and used as an overlay. RSF spatial incidence was
518 examined in relation to each thematic layer as a means of testing the explanatory power of each

519 variable listed above. In doing so, the RSFs were analysed from two perspectives: as point
520 distributions, and based on RSF polygon areas, in each case using the kernel density function
521 advocated by Silverman (1998) and readily available in ArcGIS 10.7.1. This spatial clustering metric is
522 expressed in km^{-2} and produces smoothed density gradient maps where clumpiness depends on the
523 imposed search radius. Through trial and error, the optimal search radius for this study area and
524 dataset was 10 km.
525

526 **4. Results**

527 **4.1 Spatial incidence of RSF**

528 *4.1.1 RSF type, size, area affected, and spatial density*

529 The inventory documented by remote imagery comprises 1416 RSFs (Fig. 4; Table 1). Of these, 1306
530 are rated highly probable, 88 probable, and only 22 less probable. Rockslides (RS) and rock slope
531 deformations (RSD) predominate, with 596 and 558 cases respectively (42% and 39%). Disintegrated
532 failures, i.e., rockfalls (RF) and rock avalanches (RA), together comprise 262 cases (18%), but with
533 only 15 ascertained rock avalanches among them. This three-way split in main types is almost
534 identical to that in the only other comparable study of this size, for the Scottish Highlands (Jarman
535 and Harrison, 2019).
536 Individual RSF sizes range from the 0.02 km^2 threshold to 43 km^2. Fig. 5A also indicates 53 RSDs larger
537 than 8 km^2, and 47 RS larger than 2.5 km^2. A typical lognormal size–frequency distribution is obtained
538 (Fig. 5B; cf. Wood et al., 2020). Sharp fall-offs in the various categories below 0.05 km^2 (Fig. 5C)
539 indicate sizes below which detecting them on the imagery becomes more difficult. Rockfalls are
540 naturally smallest, with an average extent of 0.22 km^2. Rockslides and rock avalanches attain
541 averages of 0.99 km^2 and 2.42 km^2, respectively. RSDs are typically very much larger, with an average
542 area of 3.15 km^2. The largest RSD (43 km^2) is the Vallée des Belleville (Vanoise), extending over the
543 entire eastern valley side and progressing from in situ fissuring to slumping.

RSF from this inventory impacts 8.8% of the total mountain area (Table 1; but see Section 5.1). Densities within massifs vary widely from <3% in most of the Prealps to a remarkable 21–23% in the Parpaillon, Beaufortain and Escreins massifs. Even higher densities have been mapped at catchment scale from fieldwork and other types of imagery, e.g., 38% in the Susa/Chisone valleys (Fioraso, 2017), but the present regional study does not drill down to that level of resolution. These dramatic variations in spatial incidence are discussed in Section 4.4.

4.1.2 RSF in relation to morphometry and topography

The peak frequency of RSF (by headscarp altitude) lies in the 1500–2300 m a.s.l. belt (Fig. 5D). Rockslides tend to be lower, with a peak at 1700 m, and RSD ~1900 m, both with Gaussian distributions. Rockfall scars are widely distributed but generally higher, with a slight peak at 2700 m (Fig. 5E).

The link between RSF occurrence and valleyside slope is less clear-cut, perhaps partly because pre-failure slopes have been relaxed by the actual RSF. The larger types (RS/RSD) range widely between 10 and 40° (Fig. 5F). A secondary peak of 65–80° for RSD can be discounted as an artefact of the DEM mapping routine, where headscarps are extensive enough to register as prevailing 'source area' slopes in their own right—as for example at the Dérochoir (Haut-Giffre massif; Goguel and Pachoud, 1981).

Local available relief (a proxy for magnitude of valley incision) does not appear to be a strong control, with RSF being broadly distributed across intermediate rather than extreme local relief (Fig. 5G). Local relief in the Western Alps can exceed 3000 m, yet there are no RSFs where local relief exceeds 2500 m, probably because the more extreme relief associates with high-strength rock types less vulnerable to RSF (e.g. granite in the still-glaciated Mont Blanc and Ecrins massifs). Differences between RSF modes can, however, be distinguished, with RSD generally falling in the 900–1400 m local relief band, RS slightly higher at 800–1700 m, while RA and RF occur randomly.

569 Slope aspect is a stronger control, with RSF occurring preferentially (by area) on NW–W–SW
570 exposures (Fig. 5H) and south aspects favouring rockslides (RS). The more northerly aspects support
571 the smaller, disintegrated types (RA, RF; Fig. 5I), partly because the prevalence of more intricate
572 cirque terrain is unconducive to large-scale RSF, and partly because more intense periglaciation
573 (frost-shattering) favours these modes.
574
575 **4.2 RSF incidence and geological factors**
576 *4.2.1 Lithology*
577 The results here (Figs. 4, 6) confirm that outcrop geology is a strong influence but not a controlling
578 one, as range-wide inventories commonly find (e.g. Jarman and Harrison, 2019): lithology
579 predisposes but does not predetermine. At a secondary level, rock type significantly influences RSF
580 mode and its agency in landscape shaping.
581 Assigning RSFs regardless of size to the four aggregated lithological classes (Fig. 4) confirms the
582 affinity of RSF with metamorphic rocks (e.g., Ballantyne, 2002; Hewitt, 2009), which may be greater
583 still if some detrital rocks display semischist fabrics as a result of weak metamorphism: metamorphic
584 rocks (n = 809), detrital rocks (n = 353), carbonate rocks (n = 216), plutonic rocks (n = 38).
585 Figure 6 provides a finer rock classification based on 15 classes aggregated out of the BRGM's
586 1:50,000 scale digital maps (see also Suppl. Table 1, Suppl. Fig. 2B). The map shows that schist, flysch,
587 and weakly metamorphosed rocks derived from detrital sedimentary protolith (i.e., sandstone,
588 greywacke) are among the most susceptible, whether in the Helvetic or Penninic domains shown in
589 Figure 2. Granite, gneiss, migmatite and limestone are among the least affected by RSF, in conformity
590 with known tendencies reported elsewhere.
591 In Figure 7, the role of lithology is quantified by relating the percentage of each rock type affected by
592 RSF to the percentage of that rock-type in the region, by area (rock categories are identical to those
593 of Figure 6). RSF lithology ratios show the strength of associations by descending order of the red
594 bars (presented separately for the French and Italian sectors since the lithology databases use

595 different classifications; Fig. 7A, B). For example (in France): 39% of all RSF by area is in schist (green
596 bar), schist only occupies 16.5% of the region (blue bar), 24% of schist outcrop area is impacted by
597 RSF (red bar).
598 The strongest associations by area, in both the Italian and French sectors, are clearly with the various
599 detrital rocks, both sedimentary and metamorphic (once gabbro and basalt are excluded as having
600 tiny outcrops). Conversely (again leaving aside lithologies of limited extent) RSF is substantially
601 underrepresented on limestone and marl, which account for 34% and 13.5% of the French sector
602 respectively: RSF impacts only 2.1% of these lithologies.
603 The Italian sector (Fig. 7B), displays a broadly similar sequence of relative impacts, with one
604 interesting statistical difference: schist is even more predominant both as a rock-type and as a host
605 for RSF, yet the relative impact (14% affected: red bar in Fig. 7B) is slightly less than west of the
606 drainage divide. This may reflect the fact that schist outcrops in Italy extend to lower altitudes, in
607 perhaps more fluvially-dissected relief where potential for RSF, and especially large-scale RSD, is thus
608 more limited than in the more elevated and glacially dissected terrain of the inner Alps.
609 At massif scale, marked differences in susceptibility emerge within lithological classes. Thus in
610 carbonate rocks, it is unsurprising that RSF densities are low in the Prealpine massifs, with massive
611 reef limestone plateaus (Urgonian facies) mainly exposing perimeter escarpments to RSF. Conversely,
612 other limestone facies, including calcarenite, display moderately higher RSF densities in more
613 dissected massifs such as Cerces, and notably in the valley of Chamonix (Chablais–Haut-Giffre),
614 deeply entrenched amid some of the highest relief of the study area. Meanwhile, granite massifs
615 such as Belledonne display only scattered handfuls of RSFs. RSDs are particularly rare in these
616 crystalline outcrops. Where present, their main distinction compared to many other RSD occurrences
617 is the conspicuousness of slope antiscarps.
618 The broad-scale correlations presented above should, of course, not understate the importance of
619 the lithological fine grain, which is often critical and can be areally extensive but evades the scale of
620 analysis chosen for this study. For example, massive sandstones usually resist RSF but may be

621 mobilised on intercalations of siltstone or clay (or their metamorphic equivalents). Likewise, flysch is
622 a fine-layered alternation of sandstone and shale, and thus effectively a dual lithology, enhancing
623 propensity to failure at favourable angles of dip. Thus in the extensive 'Zone houillère' of the
624 Western Alps (Fig. 2), with its heterolithic successions of Mesozoic detrital rocks sometimes
625 displaying semischist texture (Gidon, 1977), such internal contrasts will be more relevant to RSF than
626 geological map units suggest at face value. At still finer spatial scales, the internal fabric of bedding
627 planes, cleavage partings, and joint sets of metamorphic rocks are critical in reducing rock mass
628 strength and shaping failure envelopes with sliding and release surfaces. Different modes of RSF will
629 be promoted depending on the angle at which they intersect the topography.
630 In summary, assigning RSFs to mapped lithologies is only a first-order sorting procedure, with
631 geology becoming more influential at finer scales in controlling mode of failure, local preferential
632 orientations, and degree of disintegration. The full significance of lithology can only be determined at
633 field survey level.
634
635 *4.2.2 Geological structure, including faults and thrusts*
636 RSF incidence is routinely assigned to mappable surface lithology, yet the real locus of failure may lie
637 deeper in the stratigraphy or structure, and goes unrecorded in map view. This three-dimensional
638 mapping problem is evident in the Alps. The influential lithology—weaker, deformable, or
639 impervious—often underlies the surface rock type. This also occurs where soluble substrates
640 engender karstic processes promoting subsidence and failure, as with thick evaporites beneath
641 magmatic rocks at Friolin, in Savoie (Rovera, 1993).
642 The three-dimensional conformations summarised above are exacerbated where folding, faulting
643 and thrusting juxtapose contrasting lithologies, but no useful conclusions could be drawn from the
644 pattern of RSFs in relation to mapped faults, with only 10% of the RSF population (17% by surface
645 area) contacting them (Fig. 8). The intensely faulted Prealps, for example, almost entirely lack RSF. In
646 contrast to faults, however, the major alpine thrust fronts have 17% of the RSF population (36% by

area) touching or intersecting them (Fig. 8). Since thrusts are not noted seismic loci, but are exploited by valleys, higher RSF incidence responds to thrusts bringing susceptible lithologies into gravitational juxtaposition. This occurs in two modes:

(i) direct structural superimposition: for example, around the Annes klippe (capping the Bornes–Aravis massif; see Figs. 1, 2, 8); or at Valloire, where the PFT brings overriding detrital sediments onto weaker flysch.

(ii) karstic processes: averred subsurface rock solution in thick evaporite layers contributes to chronic instability in Beaufortain (Rovera, 1993), Aosta (Martinotti et al., 2011), and probably other areas requiring field-based documentation.

On a regional structural scale, RSF is markedly more abundant in the internal Penninic Domain, east of the PFT, than in the external Helvetic Domain (Table 2). Thus RSF is three times as widespread east of the PFT, with RSD over four times more widespread. However, the study area west of the PFT includes extensive tracts of lower elevation, plateaus, broad troughs, and unconducive lithology, notably in the Prealps.

4.2.3 Seismicity

'Postglacial rebound scarps' at Grands Moulins (Belledonne) and Peisey-Nancroix (Vanoise) (Hippolyte et al., 2006, 2009, 2012), and lineament swarms in the Swiss Alps, have been previously interpreted as seismic features (Sébrier et al., 1997; Persaud and Pfiffner 2004). Ustaszewski et al. (2008), however, preferred to view such 'composite faults' as partly gravitational rebound breakout fractures, thus caused by an RSF-related process not requiring seismicity. Debate about the local influence of seismicity on slope instability in the Western Alps is thus unsettled, but the inventory here, presented in Figure 9 as earthquake magnitude to focal-depth ratio rather than simple earthquake intensity (M_L), shows an almost total lack of correlation between the spatial incidences of RSF and current seismicity on a regional scale. Thus the 'seismic arcs' defined by Thouvenot et al. (2003) and Sue et al. (2007) bear no clear relation to the high-density RSF areas. In the Piemontais

673 arc, the Sampeyre earthquake swarm area (Godano et al., 2013) displays very few RSF occurrences.
674 Associations with seismicity in the Briançonnais arc and along the strike-slip Belledonne boundary
675 fault are barely more compelling, although creep acceleration in the well-monitored Séchilienne
676 active RSF, close to the Belledonne Fault, was reported during the 1999 M_L 3.5 Laffrey earthquake
677 (Pothérat and Effendiantz, 2009). RSF incidence also appears to associate with some earthquake
678 swarms, as in Belleville valley (Vanoise), the Aiguilles Rouges and Haut-Giffre massifs, and upper
679 Ubaye valley (Guyoton et al., 1990; Jenatton et al., 2007), but this could be a coincidence with fault-
680 exploiting topography. Likewise, the 2005 and 2017 low-magnitude tremors at Vallorcine and La
681 Chapelle recorded shallow hypocentres and occurred within an area of current landslide activity; but
682 this could also be coincidence rather than cause. Given, finally, that most historic and contemporary
683 RSFs in the Western Alps, whether large or small, have no evident seismic trigger (Eisbacher and
684 Clague, 1984; Frayssines and Hantz, 2006; Tatard et al., 2010), it seems overall that modern
685 seismicity plays a minor role, if any, in the distribution of RSF in the Western Alps.
686
687 *4.2.4 Regional tectonics and uplift*
688 RSF distribution bears some spatial association with the three main modes of tectonic strain
689 prevalent since the late Neogene and documented in Section 2.2.3 (Fig. 10): (i) extensional stress
690 occurs across 36% of the study area and hosts 69% of RSF by surface area, whereas (ii) strike-slip to
691 transtensional fault motion affects 56% of the study area but hosts only 30% of the RSF population.
692 The former operates within a broad core astride the main drainage divide, whereas the latter applies
693 to the Prealps and other peripheral massifs. Lastly, (iii) compressive stress only affects 8% of the
694 study area, again in lower-relief peripheral massifs, and a mere 1.2% of the RSF population.
695 The dome of instrumentally-measured current surface uplift rates (Fig. 11) centres on Beaufortain–
696 Vanoise, which is undoubtedly an RSF concentration (on susceptible schists), but since similar
697 concentrations occur outside the dome, where uplift rates dwindle to negligible values, there is no
698 exclusive or unique causal connection between modern uplift differentials and RSF density.

699

700 **4.3 Climatic controls on RSF incidence**

701

702 Assigning palaeoclimatic causes is inherently difficult when most RSFs are undated, and because
703 many sites fail progressively over thousands of years. They can be continuing, slow deformations;
704 dormant (metastable) masses; or displacements accelerating to final collapse. Undated extant sites
705 may thus be circumstantially assigned as Lateglacial (Ballantyne, 2013), post-Last Glacial Maximum
706 (LGM) (Augustinus, 1995), post-Little Ice Age (Holm et al., 2004; Oppikofer et al., 2008), or
707 contemporary (Blikra et al., 2006). Yet even where dates are resolved, causation may remain blurred.
708 In the Mont Blanc massif, ~50 supraglacial rockfall scars have ^{10}Be exposure ages ranging from 7 ka to
709 the LIA (Gallach, 2019), suggesting so far little more than a random succession of events.
710 Given the almost total absence of correlation found between modern rainfall patterns and RSF
711 distribution in the Western Alps (Suppl. Figure 1A even suggests an inverse relationship: drier massifs
712 host the greatest areal extent of RSF), we dwell here instead on the incidence of other climatic
713 variables: past glaciation, and permafrost.

714

715 *4.3.1 Glaciation and deglaciation*

716 In this heavily glaciated study area, 77% of RSF-related landforms are located within the boundaries
717 of the most extensive glaciation (MEG) mapped by Coutterand (2010), thus primarily in or on the
718 rims of glaciated valleys (Fig. 12). The largest RSDs are in valleys where ice thicknesses exceeded 1
719 km, notably the Maurienne, Tarentaise, Susa, and Aosta valleys. Physical debuttressing (removal of
720 ice support) undoubtedly plays its part in the timing of RSF, but is probably too simplistic to be
721 defined as a unique cause (McColl, 2015; Grämiger et al., 2017). At Séchilienne, for example,
722 debuttressing by Romanche glacier downwasting was not an immediate cause given the ~6 ka
723 recorded onset of slope deformation, long after valley deglaciation ca. 13 ka (Schwartz et al., 2017).
724 The paraglacial connection with RSF occurrence is thus nominally very widespread, but chronological
725 work on the inventory would be required to take matters further.

A more unusual feature of the regional data, however, is the substantial minority of RSFs (23%, n = 321) that occur in differing modes either above (supraglacial: n = 270) or beyond (extraglacial: n = 51) the boundaries of the Late Pleistocene MEG (Fig. 12). The majority of supraglacial RSFs (59%, n = 188) are of the RF/RA variety on possible nunatak peaks and crests above the mapped ice limits (Fig. 12B), and are thus responding to periglacial stresses. More unexpectedly, 68 supraglacial RSDs occur as split ridges, ridge rents, and ridgetop grabens. Although these RSDs only have visible expression above the MEG trimlines, some may have propagated upwards from destabilised lower slopes, with inferrable basal failure zones extending down into them (Fig. 13; see also El Bedoui et al., 2011). Such cases are thus still paraglacial. Where, however, RSDs are confined to higher levels, they can associate with broader ridges where slope stress disequilibria are more pronounced (Gerber and Scheidegger, 1973). RSD typically occurs on one flank, but occasionally both as at Mont Rognier (Belledonne massif; Hippolyte et al., 2012) and in the Aiguilles Rouges massif. The widely illustrated 'pagoda-shaped ridges' of Beck (1968) can arise thus, with true antiscarp outbreaks on both rims, but are more often false antiscarps where the headscarp daylights behind the crest, as at Croix du Berger, Beaufortain (Fig. 14). Ridge spreading is probably as much a response to long-term uplift and valley incision as to cumulative glacial overstressing, and it remains to be seen whether RSF dating could truly bring clarity to the issue of distinguishing these two causes.

The 3.6% of extraglacial RSFs occur in two contrasting contexts. In the unglaciated valleys and foothills of Italy (Chambeyron, Cottian Alps, Mt. Viso; Fig. 1B for location), RS and RSD occur in susceptible detrital and metamorphic rocks, notably the Schistes lustrés (Figs. 2, 6, 7B; Piana et al., 2017) and other schists and metavolcanic rocks (e.g., Mt. Viso). This is often in, or above, V-shaped valleys or ravines. Where removed from direct fluvial undercutting, these may be considered a 'parafluvial' (rather than 'paraglacial') mode of RSF, as identified in the eastern Pyrenees (Jarman et al., 2014). In the southwestern Prealpine massifs (Vercors, Dévoluy; Fig. 1B for location), RSF occurs primarily on escarpments owing little to glacial or fluvial steepening, and is simply contributing to the longer-term slope recession process endemic to most mountain rockfaces.

752

753 *4.3.2 Permafrost thaw*

754 As suggested by Figures 5H and 5I, the greatest influence of periglacial activity may relate to slope
755 aspect. Southerly aspects broadly favour RSF (see also Pedrazzini et al., 2015; Jarman and Harrison,
756 2019) perhaps because of greater diurnal and seasonal thermal stressing (heat and frost jacking). The
757 19% of RSFs which are supraglacial clearly fall within the periglacial zone (above at least 2000 m
758 a.s.l.), where freeze-thaw processes have been most intense, but this does not, however, necessarily
759 mean they can be attributed specifically to permafrost degradation (see Fig. 13, for a counter-
760 example concerning a large RSD). Although this inventory demonstrates a preponderance of
761 relatively smaller RSFs in this zone—59% are rockfalls, and most of the 15 rock avalanches occur in
762 that elevation band—regional mapping of undated events cannot expect to discriminate the
763 influence of permafrost thaw-related stressors. Permafrost thaw is commonly an important cause of
764 minor slope instability (Harris et al., 2009; Matthews et al., 2018; Wood et al., 2020); i.e., it mainly
765 releases abundant minor landslides and rockfalls, usually below the RSF threshold size relevant to
766 this study (Ravanel and Deline, 2011; Ravanel et al., 2017). This is possibly confirmed by the slight
767 frequency peak of RF occurrence ca. 2700 m (Fig. 5E), which is the current lower limit of permafrost
768 in the Western Alps. Its role in mobilising deeper deformations, however, is more speculative.

769

770 **4.4 Mapping overstressed slope areas in the Western Alps**

771 Here we take a spatial density approach to explore why RSF should occur intensely in some parts of
772 the Western Alps and sparsely in others, after allowing for certain lithologies being more resistant to
773 failure. Identifying such variations in spatial incidence may illuminate the significance of RSF as an
774 indicator of unusually active landscape evolution processes. For example, Jarman and Harrison
775 (2019) identified eight pronounced clusters of RSF in the Scottish Highlands. They were associated
776 with loci where concentrated erosion of bedrock (CEB) could be inferred to have destabilised
777 adjacent slopes by more than routine debuttressing-related or glacio-isostatic stress release. In that

778 regional study, CEB chiefly impacted glacial breaches of main icesheet flowline divides. Glacial
779 breaching being rare in the Western Alps, the search here is for comparable drivers and stressors.
780 An immediate problem in defining such clusters is that mapping numbers of sites per unit area will
781 play down the contribution of areally-extensive rockslides and rock slope deformation zones, while
782 mapping the area affected by RSF per square kilometre unduly favours them. Cumulatively,
783 numerous small but frequent RSFs may contribute more failed material to the slope and fluvial
784 systems for export, and a larger number of local vulnerabilities for exploitation, thus greatly
785 enhancing future erosion. In tectonically inactive mountains, however, where RF- or RA-triggering by
786 earthquakes is infrequent, this may not be a core consideration. Conversely, large slope
787 deformations may have very long residence times. In terms of delivery to the sediment cascade, or of
788 pinpointing more immediate hazards to human activity, either of these approaches has its relative
789 merits. Both bases were therefore analysed for comparison, and are presented here.
790
791 *4.4.1 RSF point-array clusters*
792 Treating RSF incidence first as a point array, Fig. 15A clearly demonstrates pronounced density–
793 sparsity contrasts across the study area. The top band of point-density (or kernel density) contour
794 values identifies seven clusters (dark blue) encompassing 33.5% of the RSF population and covering
795 9.5% of the study area. When all RSF modes are considered together (Fig. 15A), clusters of highest
796 RSF diversity (i.e., co-occurrence of RA, RF, RS and/or RSD within a small area) occur as two
797 elongated bands along the strike of the Penninic Frontal Thrust in the Beaufortain and Cerces
798 massifs, with likewise high-density polygons in the Grandes Rousses massif, the Parpaillon, and close
799 to the Alpine drainage divide in the eastern Escreins massif and the southwestern Cottian Alps /
800 eastern Queyras (Fig. 1B for location).
801 Some marked differences between RSF types become apparent in Figures 15C–E: the very small rock
802 avalanche (RA) population is rather randomly scattered, whereas the rockfall (RF) population shows a
803 few local concentrations (Fig. 15C). These trends overall suggest no strong predisposition among rock

804 types to RF and RA, both modes appearing to occur relatively evenly in all of the tectonic zones
805 defined by Fig. 2. Rockslide densities (RS) show strong peaks in most clusters, are fairly evenly
806 distributed between the Helvetic and Penninic domains, but are notably rare in the Prealps and more
807 generally in massifs dominated by brittle lithologies (e.g., Mont Blanc, Grand Paradis, Ecrins,
808 Devoluy). RSDs are prominent in all the clusters, if (naturally, given their size) less intensely. They are
809 overwhelmingly more abundant in the Penninic Domain.
810
811 *4.4.2 Area-based RSF hotspots*
812 Turning to area impacted by RSF rather than point density, the top band valuably focuses the clusters
813 into six 'RSF hotspots' (Fig. 15B, and numbered 1 to 6 in red in Figure 15F). The term hotspot is
814 borrowed here from ecology to characterise areas of high species richness (as with the clusters
815 defined in Section 4.4.1), but here also emphasising abundance in terms of quantity of rock mass
816 displacement (a substitute for biomass in the hotspot analogy). These hotspots cover 2080 km^2, i.e.,
817 7.5% of the study area and 16% of the overthrust Penninic Domain. RSF by area covers on average
818 half (48%) of the hotspot territory (i.e., in any given hotspot area, only half the rock masses are not
819 displaced), and collectively the six hotspots embrace 41% of the study area's RSF inventory by
820 surface area. Almost half the impact is thus concentrated within only 7.5% of the total study area. It
821 can be asserted on that basis that 7.5% of the study area is highly disproportionately overstressed by
822 gravitational rock mass displacement, for which predisposing factors, drivers and stressors may be
823 explored.
824 While at first glance the clusters (Fig. 15A) and hotspots (Fig. 15B) may appear to be two ways of
825 mapping the same reality, there are in fact significant differences between their patterns, as shown
826 when they are displayed together as in Figures 15F and 15G: whether first- or second-band, the
827 clusters of the Helvetic Domain, for example, fade completely, as do collections of other smaller
828 sites. Because of the weighting of RSF areally in favour of RSD, the strong Beaufortain 'Cluster 7'
829 recentres over Tarentaise (i.e. middle Isère River valley) and becomes 'Hotspot 1', while 'Cluster 9'

(Vanoise) is pulled southward to straddle the Maurienne (i.e. middle to lower Arc River valley). The extensive eastern 'Cluster 11' splits into 'Hotspot 5' (eastern Escreins and eastern Queyras massifs) and 'Hotspot 3' (which, like 'Cluster 7', is pulled northward and straddles the valley of the east-flowing Dora Riparia between Mont Cenis and the Cottian Alps).

Overall, the most striking features of RSF hotspot distribution in Figures 15B, G, and F are as follows:

(i) they all occur east of the Penninic Frontal Thrust, i.e., within the Penninic Domain (Table 2);

(ii) they are mostly aligned on, or close to the leading edge of, the PFT; or, in the case of 'Hotspot 3', of the Briançonnais Backthrust;

(iii) they cluster in the region corresponding to the core of the Pleistocene ice accumulation zone, i.e., to areas within the Penninic Domain which resided longer above the ELA than at many places in the Helvetic Domain, and thus where glacier erosive power exerted the largest stresses on preglacial slopes. The regional ELA during the Late Pleistocene most extensive glaciation (MEG) was located by Coutterand (2010) around 1300±50 m (Fig. 12A)—as opposed to 3000–3100 m at present in the Grandes Rousses and Vanoise massifs (slightly lower in the Mont Blanc: 2900 m; Six and Vincent, 2014). ELAs between MEG periods would rise rapidly, migrating east and most often remaining confined to the Penninic Domain (Séguinot et al., 2018); accordingly, large areas of the icefield ablation zone coincided mostly with the Helvetic Domain.

The two most striking differences between clusters and hotspots in Fig. 15F are as follows:

(i) clusters are mostly massif-centered, whereas hotspots straddle some major glacial valleys, where typically RSD is prevalent.

(ii) while clusters tend to straddle the PFT and, in the Chambeyron massif, the Briançonnais Backthrust (Fig. 15A), hotspots are displaced away from these major thrust fronts and, conspicuously, away from the Helvetic Domain—which, as a result, entirely lacks RSF hotspots.

The significance of these various associations is further developed in the Discussion in light of Figures 15F and 15G and other results presented in this Section 4.

5 Discussion

5.1 Comparisons between this RSF inventory and previous datasets

The inventory presented here can be compared with five existing published datasets covering all or part of the study area, while recognising that their goals and methods were different, and that data sources have improved considerably.

The 1:50,000 scale geological maps of France, for example, comprehensively map 'landslides', but unfortunately only as a standard symbol, with no indication of landslide type. About 40% of landslides on maps are not bedrock RSFs; they are often small and seated in regolith. Conversely, this study has identified ~250 previously unmapped RSFs in the French sector, some of them very large. This may partly reflect a convention that RSDs are generally not mapped as 'landslides' unless there is tangible displacement of a failed rock mass. For example, a major RSF complex identified in this study is on the SW face of the Grand Coin (Maurienne valley, Vanoise massif; Fig. 4 for location), with impressive deformation progressing to rockslide and rockfall. Within the area covered by that 1:50,000 geological sheet (Saint-Jean-de-Maurienne, see Fig. 4), the inventory identifies 55 RSFs, of which 17 cannot be correlated with BRGM landslide symbols (thus a 30% detection increase is gained for that area).

Turning to imagery-based studies, the range-wide RSD inventory of Crosta et al. (2013) utilised early versions of Google Earth, sometimes of poorer quality and before historical imagery provided multiple passes. In the French sector of the Western Alps, Crosta et al. (2013) recorded 73 DSGSDs, now augmented by 247 further RSDs from this study (current inventory total: n = 306). These additions include well-documented active sites such as Séchilienne, and other conspicuous examples shown in Fig. 3 (RSD1–RSD4). However, in the Italian sector Crosta et al. (2013) recorded 88 sites, albeit supplemented by sources additional to Google Earth, of which 15 could not be included in the present inventory as they were undetectable from the imagery, even with prior knowledge of their existence. Since the density of RSD in the present inventory (6.3%) is only slightly greater than their Alps-wide figure (5.6%), it suggests Crosta et al. underreported the French side of the study area.

882 The studies by Tonini et al. (2014) and Pedrazzini et al. (2015) of the Upper Rhône valley cover all RSF
883 modes and display limited overlap with the present study area (Fig. 1A), thereby providing narrow
884 scope for comparison. Discrepancies in the overlapping area (south of the Rhône River) are
885 negligible. The present inventory identifies at most four new RSFs (Fig. 16), evidenced by chaotic
886 debris deposits and vegetation contrasts on the imagery, and by highly irregular contours on
887 1:25,000 scale topographic maps. The newly detected RSD, indicated by ridge-splitting on the
888 imagery, is adjacent to a known rockslide (Plancherel and Broquet, 1998). Conversely, remote
889 (LiDAR) and field mapping of the Aosta valley by Martinotti et al. (2011) captures two large RSDs at
890 Hône and Villeneuve, not detectable on the imagery by the present study because they occur below
891 the treeline.
892 A valuable earlier overview by Eisbacher and Clague (1984) of catastrophic RSF in recorded history
893 identifies 15 locations in the Western Alps of France. Since it focuses on events affecting settlements
894 and infrastructure, four were not detectable on the imagery and thus not included in the inventory:
895 the rock avalanches of Tête Noire, Salvan and Pointe d'Autigny (Haut-Giffre; Chablais), and the Lullin
896 rockslide (Chablais) (Fig. 1C for location). Two other cases were retro-included in the inventory
897 because they have geomorphological impacts still visible on the imagery, with recognition criteria
898 widened by experience. The first is Mt. Granier (1248 CE). Despite being the largest rock avalanche
899 by volume in the region (500 M m^3), the fertile limestone debris was soon reclaimed and now
900 supports the famed vineyards of Apremont and Les Abymes, no longer resembling RA runout and
901 only leaving unusually convoluted elevation contours on maps as a potential clue. The second is the
902 Bourg d'Oisans palaeolake outburst of 1219 CE (Bailly-Maître et al., 1997), which inundated Grenoble
903 after destroying a rock avalanche dam impounding the Infernet valley (Taillefer massif). Only traces
904 of this event now remain. Both Granier and Infernet have left prominent scars but no obvious
905 cavities, and are not easily readable as RSFs in the absence of a conspicuously related debris mass.
906 Finally, nine RSFs monitored by CEREMA (Fig. 1C) were originally missed for being too small or within

907 forest, but prove detectable on the imagery by zooming in at sufficient magnification to see the
908 fissure-like lineaments.
909 In summary, the 30 RSFs added here to the inventory as detectable by refined study criteria (but not
910 included in the maps of this publication) are (i) the 9 CEREMA-monitored sites; (ii) the 4 undetected
911 RSFs described by Eisbacher and Clague (1984); (iii) the Hône and Villeneuve sites in Val d'Aosta; and
912 (iv) the 15 additional RSDs reported by Crosta et al. (2013) in Italy. They raise the total RSF inventory
913 for the Western Alps from 1416 to 1446. They comprise 85 km^2, increasing the total RSF area from
914 2441 km^2 to 2526 km^2 and the RSF footprint from 8.8% to 9.1% (Table 1).
915
916 **5.2 Ranking controls on rock slope susceptibility to failure**
917 While focusing on a much smaller area, but including (as in this study) all modes of slope instability,
918 Malatrait (1975) recognised the intractable aspects and various pitfalls of multivariate analysis,
919 including the difficulty of defining truly independent variables that would avoid autocorrelation and
920 circular reasoning. He opted instead for a more descriptive approach based on chosen case studies.
921 Crosta et al. (2013) later applied discriminant, principal component, and cluster analysis to define
922 predisposing and controlling factors of DSGSD incidence across the European Alps. They identified
923 foliated metamorphic rocks (especially metapelites), Late Pleistocene ice thickness, local relief, slope
924 size, drainage density, and (estimated) river stream power as the local parameters most positively
925 correlated to DSGSD occurrence. Although such analysis might be appropriate for single RSF modes,
926 the four disparate modes (RF, RA, RS and RSD) and scales of this study cannot safely be integrated to
927 explain the highly skewed spatial distribution of RSF revealed in Figure 15. Even with the single-mode
928 RSF study of Crosta et al. (2013), the authors conceded that the predisposing factor of lithology,
929 chiefly foliated metamorphic rocks, was by far the most dominant (and, therefore, once allowed for,
930 explains little else). Crosta et al. (2013) were also careful to acknowledge that the secondary
931 controlling parameters are strongly interrelated and cannot easily be disentangled. Although
932 commonly used for shallow landslides in small geographical areas where the key concern is to link

predisposing factors to triggers rather than to drivers and stressors, transposing the methods of landslide susceptibility mapping to RSF is neither straightforward nor entirely relevant given that (i) RSF triggers are most often unknown, and (ii) RSF populations are smaller than in the case of small, shallow landslides—thus making RSF also less amenable to robust statistical inference.

Considering that RSF susceptibility mapping and RSF factor ranking mostly end in stalemate, greater insight can instead be gained from the data by mapping finite areas of slope overstressing (Section 4.4), i.e., areas where massive strain relaxation by gravitational processes is interpreted as a symptom of spatially focused bedrock fatigue and failure. Such zones of extreme mass wasting are areas where positive feedback caused by various stressors further weakens the deforming region, in turn perpetuating the deformation and susceptibility to slope failure. Mapping such areas on a regional scale is a step towards explaining why they occur where they do, and to this end we focus on the areas of overlap between the previously presented clusters (Section 4.4.1) and hotspots (Section 4.4.2), naming them in this context super-hotpsots.

5.3 RSF super-hotspots

Spatial density characteristics answering simultaneously to the criteria of hotspots (Fig. 15B) and band-1 clusters (Fig. 15A), are named here super-hotspots. They are shown as cross-hatched areas of overlap in Figures 15F and 15G, and labelled *I* to *VII* (Roman numerals) in Figure 15F. More than just statistical constructs, the super-hotspots define unique spatial arenas that are sufficiently small, and thus suitably tractable, for attempting to interpret RSF occurrence and capture causal patterns on a level that transcends the single-RSF monograph. Super-hotspots are areas where displaced masses of rock, predominantly in the form of RSDs, are the most pervasive, and where contribution of failed material to the sediment cascade and to local rivers is potentially highest within a region. Based on Figures 15F and 15G, the geographic location and other attributes of the seven super-hotspots of the study area are summarised in Table 3.

959 The locations of these seven, exceedingly overstressed slope areas in the Western Alps can be
960 interpreted from the perspective of first-order geological predisposition as well as drivers and
961 stressors. Thus super-hotspot *I*, for example, encompasses the closely-spaced Lower Penninic and
962 Middle Penninic thrusts and their thrust fronts (visible in Fig. 8), i.e. the Valais, Sub-Briançonnais, and
963 Briançonnais zones (Figs. 2, 15G), juxtaposing structurally stacked, rapid successions of highly
964 susceptible, ductile schist- or semischist-fabric lithologies derived from sedimentary detrital
965 protolith: typically flysch, greywacke, fine sandstone, bedded conglomerate, marl, claystone, and
966 evaporites (Fig. 6). As shown in Fig. 12A, the middle Isère valley (alias Tarentaise) is also a glacial
967 accumulation zone where LGM valley ice was thickest (up to 2 km). Along with super-hotspot *II*
968 (middle Arc valley, alias Maurienne; Fig. 15F), the pattern suggests that the most intensely
969 overstressed areas of the Western Alps have occurred at sites where highly dynamic, thick, warm-
970 based glaciers above the equilibrium line altitude in E–W transverse valleys, such as the Arc and
971 Isère, either intersected (Maurienne) or followed the strike of (Tarentaise) N–S bands of susceptible
972 lithologies and structures (Figs. 5, 15G). The wide and low-gradient valleys of the Helvetic Domain to
973 the west could accommodate large masses of ice, but these lay for relatively much longer periods
974 below the regional ELA, and west of the susceptible lithologies typical of the Penninic Domain.
975 The remaining six super-hotspots *II* to *VII* can be analysed on a similar basis from an inspection of
976 Table 3. The outstanding features of super-hotspots arising from Table 3 are listed as follows:
977 (i) They all occur in the Penninic Domain or along its tectonic boundary, the PFT, where the crust
978 passed its peak of intense denudation somewhat earlier than the Helvetic Domain (Schildgen et
979 al., 2018), and thus finds itself in a state of relative post-orogenic relaxation dominated by an
980 extensional stress regime (Fig. 10). These regional, long-term state changes qualify here as
981 drivers of RSF promotion.
982 (ii) They mostly occur between the Penninic Frontal Thrust and the Briançonnais Backthrust, i.e.,
983 where the pre-Alpine continental margins were most intensely squeezed by syntectonic

convergence and where the crust is thickest; super-hotspots *V* and *VI*, which lie east of the Briançonnais Backthrust, are relative exceptions.

(iii) Lithology is a constant denominator of RSF susceptibility, from two perspectives: rock type, with flysch and Schistes lustrés as the two main players by areal extent; and fine-scale outcrop heterogeneity, where three-dimensional outcrop geometry and juxtaposition of susceptible lithologies multiply opportunities for bedrock decohesion, slope undercutting, and mass failure (type areas: Beaufortain, parts of the Vanoise, Arves, and Cerces; Fig. 1B for location). The Lower and Middle Penninic zones and Ultra-Dauphinois Zone (Fig. 2) focus these characteristics.

(iv) Recent seismicity plays no palpable part in RSF super-hotspot location. The Parpaillon massif, for example, is situated outside the adjacent Briançonnais seismic arc as well as the Ubaye seismic swarm. Finer analysis of the structural aspects would require different tools and scales.

(v) Massif altitude criteria highlight preferential RSF occurrence at intermediate rather than at higher or lower elevations. This 'goldilocks' feature is perhaps characteristic of the unit rock-mass strength intrinsic to the ductile rocks in which the RSFs are most abundant, widespread, and diverse. This critical attribute is evident, for example, in the Guisane River valley (super-hotspot *V*), where crystalline rocks such as granite are situated outside polygon *V* (i.e., a little further west in the Ecrins Massif) and uphold summits and ridges that are easily 1000 m higher than within polygon *V*.

(vi) Relative relief within the super-hotspot area of interest augments gravitational potential for RSD. It also generates overall longer slopes, thus with greater opportunities for rock failure following other RSF modes. Large magnitudes of relative relief are clearly not a control on RSF, with thus another 'goldilocks' effect in the internal massifs of the Upper Penninic Domain (super-hotspots *IV* to *VII*). RSF, therefore, thrives in areas of intermediate relief. This probably highlights an upper limit to the capacity for relatively uniform masses of ductile rock to sustain deep valleys alongside elevated summits without succumbing to relief reduction by mass wasting—a 'rock-mass-strength buzz-saw' effect acting as a critical limit on relief (where changes in rock uplift rate

are expected to influence erosion rates through adjustments in the frequency and magnitude of slope failure). Areas of maximum local relief in the study area (up to 2500 m in the presence of RSF, see Fig. 5G), attain 3060 m in the crystalline massifs (Mont Blanc, Ecrins, southern Belledonne). These External Crystalline Massifs are areas of RSF scarcity, although rockfall below the detection threshold of this study may be active in such areas. The exceptions in Table 3 are the middle Maurienne ('twin' super-hotspots *II* and *III*) and middle Tarentaise (super-hotspot *I*), where overdeepening of these transverse valleys by stream power and Quaternary glaciers was clearly substantial.

(vii) Causes of slope overstressing appear unsystematic from one area to the next. Paraglacial processes would appear most plausible in the middle Tarentaise (*I*), where ice was thickest; and RSF prevalence has perhaps been exacerbated by more active surface uplift in the Beaufortain and Vanoise massifs (in Figure 11, maximum rates of surface uplift encompass hotspots 1 and 2, and thus also super-hotspots *I* and *II*). This spatial coincidence is notionally consistent with more intense glacial erosion and greater isostatic rebound in these massifs, even though it does not readily explain other hotspots and clusters. Overstressing by thick and dynamic ice in association with high relief sets the middle Tarentaise super-hotspot in a similar league to the upper Rhône (Pedrazzini et al., 2015) and Val d'Aosta (Martinotti et al., 2011), neither fully included in the present study but equally good candidates to super-hotspot status.

Two smaller, secondary super-hotspots, which coincide with the intersection between a hotspot and a second-band cluster, can also be defined: such is the case for 'Hotspot 1' and 'Cluster 17', and 'Hotspot 3' and 'Cluster 19', respectively (Figs. 15F, G). These small areas are not listed in Table 3 but correspond to: a portion of the north Vanoise, and to the boundary between NE Cerces and western Mont Cenis (Plaistocene icefield flowline divide), respectively.

Detailed analysis of second-band clusters (Figs. 15A, F, G) and first-band clusters that do not intersect hotspots (e.g. Cluster 8, and parts of Cluster 10 and Cluster 11) would yield meaningful interpretations only from field studies and inclusion of considerations such as three-dimensional

geology and local structure. Drilling down to such levels of detail is beyond the scope of this macroscopic regional study, but Figure 12A shows that both these areas share the characteristic of having hosted the thickest Late Pleistocene ice. Given also their positions close to the drainage divide and to internal to massifs still hosting glaciers, they resided for long periods above the ELA. Accordingly, further research into the two small super-hotspots situated on the Alpine drainage divide could also provide insights into a possible contribution to overstressing by glacial breaching of the icefield divide, such as reported in the case of the Scottish icesheet by Jarman and Harrison (2019).

5.4 The top 100 largest rockslides and slope deformation areas

The RSF inventory displays a conventional lognormal size distribution (Fig. 5B), with the usual tail-off at threshold sizes for each type. While the RSDs can exceed 40 km^2, they are not exceptionally large by global standards, or even extreme within the Alps. The largest RSD and rockslide units populate the upper whiskers of the box plots in Fig. 5A (by coincidence: n = 100). They are geologically and geographically located in Figures 6 and 15F, respectively. Their outstanding features are as follows:

(i) they are not confined to the Penninic Domain, as about 30% of them occur in the Helvetic Domain;

(ii) they only partly concentrate in hotspots (65% of RSDs occur in hotspots) and, in that context or otherwise, often associate with large glacial troughs formed by transverse valleys (middle Tarentaise, Val d'Aosta, upper Dora Riparia);

(iii) they are otherwise mostly quite scattered and, as such, invite a case by case investigation of three-dimensional geological constraints and structure best appreciated in the field.

(iv) The Helvetic Domain is largely devoid of large RSDs but hosts almost half of the top 100 rockslides. The low RSD numbers are notionally consistent with the fact that the larger valleys of the Helvetic Domain during the Quaternary most often extended below the regional ELA (External Crystalline Massifs excepted), thereby restricting their exposure to

intense glacial erosion. Control factors for the large rockslides are difficult to generalise and would call for case by case investigation of local predisposing and preparatory factors. The much higher annual precipitation in the Helvetic Domain compared to the Penninic Domain (see Suppl. Fig. 1B) could be a contributing cause, but the connection seems tenuous.

(v) out of the 47 largest rockslides, 13 are previously unreported, and only four out of the 53 RSDs are likewise new to this inventory. The 81 remaining biggest sites were thus mostly already known, but chiefly in the sense of having been marked by a generic landslide symbol on geological maps rather than of having been classified, studied, dated, and monitored.

The size threshold adopted here is clearly an arbitrary statistical derivation of Fig. 5A. Séchilienne, for example, lies just below the threshold (although field studies have shown that Séchilienne is actually larger than the conservative figure provided by this study using Google Earth), and is one of the most threatening RSDs of the Western Alps. The inventory results nonetheless show that RSF size and recognised RSF hazard intensity are almost entirely uncorrelated: this is apparent in the fact that none of the 38 dated and/or monitored sites listed in Fig. 1C—apart from Aiguilles de Grives—belong to the top size category defined here. CEREMA, for example, is monitoring smaller hazardous occurrences, some of them (see Section 5.1) not detectable by the remote methods used in this study. Such a result also suggests that a proportion of the hitherto unreported RSFs revealed by this study may be hazardous regardless of their size—a topic requiring to be investigated in finer detail but beyond the scope of this work.

5.5 The Western Alps in global context

The overall spatial incidence of RSF in the study area appears to be considerably greater than in the few other mountain ranges for which densities are available, in all cases derived from systematic RSF mapping, and summarised in Table 4. The already high density of 5.6% obtained for DSGSD alone in the European Alps by Crosta et al. (2013) is now further increased to 6.3% in the Western Alps (Table 1), aided by closer scrutiny with better imagery. These contrasts, however, must be viewed with

caution, since the study methods and criteria vary enormously. Thus the result for RSF in the Southern Alps of New Zealand derives predominantly from traditional field mapping, and almost half the surveyed area is till-covered or alluvial plains. The glaciation–landsliding cycle has nonetheless been well studied in New Zealand, where coseismic landsliding is endemic and large (but shallow) landslides dominate sediment production. The predominant lithologies are susceptible greywackes and schists, and the mountain range is noted for its intense seismic activity and tectonic deformation. The slope evolution cycle characteristic of New Zealand has been summarised by Davies (2017) as follows, and provides a meaningful counterpoint to the features and conditions highlighted in this study:

(i) seismic shaking is amplified on mountain ridges and peaks (Büch et al., 2010), potentially initiating large landslides and implying that ridge elevations might be higher if seismicity were absent. In Europe's Western Alps, such a kind of 'seismic buzz-saw' is inexistent, and limitation to relief appears instead to be set by the widespread occurrence of susceptible ductile bedrock being subjected to extensional stresses, of which RSF (particularly RSD) is a widespread symptom.

(ii) In New Zealand, the generation of deep-seated failure surfaces, probably by resonant response of the upper mountain ridges to the 1–10 Hz frequencies that contain most seismic energy, is believed to result in characteristically more bowl-shaped and deeper landslide source areas than in the case of aseismic landslides. Within the western European Alps, and without detailed field work, this distinction is difficult to appreciate from the remote data acquired for the present study, but could be a topic for further investigation.

(iii) As in any glaciated mountain range, during major glaciations the presence of ice caps and thick valley glaciers will tend to buttress the higher slopes because, at the high strain rates associated with seismic shaking, ice behaves as a strong rigid solid. The net effect is the reduction of coseismic landsliding during glacial periods, which in the New Zealand Alps

allows mean elevations to increase by uplift while valleys are being deepened by glacial erosion, thereby increasing total relief substantially (e.g., the fjords).

(iv) Deglaciation is associated with increased coseismic landsliding, perhaps generating a prevalence of large Holocene landslide 'events', all occurring within a narrow time band in the case of New Zealand. Such a pattern seems less likely in the Western Alps, with evidence of continuous, self-perpetuating displacement on large RSDs such as Séchilienne (Schwartz et al., 2017), and rockfall occurring on Mont Blanc throughout the Holocene to the Present (Gallach, 2019). Thus in spite of the fact that New Zealand's Southern Alps were extensively glaciated during the LGM, limited geomorphological evidence of this remains in the form of characteristic glacial landforms. The reason is that 20,000 years of uplift and landslide-driven denudation since the LGM (average rate of several mm/yr) have eroded at least 100 m of land surface and generated a modern landscape dominated by mass-movement morphologies. The legacy in the Western Alps is clearly more nuanced, hybrid and, as a result, difficult to interpret in categorical ways.

Until comparable data become available for more ranges spanning orogenic ages and uplift rates, it will remain difficult to advocate more clear-cut or systematic reasons for the prevalence of RSF in the Western Alps. Existing candidates for comparison would include the Carpathians, which are comparably 'alpine' in origin and possess extensive susceptible lithologies. They are only half the height of the Alps, and often display cirque rather than full-scale valley glaciation. The eastern Pyrenees also have less relief and glacial imprint (dry, sunny climate), and additionally rather lack conducive lithologies (Jarman et al., 2014). The Scottish Highlands are an ancient orogen reduced to moderate relief, yet with significant glaciation and abundant susceptible geology can attain high local densities of RSF (Jarman and Harrison, 2019).

In summary, RSD and RS appear to be more widespread in portions of mountain belts (i) that have attained a post-orogenic stage in which crustal extension has taken over as the dominant regime; (ii) where seismicity is limited; (iii) where intensities of crustal denudation slackened sooner (Penninic

1139 Domain) rather than later (Helvetic Domain) during the Neogene and Quaternary (Schildgen et al.,
1140 2018); and (iv) where current surface uplift magnitudes are low to moderate (Fig. 11). This profile fits
1141 the extensive Penninic Domain of the Western Alps, which hosts a small proportion (<7.5% of the
1142 total study area) of exceptionally overstressed areas controlled by factors summarised in Table 3. In
1143 mountain ranges that are still undergoing high-frequency and high-magnitude seismicity with rapid
1144 increases in relative relief, such as the Fiordland of New Zealand (Schildgen et al., 2018), valley-
1145 shaping processes are granted insufficient time to widen out (fluvially and glacially) and thus to
1146 generate slope stresses capable of provoking, for example, RSD. Catastrophic rock avalanches, which
1147 are rare in the Western Alps (n = 15, perhaps slightly more: see Section 5.1), would thus be
1148 signatures of tectonically more active glaciated orogens such as the Himalaya (Hewitt et al., 2008)
1149 and New Zealand's Southern Alps (Allen et al., 2011; Davies, 2017)—where coseismic rockfalls and
1150 shallow landsliding are likewise intense.
1151 In the more outstanding cases of hotspots 1, 2, and 3 (Figs. 15F, G), there may be scope for testing
1152 the hypothesis associating slope failure in these intensely overstressed areas with concentrated
1153 erosion of bedrock (CEB) as propounded by Jarman and Harrison (2019) in the Scottish context. The
1154 concept is based on antecedents addressed from the perspective of rock mechanics (Matheson and
1155 Thomson, 1973) and goes beyond glacio-isostatic recovery (which, in any case, in the Western Alps is
1156 pervasive and endemic: Sternai et al., 2019) to geographically-focused bedrock rebound of valley
1157 floors, which can be locally intense and has repercussions on the mechanical response of valley
1158 slopes and rims (Matheson and Thomson, 1973). To achieve differential rebound stresses large
1159 enough to provoke and perpetuate RSF super-hotspots, CEB would have to be intense in both space
1160 and time, and preferably within the last glacial cycle(s). This would require fast rates of Quaternary
1161 valley incision, such as appears to have been the case, for example, in the upper Rhône valley (Valla
1162 et al., 2012). If so, this implies that glacial incision can occasionally or locally operate at a
1163 'catastrophic' rate, with the most conspicuous concentrated erosion of bedrock of the study area
1164 occurring along the transverse Alpine valleys of the middle Maurienne and middle Tarentaise, i.e., at

the intersection between areas of peak E–W glacial erosion and N–S bands of the weakest rocks of the Alpine fabric: typically the 'Zone Houillère' and the tight succession of Middle and Lower Penninic thrust units.

6 Conclusions

(i) Almost 1450 RSFs were inventoried in the Western Alps study area, impacting about 9% of the region's land surface. This ratio is substantially higher than in the few previous comparable range-wide studies, and not easy to explain beyond the classic predisposing influence of rock susceptibility.

(ii) The remote identification appears comprehensive but would be enlargeable with field mapping, which would ideally utilise LiDAR imagery in forest areas. The 22 'less probable' RSFs of the inventory would require ground control, but it can be anticipated that, with improved detection possibilities in the future, the inventory on average will grow rather than shrink. Overall, the panoptic approach provided here, i.e., addressing RF, RA, RS and RSD together rather than separately, forms a comprehensive basis for future local monographs and for undertaking instrumental monitoring (Blondeau et al., 2019).

(iii) In roughly 40% / 40% / 20% proportions, the RSF population comprises rock slope deformations (RSD); coherent, shorter-travel rockslides (RS); and disintegrated longer-travel rockfalls (RF, RA). The surprisingly tiny subset of rock avalanches would suggest a lack of system energy compared with more active ranges where coseismic landslides are endemic.

(iv) The inventory displays the usual broad association between RSF and the more vulnerable lithologies, which are chiefly metasedimentary phyllites but here equally include all clastic sediments—weakly and un-metamorphosed when present. However, geology really only predisposes and does not account for large spatial variations in overstressing within these rock types. There are significant RSF occurrences on most other lithologies, some of them large, and future studies could focus on conducting field-based analyses within each major lithology.

(v) Three-dimensional geology is influential but hard to assign from two-dimensional geological maps. As a result, either the effective underlying strata go unmapped; or intra-rockmass lithological and fabric variations driving local RSF incidence occur at scales too small to map other than in field reports. Likewise, Quaternary deposits (e.g. talus, moraine) may mask the RSF-generating bedrock of interest. Focused field investigations, beyond the scope of this reconnaissance study, are required.

(vi) Standard factors including topography, fault and fracture alignments, seismicity, glaciation extent, and periglaciation have variable influence on RSF spatial distribution, best investigated at local scale and from the field. Slope aspect has an effect, but also at local, not massif scale.

(vii) Although the RSF population is primarily paraglacial in context, a small minority (n = 51, i.e. ~3.6%) occurs beyond the Late Pleistocene maximum ice limits. These occurrences thus belong to a fluvial or parafluvial context and, as such, requires further investigation.

(viii) Analysing RSF distribution by density of occurrence yielded twenty-two point-density clusters containing 0.1 to 0.22 RSF/km^2 in any of the four RSF modes. These clusters are thus areas of high landslide geodiversity, of some interest to hazard investigation as well as to geoheritage concerns (educational value for geotourism when a diversity of landslide types co-occur in a small area). They are distributed across the Penninic Domain in the east as well as the Helvetic Domain in the west. Mapping and monitoring each of these in finer detail is work for future local monographs.

(ix) Analysing RSF distribution by area impacted sharpens RSF clustering into six 'hotspots' (7.5% of the study area), all located in the overthrust Penninic Domain and covering 41% by area of the total RSF inventory.

(x) The intersection between clusters and hotspots, which overlap in some key areas, defines nine RSF super-hotspots (seven major and two subsidiary). Super-hotspots are areas where contribution of failed bedrock material to the sediment cascade and to local rivers is potentially very high, and where displaced (but temporarily arrested) masses of rock, predominantly in the

1217 form of RSDs, are the most extensive. At the scale of the Western Alps, these overstressed areas
1218 are where landscape-scale erosion rates most intensely refresh the gradient of the landslide-
1219 dominated slopes and release larger-than-average volumes of gravitationally-released debris into
1220 the sediment cascade.

1221 (xi) Super-hotspots occur among uniform or highly heterogeneous outcrops of susceptible ductile
1222 lithologies, and exclusively in areas of the Penninic Domain—independently documented as
1223 being in a state of post-orogenic crustal extension. Overstressing by the thickest warm-based
1224 iceways of the region during the LGM (and presumably earlier) is verified for the steeper portions
1225 of the strike-transverse Isère and Arc valleys, which remained longest above the regional
1226 equilibrium line altitude (ELA); but less conspicuously elsewhere, and even less so in the Helvetic
1227 Domain where large valley glaciers during the Quaternary were most often in a state of
1228 accumulation below the ELA despite being wide and extensive. A finer analysis of these patterns
1229 would gain from being articulated with detailed knowledge about the chronology and spatial
1230 fluctuations of local ELAs on a massif-by-massif basis, thus contributing to test with greater
1231 precision than outlined here the strength of association between ELA position and RSF incidence.

1232 (xii) A 'goldilocks' effect applies to super-hotspot areas, whereby the highest area densities of RSF
1233 occur in massifs where elevation and relative relief are intermediate rather than large or small.

1234 (xiii) The contribution from modern seismicity is negligible; but a strong spatial association
1235 between hotspots and the Penninic Frontal Thrust, Briançonnais Backthrust and other subsidiary
1236 Alpine thrust fronts, especially in the case of RSD, is remarkable (~36% of RSF by area intersects a
1237 mapped thrust front), confirming the long-lasting state of stress at these tectonic boundaries also
1238 reported more widely in the rest of the Alps by Crosta et al. (2013).

1239 (xiv) The largest 100 RSFs are scattered across the region according to criteria that only partly
1240 meet those tentatively relevant to the hotspot approach. Their analysis would require a
1241 monographic, field-based approach beyond the scope of this study. In terms of natural hazards,
1242 the link between RSF size and threat intensity is very weak (Fig. 1C): whereas none of the 14

historically catastrophic RSFs inventoried by Eisbacher and Clague (1984) were particularly large, and while CEREMA currently monitors RSFs of a size falling within the interquartile range of the inventory, many large RSDs could remain metastable for the next several thousand years.

(xv) Drilling down to massif- or valley-scale monographs on the basis of the broad inventory presented in this study, it would be fruitful to further evaluate its findings by (1) investigating tectonic signals and rock mass behaviours within and between all clusters and hotspots; (2) performing hypsometric and finer-scale morphometric analysis to detect conducive topographies; and (3) identifying in finer local detail processes and contexts that generate concentrated erosion of bedrock (CEB), such as: in locally overdeepened troughs; or on the Alpine drainage divide where glacial breaches at two subsidiary super-hotspots may have occurred, possibly amplifying rebound stresses sufficiently to promote unusually intense RSF.

(xvi) A comparison between the Western Alps, where rockslides and slope deformation areas are abundant, and New Zealand's Southern Alps, where instead coseismic rockfalls and rock avalanches are widespread, highlights the importance of regional tectonic regime in controlling landscape evolution style and character. It hypothetically suggests two contrasting evolutionary models of mountain relief under a 'buzz-saw effect' whereby changes in rock uplift rate influence erosion rates through adjustments in the frequency and magnitude of slope failure: one buzz-saw effect is primarily controlled by limits in rock mass strength, attenuating or cancelling glacio-isostatic or other potential drivers of ongoing uplift (Alps); the other is controlled by active tectonics and seismicity (Fiordland).

Acknowledgements. We thank Hélène Tissoux at the Bureau des Recherches Géologiques et Minières for providing a set of vector 1:50,000 scale geological maps of most of the study area, and François Thouvenot for providing access to the SISMALP earthquake database. Two anonymous reviewers provided thoughtful comments for which we are very grateful.

References

Agliardi, F., Crosta, G.B., Frattini, P., 2012. Slow rock-slope deformation. In: Clague, J.J., Stead, D. (eds), Landslides: types, mechanisms and modeling. Cambridge University Press, pp. 207–221.

Agliardi, F., Crosta, G.B., Frattini, P., Malusà, M.G., 2013. Giant non-catastrophic landslides and the long–term exhumation of the European Alps. Earth Planet. Sci. Lett. 365, 263–274.

Allen, S.K., Cox, S.C., Owens, I.F., 2011. Rock avalanches and other landslides in the central Southern Alps of New Zealand: a regional study considering possible climate change impacts. Landslides 8, 33–48.

Antinao, J.L., Gosse, J., 2009. Large rockslides in the Southern Central Andes of Chile (32–34.5°S): tectonic control and significance for Quaternary landscape evolution. Geomorphology 104, 117–133.

Augustinus, P., 1995. Rock mass strength and the stability of some glacial slopes. Z. Geomorph. 39, 55–68.

Bailly–Maître, M.C., Montjuvent, G., Mathoulin, V., 1997. Les quatre anciens lacs de l'Oisans (Alpes françaises du Nord). Rev. Géogr. Alp. 85, 33–52.

Ballantyne, C.K., 2002. Paraglacial geomorphology. Quat. Sci. Rev. 21, 1935–2017.

Ballantyne, C.K., 2013. Lateglacial rock–slope failures in the Scottish Highlands. Scot. Geogr. J. 129, 67–84.

Bălteanu, D., Chendeş, V., Sima, M., Enciu, P., 2010. A country–wide spatial assessment of landslide susceptibility in Romania. Geomorphology 124, 102–112.

Beck, A.C., 1968. Gravity faulting as a mechanism of topographic adjustment; N. Z. J. Geol. Geophys. 11, 191–199.

Bergemann, C.A., Gnos, E., Whitehouse, M.J., 2019. Insights into the tectonic history of the Western Alps through dating of fissure monazite in the Mont Blanc and Aiguilles Rouges Massifs. Tectonophysics 750, 203–212.

1294 Blondeau, S., Thiery, Y., Gunnell, Y., Jarman, D., 2019. Les ruptures de versant rocheux : de
1295 l'observation à l'évaluation du risque, Géosciences 23, 14–29.
1296 Blikra, L.H., Longva, O., Braathen, A., A.da, E., Dehls, J.F., Stalsberg, K., 2006. Rock slope failures in
1297 Norwegian fjord: examples, spatial distribution and temporal pattern. In: Evans, S.G., Scarascia,
1298 Mugnozza, G., Strom, A., Hermanns, R.L. (eds): Landslides from massive rock slope failure.
1299 NATO Science Series IV, Earth and Environmental Sciences 49, Springer, pp. 475–496.
1300 Bodin, X., Schoeneich, P., Deline, P., Ravanel, L., Magnin, F., Krysiecki, J.M., Echelard, T., 2015. Le
1301 permafrost de montagne et les processus géomorphologiques associés : évolutions récentes dans
1302 les Alpes françaises. Rev. Géogr. Alp. 103, http://journals.openedition.org/rga/2806.
1303 Boeckli, L., Brenning, A., Gruber, S., Noetzli, J., 2012. Permafrost distribution in the European Alps:
1304 calculation and evaluation of an index map and summary statistics. Cryosphere 6, 807–820.
1305 Böhme, M., Saintot, A., Henderson, I.H.C., Henriksen, H., Hermanns, R.L., 2011. Rock slope
1306 instabilities in Sogn and Fjordane County, Norway: a detailed structural and geomorphological
1307 analysis. In: Jaboyedoff, M. (Ed.), Slope tectonics. Geol. Soc. Lond., Spec. Publ. 351, 97–111.
1308 Boutoux, A., Bellahsen, N., Nanni, U., Pik, R., Verlaguet, A., Rolland, Y., Lacombe, O., 2016. Thermal
1309 and structural evolution of the external Western Alps: insights from (U–Th–Sm)/He
1310 thermochronology and RSCM thermometry in the Aiguilles Rouges/Mont Blanc Massifs.
1311 Tectonophysics 683, 109–123.
1312 Braathen, A., Blikra, L.H., Berg, S.S., Karlsen, F., 2004. Rock-slope failures in Norway; type, geometry,
1313 deformation mechanisms and stability. Nor. J. Geol. 84, 67–88.
1314 Brideau, M.A., Roberts, N.J., 2015. Mass movement in bedrock. In: Davies, T. (Ed.), Landslide hazards,
1315 risks, and disasters. Elsevier, Amsterdam, pp. 43–90.
1316 Büch, F., Davies, T.R.H., Pettinga, J.R., 2010. The Little Red Hill seismic experimental study:
1317 Topographic effects on ground motion at a bedrock-dominated mountain edifice. Bull. Seismol.
1318 Soc. Am. 100, 2219–2229.

1319 Calais, E., Bayer, R., Chéry, J., Cotton, F., Flouzat, M., Jouanne, F., Martinod, J., Mathieu, F., Scotti, O.,
1320 Tardy, M., Vigny, C., 2000. REGAL: a permanent GPS network in the French Western Alps —
1321 Configuration and first results. C. R. Acad. Sci. Paris 331, 435–442.
1322 Coutterand, S., 2010. Etude géomorphologique des flux glaciaires dans les Alpes nord–occidentales
1323 au Pléistocène récent. Du maximum de la dernière glaciation aux premières étapes de la
1324 déglaciation. Unpubl. PhD thesis, Université de Savoie, 468 p.
1325 Coutterand, S., 2017. Les glaciers des Alpes. Vandelle, 176 p.
1326 Crosta, G., Zanchi, A., 2000. Deep seated slope deformations: huge, extraordinary, enigmatic
1327 phenomena. In: Bromhead, E., Dixon, N. (Eds.), Landslides in research, theory and practice, Proc.
1328 8th Int. Symp. on Landslides, Cardiff. Thomas Telford, London, pp. 351–358.
1329 Crosta, G.B., Chen, H., Lee, C.F., 2004. Replay of the 1987 Val Pola Landslide, Italian Alps.
1330 Geomorphology 60, 127–146.
1331 Crosta, G.B., Frattini, P., Agliardi, F., 2013. Deep seated gravitational slope deformations in the
1332 European Alps. Tectonophysics 605, 13–33.
1333 Davies, T.R.H., 2017. Mountain process geomorphology: conceptual progress in the Southern Alps.
1334 In: Shulmeister, J. (Ed.), Landscape and Quaternary environmental change in New Zealand. Atlantis
1335 Advances in Quaternary Science 3, Atlantis Press, pp. 205–233.
1336 Debelmas, J., 1979. Découverte géologique des Alpes du Nord. BRGM Editions, Orléans, 84 p.
1337 Delacou, B., Sue, C., Champagnac, J.D., Burkhard, M., 2004. Present-day geodynamics in the bend of
1338 the western and central Alps as constrained by earthquake analysis. Geophys. J. Int. 158, 753–
1339 774.
1340 Deline, P., Alberto, W., Broccolato, M., Hungr, O., Noetzli, J., Ravanel, L., Tamburini, A., 2011. The
1341 December 2008 Crammont rock avalanche, Mont Blanc massif area, Italy. Nat. Haz. Earth Syst.
1342 Sci., 11, 3307–3318.

1343 Delunel, R., Hantz, D., Braucher, R., Bourlès, D., Schoeneich, P., Deparis, J., 2010. Surface exposure
1344 dating and geophysical prospecting of the Holocene Lauvitel rock slide (French Alps). Landslides 7,
1345 393–400.
1346 Dramis, F., Sorriso-Valvo, M., 1994. Deep–seated gravitational slope deformations related landslides
1347 and tectonics. Eng. Geol. 38, 231–243.
1348 Eeckhaut van den, M., Hervás, J., 2012. State of the art of national landslide databases in Europe and
1349 their potential for assessing landslide susceptibility, hazard and risk. Geomorphology 139–140,
1350 545–548.
1351 Eisbacher, G.H., Clague, J.J., 1984. Destructive mass movements in high mountains: hazard and
1352 management. Geol. Surv. Canada Paper 84–16, 229 p.
1353 El Bedoui, S., Bois, T., Jomard, H., Sanchez, G., Lebourg, T., Trics, E., Guglielmi, Y., Bouissou, S.,
1354 Chemenda, A., Rolland, Y., Corsini, M., Pérez, J.L., 2011. Paraglacial gravitational deformations in
1355 the SW Alps: a review of fields investigations, ^{10}Be cosmogenic dating and physical modelling. In
1356 Jaboyedoff, M. (Ed.), Slope Tectonics, Geol. Soc. Lond., Spec. Publ. 351, pp. 11–25.
1357 Evans, S.G., Scarascia–Mugnozza, G., Strom, A.L., Hermanns, R.L., Ischuk, A., Vinnichenko, S., 2006.
1358 Landslides from massive rock slope failure and associated phenomena. In: Evans, S.G., Scarascia,
1359 Mugnozza, G., Strom, A., Hermanns, R.L. (eds), Landslides from massive rock slope failure,
1360 NATO Science Series IV, Earth and Environmental Sciences 49, Springer, pp. 3–52.
1361 Fioraso, G., 2017. Impact of massive deep-seated rock slope failures on mountain valley morphology
1362 in the northern Cottian Alps (NW Italy). J. Maps 13, 575–587.
1363 Fioraso, G., Baggio, P., 2013. Geological map of the Mount Ciantiplagna rock avalanche (Chisone
1364 valley, Italian Western Alps). J. Maps 9, 336–342.
1365 Forcella, F., 1984. The sackung between Mount Padrio and Mount Varadega, Central Alps, Italy: a
1366 remarkable example of slope gravitational tectonics. Méditerranée 51, 81–92.
1367 Frayssines, M., Hantz, D., 2006. Failure mechanisms and triggering factors in calcareous cliffs of the
1368 Subalpine ranges (French Alps). Eng. Geol. 86, 256–270.

1369 Fréchet, J., Thouvenot, F., Frogneux, M., Deichmann, N., Cara, M., 2010. The M_W 4.5 Vallorcine
1370 (French Alps) earthquake of 8 september 2005 and its complex aftershock sequence. J. Seismol.
1371 15, 43–58.
1372 Gallach, X., 2019. Reconstitution de la fréquence des écroulements rocheux post–LGM dans le massif
1373 du Mont Blanc. Unpubl. PhD thesis, Communauté universitaire Grenoble–Alpes, 250 p.
1374 Gardent, M., Rabatel, A., Dedieu, J.P., Deline, P., 2014. Multitemporal glacier inventory of the French
1375 Alps from the late 1960s to the late 2000s. Glob. Planet. Change 120, 24–37.
1376 Gidon, M. 1977. Carte géologique simplifiée des Alpes occidentales (scale: 1:250,000). BRGM and
1377 Editions Didier Richard.
1378 Godano, M., Larroque, C., Bertrand, E., Courboulex, F., Deschamps, A., Salichon, J., Blaud-Guerry, C.,
1379 Fourteau, L., Charléty, J., Deshayes, P., 2013. The October–November 2010 earthquake swarm
1380 near Sampeyre (Piedmont region, Italy): A complex multicluster sequence. Tectonophysics 608,
1381 97–111.
1382 Goguel, B., 1989. Le glissement du Friolin, en Savoie : un mouvement majeur révélé par les
1383 photographies. Rev. Fr. Géotech. 48, 55–64.
1384 Goguel, J., Pachoud, A., 1981. Les mouvements de terrain du versant sud du massif de Platé, Haute–
1385 Savoie, France. Bulletin de Liaison du Laboratoire des Ponts et Chaussées, XXVIe Congrès
1386 géologiques international, pp. 15–25.
1387 Gosar, A., 2017. Earthquake–induced rockfalls caused by 1998 M_w5.6 earthquake in Krn Mountains
1388 (NW Slovenia) and ESI 2007 intensity scale. In: Mikos, M., Tiwari, B., Yin, Y., Sassa, K. (eds),
1389 Advancing culture of living with landslides, vol. 4. Springer, pp. 131–139.
1390 Gottardi, F., 2009. Estimation statistique et réanalyse des précipitations en montagne. Utilisation
1391 d'ébauches par types de temps et assimilation de données d'enneigement. Application aux grands
1392 massifs montagneux français. PhD thesis, Institut National Polytechnique, Grenoble, 144 p.
1393 Graciansky, P.C. de, Roberts, D.G., Tricart, P., 2011. The Western Alps, from rift, to passive margin
1394 to orogenic belt: an integrated geoscience overview. Elsevier, 398 p.

1395 Grämiger, L.M., Moore, J.R., Gischig, V.S., Ivy-Ochs, S., Loew, S., 2017. Beyond debuttressing:
1396 mechanics of paraglacial rock slope damage during repeat glacial cycles. J. Geophys. Res., Earth
1397 Surf. 122,1004–1036.
1398 Guyoton, F., Fréchet, J., Thouvenot, F., 1990. La crise sismique de janvier 1989 en Haute-Ubaye
1399 (Alpes-de-Haute-Provence, France) : étude fine de la sismicité par le nouveau réseau SISMALP.
1400 Compte Rendu de l'Académie des Sciences, Paris, 311, 985–991.
1401 Guzzetti, F., Ardizzone, F., Cardinali, M., Galli, M., Reichenbach, P., Rossi, M., 2008. Distribution of
1402 landslides in the Upper Tiber River basin, central Italy. Geomorphology 96, 105–122.
1403 Harris, C., Arenson, L.U., Christiansen, H.H., Etzelmüller, B., Frauenfelder, R., Gruber, S., Haeberli, W.,
1404 Hauck, C., Hölzle, M., Humlum, O., Isaken, K., Kääb, A., Kern-Lütschg, M.A., Lehning, M.,
1405 Matsuoka, N., Murton, J.B., Nötzli, J., Phillips, M., Ross, N., Seppälä, M., Springman, S.M., Vonder
1406 Mühll D., 2009. Permafrost and climate in Europe: monitoring and modelling thermal,
1407 geomorphological and geotechnical responses. Earth-Sci. Rev. 92, 117–171.
1408 Heim, A., 1932. Der Bergsturz und Menschenleben. Fretz und Wasmuth, Zürich, 218 p.
1409 Hewitt, K., 2009. Catastrophic rock slope failures and late Quaternary developments in the Nanga
1410 Parbat–Haramosh massif, upper Indus basin, northern Pakistan. Quat. Sci. Rev. 28, 1055–1069.
1411 Hewitt, K., Clague, J.J., Orwin, J.F., 2008. Legacies of catastrophic rock slope failures in mountain
1412 landscapes. Earth-Sci. Rev. 87, 1–38.
1413 Hibert, C., Grandjean, G., Bitri, A., Travelletti, J., Malet, J.P., 2012. Characterizing landslides through
1414 geophysical data fusion: Example of the La Valette landslide (France). Eng. Geol. 128, 23–29.
1415 Hippolyte, J.C., Brocard, G., Tardy, M., Nicoud, G., Bourlès, D., Braucher, R., Ménard, G., Souffaché,
1416 B., 2006. The recent fault scarps of the Western Alps (France): Tectonic surface ruptures or
1417 gravitational sackung scarps? A combined mapping, geomorphic, levelling, and ^{10}Be dating
1418 approach. Tectonophysics 418, 255–276.

1419 Hippolyte, J.C., Bourlès, D., Braucher, R., Carcaillet, J., Léanni, L., Arnold, M., Aumaître, G., 2009.
1420 Cosmogenic ^{10}Be dating of a sackung and its faulted rock glaciers, in the Alps of Savoy (France).
1421 Geomorphology 108, 312–320.
1422 Hippolyte, J.C., Bourlès, D., Léanni, L., Braucher, R., Chauvet, F., Lebatard, A.E., 2012. ^{10}Be ages reveal
1423 >12 ka of gravitational movement in a major sackung of the Western Alps (France).
1424 Geomorphology 171–172, 139–153.
1425 Holm, K., Bovis, M., Jakob, M., 2004. The landslide response of alpine basins to post–Little Ice Age
1426 glacial thinning and retreat in southwestern British Columbia. Geomorphology 57, 201–216.
1427 Hungr, O., Leroueil, S., Picarelli, L., 2014. The Varnes classification of landslide types, an update.
1428 Landslides 11, 167–194.
1429 Jarman, D., Ballantyne, C.K., 2002. Beinn Fhada, Kintail: a classic example of paraglacial rock slope
1430 deformation. Scot. Geogr. J. 118, 59–68.
1431 Jarman D., 2006. Large rock slope failures in the Highlands of Scotland: characterisation, causes and
1432 spatial distribution. Eng. Geol. 83, 161–182.
1433 Jarman D, Wilson P, Harrison, S., 2013. Are there any relict rock glaciers in Britain? J. Quat. Sci. 28,
1434 131–143.
1435 Jarman, D., Calvet, M., Corominas, J., Delmas, M., Gunnell, Y., 2014. Large–scale rock slope failure in
1436 the eastern Pyrenees: identifying a sparse but significant population in paraglacial and parafluvial
1437 contexts. Geogr. Ann., Ser. A: Phys. Geogr. 96, 357–391.
1438 Jarman, D., Harrison, S., 2019. Rock slope failure in the British Mountains. Geomorphology 340, 202–
1439 233.
1440 Jenatton, L., Guiguet, R., Thouvenot, T., Daix, N., 2007. The 16,000-event 2003–2004 earthquake
1441 swarm in Ubaye (French Alps). J. Geophys. Res. 112, DOI: 10.1029/2006JB004878.
1442 Jibson, R.W., 2009. Using landslides for paleoseismic analysis. In: McCalpin, J.P. (Ed.),
1443 Paleoseismology. Academic Press, New York, pp. 565–601.

1444 Jibson, R.W., 2013. Mass-movement causes: earthquakes. In: Shroder, J. (Editor in Chief), Marston,
1445 R.A., Stoffel, M. (eds), Treatise on geomorphology. Academic Press, San Diego, vol. 7, Mountain
1446 and Hillslope Geomorphology, pp. 223–229.
1447 Kästle, E.D., Rosenberg, C., Boschi, L., Bellahsen, N., Meier, T., El-Sharkawy, A., 2019. Slab break-offs
1448 in the Alpine Subduction Zone. Solid Earth Disc., 16 p., https://doi.org/10.5194/se-2019-17.
1449 Korup, O., 2005. Distribution of landslides in southwest New Zealand. Landslides 2, 43–51.
1450 Korup, O., 2006. Effects of large deep–seated landslides on hillslope morphology, western Southern
1451 Alps, New Zealand. J. Geophys. Res. F01018, doi:10.1029/2004JF000242.
1452 Kremer, K., Simpson, G., Girardclos, S., 2012. Giant Lake Geneva tsunami in AD 563. Nature Geosci.,
1453 5, 756–757.
1454 Kremer, K., Marillier, F., Hilbe, M., Simpson, G., Dupuy, D., Yrro, B.J.F., Rachoud–Schneider, A.M.,
1455 Corboud, P., Bellwald, B., Wildi, W., Girardclos, S., 2014. Lake dwellers occupation gap in Lake
1456 Geneva (France–Switzerland) possibly explained by an earthquake–mass movement–tsunami
1457 event during Early Bronze Age. Earth Planet. Sci. Lett. 385, 28–39.
1458 Malatrait, A., 1975. Analyse et classement des mouvements gravitaires – Feuille St Jean de
1459 Maurienne au 1/50 000e. Unpubl. PhD thesis, Université de Grenoble, 219 p.
1460 Malatrait, A., Sabatier, F., 1996. Le glissement de la Montagne des Piniès à l'origine des coulées de
1461 Boulc-en-Diois (Drôme) : évolution et mécanismes. Rev. Fr. Géotech. 75, 45–53.
1462 Marcer, M. Bodin, X., Brenning, A., Schoeneich, P., Charvet, R., Gottardi, F., 2017. Permafrost
1463 favorability index: spatial modeling in the French Alps using a rock glacier inventory. Front. Earth
1464 Sci., DOI: 10.3389/feart.2017.00105.
1465 Martinotti, G., Giordan, D., Giardino, M., Ratto, S., 2011. Controlling factors for deep–seated
1466 gravitational slope deformation (DSGSD) in the Aosta Valley (NW Alps, Italy). In: Jaboyedoff, M.
1467 (Ed.), Slope tectonics. Geol. Soc. Lond., Spec. Publ. 351, pp. 113–131.
1468 Matheson, D.S., Thomson, S., 1973. Geological implications of valley rebound. Can. J. Earth Sci. 10,
1469 961–978.

1470 Matthews, J.A., Winkler, S., Wilson, P., Tomkins, M.D., Dortch, J.M., Mourne, R.W., Hill, J.L., Owen,
1471 G., Vater, A.E., 2018. Small rock-slope failures conditioned by Holocene permafrost degradation: a
1472 new approach and conceptual model based on Schmidt-hammer exposure-age dating,
1473 Jotunheimen, southern Norway. Boreas 47, 1144–1169.
1474 McColl, S.T., 2012. Paraglacial rock-slope stability. Geomorphology 153–154, 1–16.
1475 McColl, S.T., 2015. Landslide causes and triggers. In: Davies, T. (Ed.), Landslide hazards, risks, and
1476 disasters. Elsevier, Amsterdam, pp. 17–42.
1477 Mortara, G., Sorzana, P.F., 1987. Fenomeni di deformazione gravitativa profonda nell'Arco Alpino
1478 Occidentale Italiano. Considerazioni lito-strutturali e morfologiche. Boll. Soc. Geol. Ital. 106, 303–
1479 314.
1480 Němčok, A., 1972. Gravitational slope deformation in high mountains. Proceedings of the 24th
1481 International Geological Congress, Montreal, 13, pp. 132–141.
1482 Nocquet, J.M., Sue, C., Walpersdorf, A., Tran, T., Lenôtre, N., Vernant, P., Cushing, M., Jouanne, F.,
1483 Masson, F., Baize, S., Chéry, J., van der Beek, P.A., 2016. Present–day uplift of the western Alps.
1484 Sci. Rep. 6. DOI: 10.1038/srep28404.
1485 Oppikofer, T., Jaboyedoff, M., Keusen, H.R., 2008. Collapse at the eastern Eiger flank in the Swiss
1486 Alps. Nature Geosci. 1, 531–535.
1487 Oppikofer, T., Saintot, A., Hermanns, R.L., Böhme, M., Scheiber, T., Gosse, J., Dreias, G.M., 2017.
1488 From incipient slope instability through slope deformation to catastrophic failure—Different
1489 stages of failure development on the Ivasnasen and Vollan rock slopes (western Norway).
1490 Geomorphology 289, 96–116.
1491 Ortuño, M., Guinau, M., Calvet, J., Furdada, G., Bordonau, J., Ruiz, A., Camafort, M., 2017. Potential
1492 of airborne LiDAR data analysis to detect subtle landforms of slope failure: Portainé, Central
1493 Pyrenees. Geomorphology 295, 364–382.
1494 Pachoud, A., 1991. Une catastrophe naturelle majeure : l'écroulement du Mont Granier dans le
1495 massif de la Chartreuse au XIIIe siècle. La Houille Blanche 5, 327–332.

1496 Palis, E., Lebourg, T., Tric, E., Malet, J.P., Vidal, M., 2017. Long–term monitoring of a large deep–
1497 seated landslide (La Clapière, south–east French Alps): initial study. Landslides 14, 155–170.
1498 Pánek, T., Mentlík, P., Ditchburn, B., Zondervan, A., Norton, K., Hradecký, J., 2015. Are sackungen
1499 diagnostic features of (de)glaciated mountains? Geomorphology 248, 396–410.
1500 Pánek, T., Klimeš, J., 2016. Temporal behavior of deep-seated gravitational slope deformations: a
1501 review. Earth-Sci. Rev. 156, 14–38.
1502 Pánek, T., Korup, O., Lenart, J.,Hradecký, J., Březný, M., 2018. Giant landslides in the foreland of the
1503 Patagonian Ice Sheet. Quat. Sci. Rev. 194, 39–54.
1504 Pedrazzini, A., Humair, F., Jaboyedoff, M., Tonini, M., 2015. Characterization and spatial distribution of
1505 gravitational slope deformations in the upper Rhone catchment (Western Swiss Alps). Landslides
1506 13, 1–19.
1507 Peras, A., Decaulne, A., Cossart, E., Coquin, J., Mercier, D., 2016. Distribution and spatial analysis of
1508 rockslides failures in the Icelandic Westfjords: first results. Géomorph. Rel. Proc. Env. 22, 25–35.
1509 Perrone, G., Eva, E., Solarino, S., Cadoppi, P., Balestro, G., Fioraso, G., 2010. Seismotectonic
1510 investigations in the inner Cottian Alps (Italian Western Alps): an integrated approach.
1511 Tectonophysics 496, 1–16.
1512 Persaud, M., Pfiffner, O.A., 2004. Active deformation in the eastern Swiss Alps: Post-glacial faults,
1513 seismicity and surface uplift. Tectonophysics 385, 59–84
1514 Pfiffner, A.O., 2014. Geology of the Alps. Wiley, 376 p.
1515 Piana, F., Fioraso, G., Irace, A., Mosca, P., d'Atri, A., Barale, L., Falletti, P., Monegato, G., Morelli, M.,
1516 Tallone, S., Vigna, G.B., 2017. Geology of Piemonte region (NW Italy, Alps-Apennines interference
1517 zone). J. Maps 13, 395–405.
1518 Plancherel R., Broquet P., 1998. Geological map of Samoëns–Pas de Morgins (1:50,000 scale),
1519 Explanatory handbook. BRGM editions, Orléans, 112 p.
1520 Pollet, N., 2004. Significance of source areas and deposits in the analysis of highspeed rock
1521 movements: Alpine examples. Bull. Eng. Geol. Env. 63, 353–365.

1522 Poschinger von, A., 2002. Large rockslides in the Alps: a commentary on the contributions of G. Abele
1523 (1937–1994) and a review of some recent developments. Rev. Eng. Geol. 15, 237–255.
1524 Pothérat, P., Effendiantz, L., 2009. Néotectonique et grands mouvements de versant. Le cas de
1525 Séchilienne (Isère, France). Bull. Eng. Geol. Env. 68, 567–577.
1526 Ravanel, L., Deline, P., 2011. Climate influence on rockfalls in high–Alpine steep rockwalls: the north
1527 side of the Aiguilles de Chamonix (Mont Blanc massif) since the end of the 'Little Ice Age'. The
1528 Holocene 21, 357–365.
1529 Ravanel, L., Magnin, F., Deline, P., 2017. Impacts of the 2003 and 2015 summer heatwaves on
1530 permafrost–affected rock–walls in the Mont Blanc massif. Sci. Total Env. 609, 132–143.
1531 Roback, K., Clark, M.C., West, J., Zekkos, D., Gen, L., Gallen, S.F., Chamlagain, D., Godt, J., 2018. The
1532 size, distribution, and mobility of landslides caused by the 2015 M_w7.8 Gorkha earthquake, Nepal.
1533 Geomorphology 301, 121–138.
1534 Rovera, G., 1993. Instabilité des versants et dissolution des évaporites dans les Alpes internes :
1535 l'exemple de la montagne de Friolin (Peisey-Nancroix, Savoie). Rev. Géogr. Alp. 81, 71–84.
1536 Sartori, M., Baillifard, F., Jaboyedoff, M., Rouiller, J.-D., 2003. Kinematics of the 1991 Randa
1537 rockslides (Valais, Switzerland). Nat. Haz. Earth Syst. Sci. 3, 423–433.
1538 Schildgen, T., van der Beek, P.A., Sinclair, H., Thiede, R.C., 2018. Spatial correlation bias in late-
1539 Cenozoic erosion histories derived from thermochronology. Nature 559, 89–93.
1540 Schwartz S., Zerathe S., Jongmans D., Baillet L., Carcaillet J., Audin L., Dumont T., Bourlès D., Braucher
1541 R., Lebrouc V., 2017. Cosmic ray exposure dating on the large landslide of Sechilienne (Western
1542 Alps): a synthesis to constrain the slope evolution. Geomorphology, 278, 329–344.
1543 Sébrier, G., Ghafiri, A., Blès, J.-L., 1997. Paleoseismicity in France: fault trench studies in a region of
1544 moderate seismicity. J. Geodyn., 24, 207–217.
1545 Séguinot, J., Jouvet, G., Huss, M., Funk, M., Ivy-Ochs, S., Preusser, F., 2018. Modelling last glacial cycle
1546 dynamics in the Alps. The Cryosphere Discuss., https://doi.org/10.5194/tc-2018-8.
1547 Silverman, B.W., 1998. Density estimation for statistics and data analysis. Chapman and Hall, 175 p.

1548 Six, D., Vincent, C., 2014. Sensitivity of mass balance and equilibrium line altitude to climate change
1549 in the French Alps. J. Glaciol. 60, 874–878.
1550 Stead, D., Wolter, A., 2015. A critical review of rock slope failure mechanisms: the importance of
1551 structural geology. J. Struct. Geol. 74, 1–23.
1552 Sternai, P., Sue, C., Husson, L., Serpelloni, E., Becker, T.W., Willett, S.D., Faccenna, C., Di Giulio, A.,
1553 Spada, G., Jolivet, L., Valla, P., Petit, C., Nocquet, J.M., Walpersdorf, A., Castelltort, S., 2019.
1554 Present–day uplift of the European Alps: evaluating mechanisms and models of their relative
1555 contributions. Earth-Sci. Rev. 190, 589–604.
1556 Strom, A.L., Korup, O. 2006. Extremely large rockslides and rock avalanches in the Tien Shan,
1557 Kyrgyzstan. Landslides 3, 125–136.
1558 Sue, C., Delacou, B., Champagnac, J.D., Allanic, C., Tricart, P., Burkhard, M., 2007. Extensional
1559 neotectonics around the bend of the Western/Central Alps: an overview. Int. J. Earth Sci. 96,
1560 1101–1129.
1561 Tatard, L., Grasso, J.R., Helmstetter, A., Garambois, S., 2010. Characterization and comparison of
1562 landslide triggering in different tectonic and climatic settings. J. Geophys. Res., Earth Surf. 115,
1563 DOI: 10.1029/2009JF001624.
1564 Thiery Y., 2007. Landslide susceptibility in the Barcelonnette basin (French South Alps):
1565 morphodynamic cartography, spatial analysis and probabilistic modelling. Unpubl. PhD thesis,
1566 Université de Caen.
1567 Thouvenot, F., Fréchet, J., Jenatton, L., Gamond, J.F., 2003. The Belledonne Border Fault:
1568 identification of an active seismic strike–slip fault in the western Alps. Geophys. J. Int. 155, 174–
1569 192.
1570 Thouvenot, F., Fréchet, J., 2006. Seismicity along the northwestern edge of the Adria microplate. In
1571 Pinter, N., Grenerczy, G., Weber, J., Stein, S., Medak, D. (eds), The Adria Microplate: GPS geodesy,
1572 tectonics and hazards. NATO Science Series (IV), Earth and Environmental Sciences 61, pp. 335–
1573 349.

1574 Tiwari, B. Ajmera, B., 2017. Landslides Triggered by Earthquakes from 1920 to 2015. In Mikos, M.,
1575 Tiwari, B., Yin, Y., Sassa, K. (eds), Advancing culture of living with landslides, volume 5, WLF 2017.
1576 Springer, pp. 5–15.
1577 Tonini, M., Pedrazzini, A., Penna, I., Jaboyedoff, M., 2014. Spatial pattern of landslides in the Swiss
1578 Rhône Valley. Nat. Haz. 73, 97–110.
1579 Tricart, P., Lardeaux, J.M., Schwartz, S., Sue, C., 2006. The late extension in the inner western Alps: a
1580 synthesis along the south–Pelvoux transect. Bull. Soc. Géol. Fr. 77, 299–310.
1581 Truche M., 2019. Le glissement de terrain du Pas de l'Ours. Dixièmes Journées Nationales de
1582 Géotechnique et de Géologie de l'Ingénieur, Comité Français de Géologie de l'Ingénieur et de
1583 l'Environnement. Oral presentation, Lyon, October 3, 2019.
1584 Tsou, C.Y., Chigira, M., Matsushi, Y., Chen, S.C., 2015. Deep–seated gravitational deformation of
1585 mountain slopes caused by river incision in the Central Range, Taiwan: spatial distribution and
1586 geological characteristics. Eng. Geol. 196, 126–138.
1587 Ustaszewski, M.E., Hampel, A., Pfiffner, O., 2008. Composite faults in the Swiss Alps formed by the
1588 interplay of tectonics, gravitation and postglacial rebound: an integrated field and modelling
1589 study. Swiss J. Geosci. 101, 223–235.
1590 Valla, P.G., van der Beek, P.A., Shuster, D.L., Braun, J., Herman, F., Tassan–Got, L., Gautheron, C.,
1591 2012. Late Neogene exhumation and relief development of the Aar and Aiguilles Rouges massifs
1592 (Swiss Alps) from low-temperature thermochronology modeling and $^{4}He/^{3}He$
1593 thermochronometry. J. Geophys. Res. 117, F01004, Doi: 10.1029/2011JF002043.
1594 Varnes, D.J., 1978. Slope movement types and processes. In: Schuster, R.L., Křižek, R.J. (eds),
1595 Landslides, Analysis and Control, Spec. Rep. 176, Transportation Research Board. National
1596 Academy of Sciences, Washington, D.C., pp. 11–33.
1597 Vengeon, J.M., Couturier, B., Antoine, P., 1999. Déformations gravitaires post glaciaires en terrains
1598 métamorphiques. Comparaison des indices de déformation du versant sud de la Toura (Saint-

Christophe-enOisans, France) avec le phénomène de rupture interne du versant sud du Mont Sec (Séchilienne, France). Bull. Eng. Geol. Env. 57, 387–395.

Vick, L.M., Böhme, M., Rouyet, L., Bergh, S.G., Corner, G.D., Lauknes, T.R., 2020. Structurally controlled rock slope deformation in northern Norway. Landslides, DOI 10.1007/s10346-020-01421-7.

Whalley, W.B., Douglas, G.R., Jonsson, A., 1983. The magnitude and frequency of large rock slides in Iceland during the postglacial. Geogr. Ann. Ser. A: Phys. Geogr. 65, 99–109.

Wood, J.L., Harrison, S., Reinhardt, L., 2020. Landslide inventories for climate impacts research in the European Alps. Geomorphology 228, 398–408.

Figure captions

Fig. 1. The Western Alps study area: key characteristics. A: Alps context, with areas covered by previous work. The whole-range studies by Crosta et al. (2013) and Eisbacher and Clague (1984) were restricted to DGSGSD and catastrophic historical mass movements, respectively. B: study area with main river, massif, and other place names mentioned in the text. Elevation data source: ALOS World 3D elevation model. C: additional site identification sources; RSF monitored by CEREMA (Centre d'Etudes et d'expertise sur les Risques, l'Environnement, la Mobilité et l'Aménagement) for hazard potential (1–17); recorded by Eisbacher and Clague (1984) (18–31), and documented by radiometric dating methods (32–38).

Fig. 2. Tectonic zones of the Western Alps, and modern crustal stress regimes (inset). The units correspond to pre-Alpine palaeogeographic subdivisions today crushed into tectonic belts with distinct characteristics. Source: (Gidon, 1977), modified and updated. Note the thin bands of the Ultra-Dauphinois, Sub-Briançonnais and Valais zones forming a closely-spaced, foreland-vergent imbricate system overthrust on the Helvetic domain along the Penninic Frontal Thrust. Dominant

1625 lithologies within each zone are provided in Figure 6. Inset: documented stress field in the Western
1626 Alps; 1: compressive; 2: extensional; 3: strike-slip (after Delacou et al., 2004).
1627
1628 Fig. 3. Illustrations of the RSF classification based on satellite and field images from the study area.
1629 Rock avalanches (RA), rockfalls (RF), rockslides (RS), and rock slope deformation (RSD) are labelled
1630 accordingly in image pairs. RF1 (runout: 650 m) is in highly fractured dolomitic limestone. Note that
1631 RS1 displays hummocky surface topography reminiscent of an earthflow (high plasticity of the
1632 bedrock); RS2 is a compound site involving more displacement than just downhill creep: clear
1633 rupture scars (scarps 3–5 m high) forming a joined-up arc despite limited travel distance, and shallow
1634 secondary landslides. Both RS sites are in highly fissile Jurassic shale and calcareous sand. Satellite
1635 imagery: as provided by Google Earth. Credits: S. Blondeau.
1636
1637 Fig. 4. RSF inventory of the Western Alps in relation to topography. RSF is endemic in the main
1638 massifs, but sparser in the highest and Prealpine massifs. Sites are additionally classified by four
1639 broad lithological groups. Graphs show relative frequency of RSF types in these groups.
1640
1641 Fig. 5. RSF attributes as a function of spatial and topographic variables. A: box-and-whisker plots of
1642 surface-area distributions by RSF mode. Main boxes define the interquartile range (IQR), showing
1643 median (horizontal line) and mean (cross). Whiskers are positioned at 1.5 IQR, thus leaving
1644 headroom for displaying the distribution of 'outsize' RSF. These are clearly dominated by RS (n = 47)
1645 and RSD (n = 53). Note that a single data point on the graph at this resolution may represent several
1646 closely-spaced values. B: RSF size–frequency distribution; long tail of 39 RSDs > 10 km^2 not shown
1647 (see box plots). Types clearly aggregate to log-normal distribution. Note that numbers fall off rapidly
1648 below 0.4 km^2 for RS and RSD. C: RSF size detection thresholds. Enlarged first two increments of
1649 graph (B) to 0.2 km^2. Numbers fall off sharply below 0.04 km^2 for RF, and RS and RSD numbers
1650 remain 'noisily' low within that size band. D: altitude of RS and RSD headscarps, by percentage of

1651 total area affected. E: RSF headscarp altitude, by numbers of each type. F: slope angle at RS and RSD
1652 headscarps, by percentage of total area affected. G: local relief (computed from the ALOS DEM using
1653 a 3x3 km moving window), by percentage of total area affected (all RSF types). H: RSF aspect (red)
1654 contrasted with overall hillslope aspect for entire study area (blue). I: aspect variation between RSF
1655 types.
1656
1657 Fig. 6. RSF inventory for the Western Alps as a function of lithology. Lithological base map, here
1658 consisting of 15 classes, was elaborated (A) out of the 178 lithological taxa provided by the BRGM
1659 1:50,000-scale digital maps of France, and (B) from the 1:250,000-scale map of Piemonte by Piana et
1660 al. (2017). Given the pre-ordained nomenclature of existing geological maps, lithology polygons
1661 emphasise pre-tectonic protolith rather than metamorphic grade or texture (see text). Massif
1662 outlines as in Fig. 1B. Blank areas are Val d'Aosta and Swiss border area, which lack compatible
1663 geological maps; the far south, where the digital database is corrupted; and Quaternary deposits.
1664 Green and red circles locate the outsize RS and RSD plotted in Figure 5A.
1665
1666 Fig. 7. Lithology as a predisposing factor of RSF incidence in the Western Alps. The association is
1667 obtained as a function of the three ratios specified in the keybox. The strength of association is
1668 indicated by the red bars, in decreasing order. Blank areas in Fig. 6 are excluded. Sources: A – France,
1669 from BRGM 1:50,000 scale geological maps; B – Italy, from 1:250,000 scale geological map by Piana
1670 et al. (2017), which also displays RSF locations mapped by Fioraso (2017).
1671 Fig. 8. RSF incidence and tectonic lineaments. Table gives proportions of RSF (by numbers and
1672 surface area) that intersect a lineament displayed on the 1:250,000 scale geological BRGM maps of
1673 the region.
1674
1675 Fig. 9. RSF and seismic activity. Earthquake magnitude/depth ratio (bigger circles suggest large,
1676 shallow earthquakes). Seismic database after Thouvenot and Fréchet (2006).

Fig. 10. Present-day regional tectonic stress field. Source: Delacou et al. (2004), simplified. Table showing proportions of RSF in each zone is by RSF surface area.

Fig. 11. Present-day uplift rates (source: Nocquet et al., 2016). The elongated dome of highest values centres on the Beaufortain–Vanoise massifs and Tarentaise (middle Isère) valley, but overall RSF distribution is unrelated.

Fig. 12. RSF incidence in relation to maximum ice thickness during the Late Pleistocene most extensive glaciation (MEG). A: spot ice depths derived from Coutterand's (2010) contour maps of the LGM icefield (glaciated piedmont farther west not shown). Dashed red line: equilibrium line altitude (ELA) during the MEG, ca. 1300 ± 50 m. B: box-and-whisker plots of RSF distribution by type as a function of ice thickness based on map A. Ice thickness was measured at headscarp altitudes for RA and RF (hence the small values), and at altitudes of displaced-mass base for RS and RSD because this is where any glacial debuttressing would focus.

Fig. 13. Example of upslope-directed RSD propagation into the periglacial zone. A: RSD near Pic Ségure (Guil River valley, Queyras massif). B: rockslide at the base of Pointe de la Sana (Vanoise massif). Current permafrost distribution after Boeckli et al. (2012).

Fig. 14. Croix du Berger RSF, 2250 m a.s.l., Beaufortain massif. Primarily a strikingly well-developed RSD, with 'false antiscarps' where multiple-source scarps daylight behind the crest, it also progresses to RS and RF modes. Credits: S. Blondeau.

Fig. 15. RSF clusters, hotspots, and super-hotspots in the Western Alps. A: RSF clusters (blue and dark blue combined), here defined from a point-based (or kernel) density map using RSF centroids as data

1703 points and applying a search radius of 10 km. Massif outlines (black lines) as in Fig. 1B, and major
1704 thrust fronts (BB and PFT) as in other figures. B: RSF hotspots (red and orange combined), here
1705 defined from a density map based on RSF surface area (same conditions as in 15A). C, D, E: point
1706 density clusters mapped for rockfalls and rock avalanches (C), rockslides (D), and RSD (E). F: co-
1707 occurrence of highest-density clusters (blue polygons in map A) and hotspots (red and orange
1708 polygons in map B). Intersections between the two categories are termed super-hotspots (labelled
1709 with Roman numerals). G: RSF clusters, hotspots and super-hotspots (as in map F) in relation to main
1710 tectonic units.
1711
1712 Fig. 16. Four new RSF units identified by this study in the Upper Rhône valley, augmenting the
1713 inventory of Pedrazzini et al. (2015). In B, the large Tour de Don rockfall has wide open fissures along
1714 the ridge, suggesting incipient further phases. Note that the feature interpreted as a rockslide in Fig.
1715 16B has been reported as moraine on Swiss maps; field control is required to adjudicate.

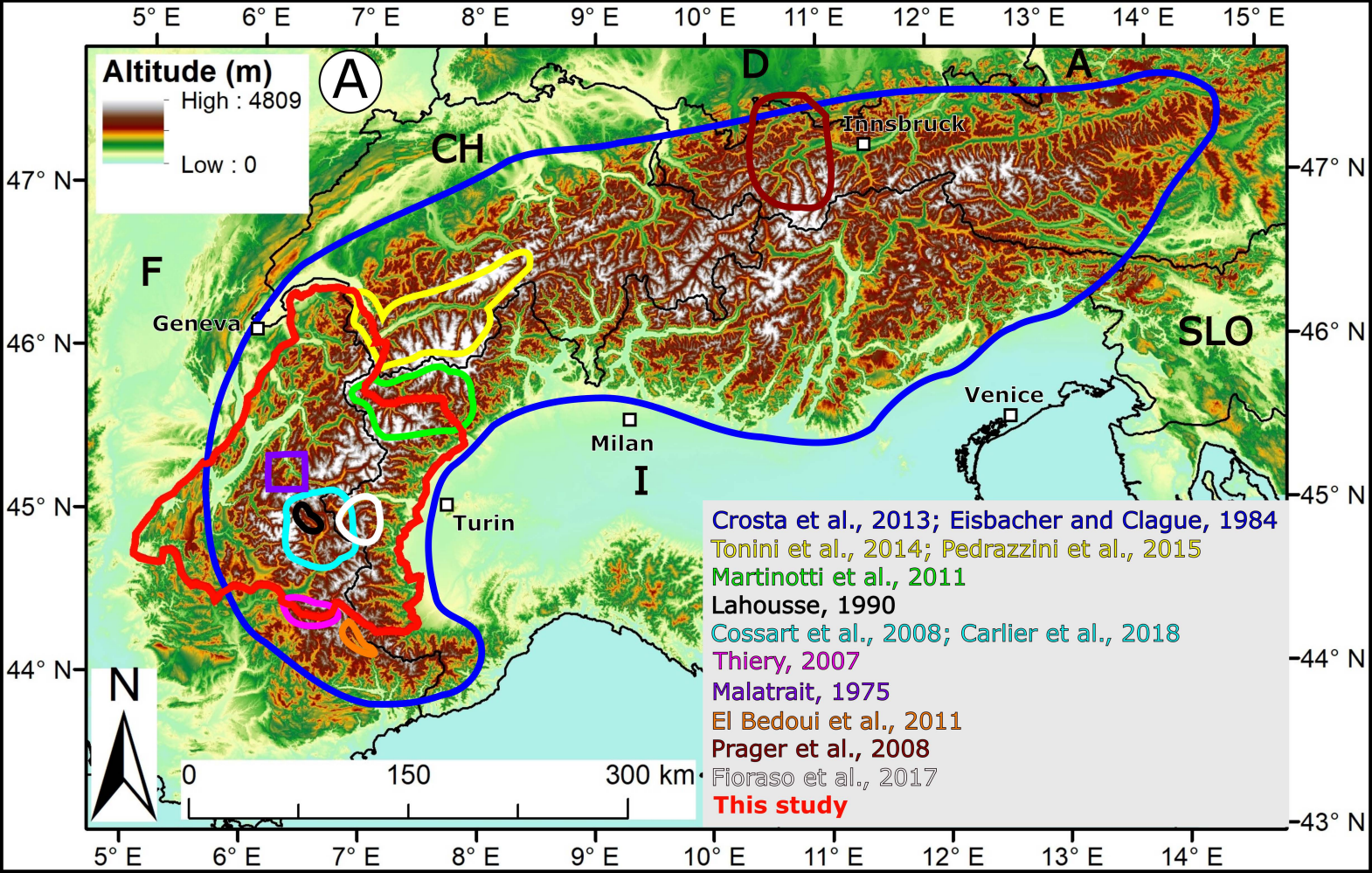
Altitude (m)
High : 4809
Low : 0
A
CH
D
A
Innsbruck
F
Geneva
SLO
Venice
Milan
I
Turin
N
0
150
300 km
5° E
6° E
7° E
8° E
9° E
10° E
11° E
12° E
13° E
14° E
15° E
47° N
46° N
45° N
44° N
43° N
Crosta et al., 2013; Eisbacher and Clague, 1984
Tonini et al., 2014; Pedrazzini et al., 2015
Martinotti et al., 2011
Lahousse, 1990
Cossart et al., 2008; Carlier et al., 2018
Thiery, 2007
Malatrait, 1975
El Bedoui et al., 2011
Prager et al., 2008
Fioraso et al., 2017
This study

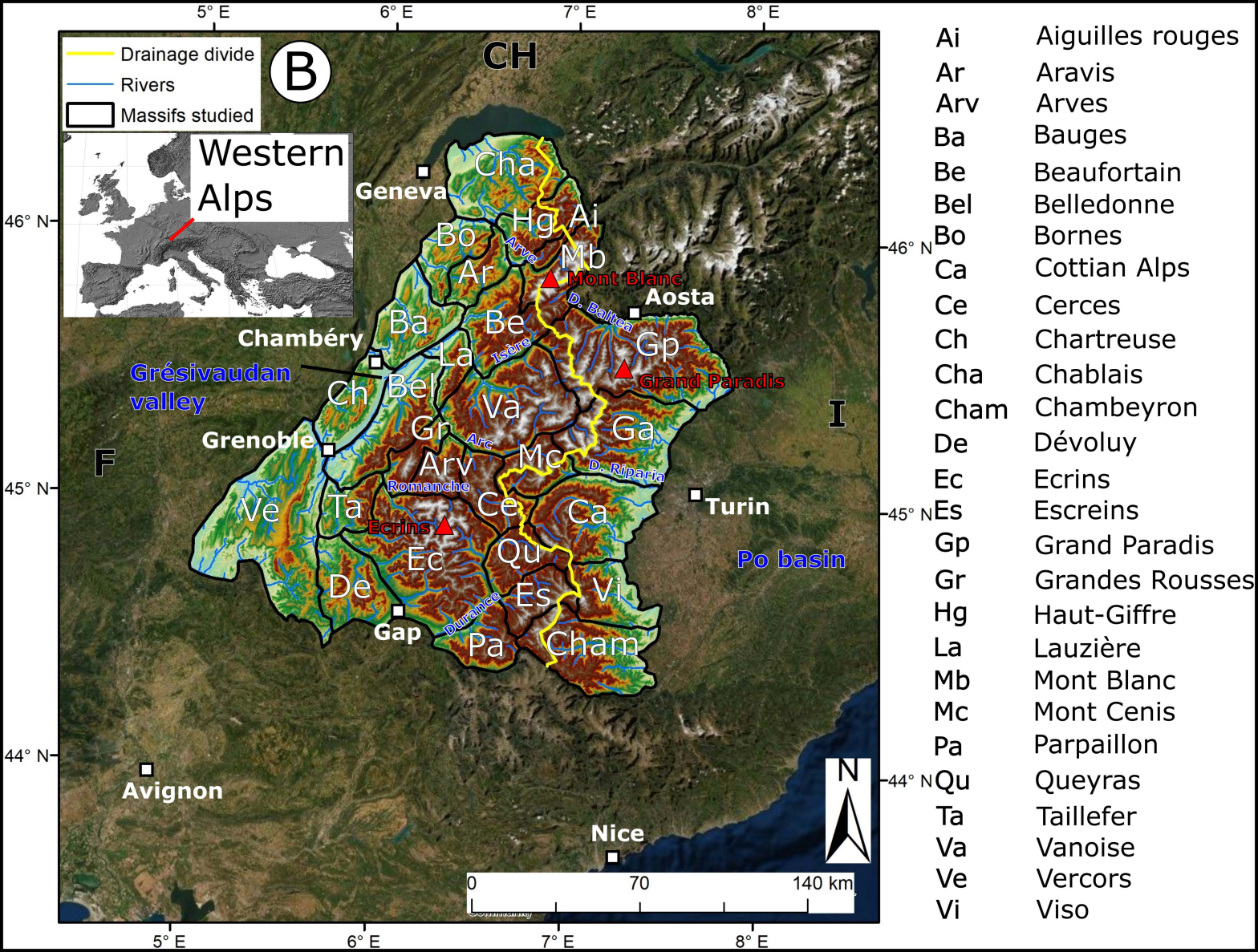

Ai	Aiguilles rouges
Ar	Aravis
Arv	Arves
Ba	Bauges
Be	Beaufortain
Bel	Belledonne
Bo	Bornes
Ca	Cottian Alps
Ce	Cerces
Ch	Chartreuse
Cha	Chablais
Cham	Chambeyron
De	Dévoluy
Ec	Ecrins
Es	Escreins
Gp	Grand Paradis
Gr	Grandes Rousses
Hg	Haut-Giffre
La	Lauzière
Mb	Mont Blanc
Mc	Mont Cenis
Pa	Parpaillon
Qu	Queyras
Ta	Taillefer
Va	Vanoise
Ve	Vercors
Vi	Viso

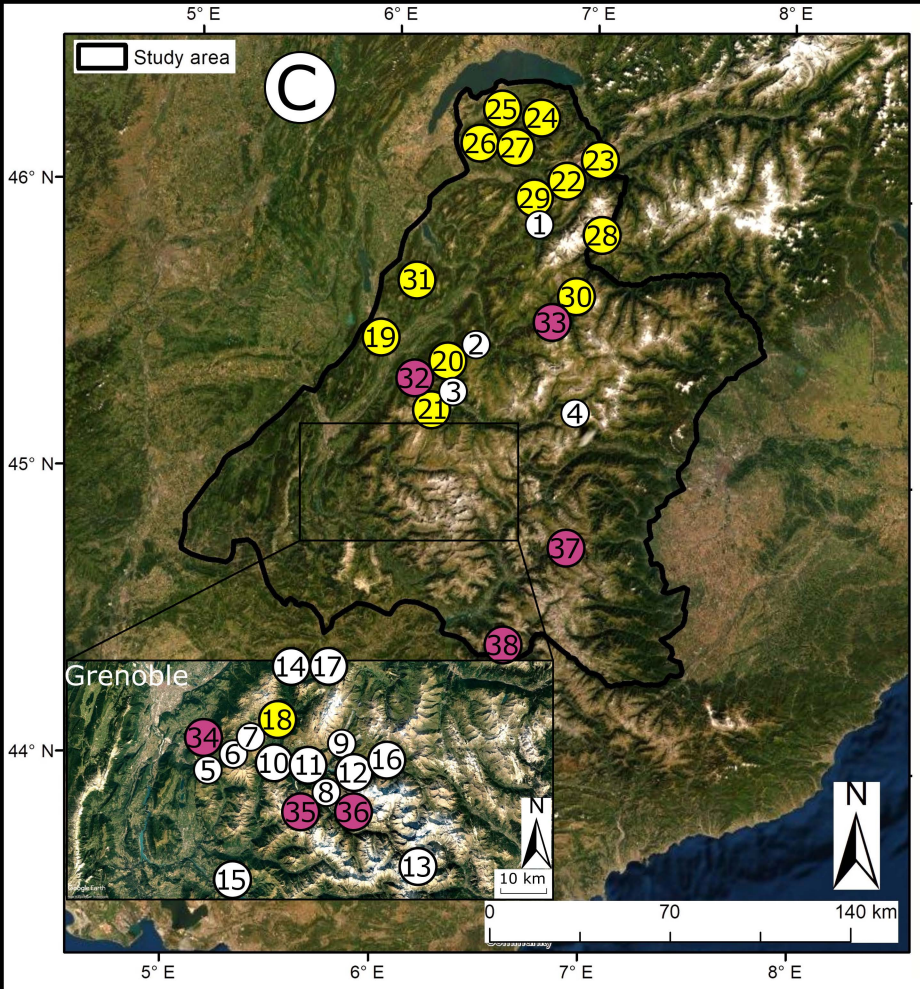

Eisbacher and Clague, 1984

18 Infernet (RA)
19 Granier (RA)
20 La Chapelle (RA)
21 Saint-Jean-de-Maurienne (RS)
22 Tête Noire (RA)
23 Salvan (RF)
24 Pointe d'Autigny (RF)
25 Lullin (RS)
26 Viuz-en-Sallaz (RS)
27 Bellevaux (RS)
28 Val-Ferret (RA and RF)
29 Massif de Platé (RSD)
30 Bec Rouge (RF)
31 Le Châtelard (RS)

CEREMA

① Egratz road (RF)
② Combelouvière (RS)
③ Madeleine SNCF tunnel (RSD)
④ Mont Cenis (RSD)
⑤ Granges (RS)
⑥ Tête de Sauve (RSD)
⑦ Pte de l'Aiguille (RSD)
⑧ Collet (RS)
⑨ Croix de Cassini (RS and RSD)
⑩ Oulles (RF)
⑪ Charmonetier (RF)
⑫ Chambon dam (RS)
⑬ Pilatte refuge (RSD)
⑭ Pic Bunard (RF)
⑮ Mont Chauvet (RS)
⑯ Clot de Pertuis (RF)
⑰ Billan (RS)

Other studies

32 Mont Rognier (Hippolyte et al., 2012)
33 Aiguilles de Grives (Hippolyte et al., 2009)
34 Séchilienne (Schwartz et al., 2017)
35 Lauvitel (Delunel et al., 2010)
36 Toura (Vengeon et al., 1999)
37 Pas de l'Ours (Truche, 2019)
38 La Valette (Hibert et al., 2012)

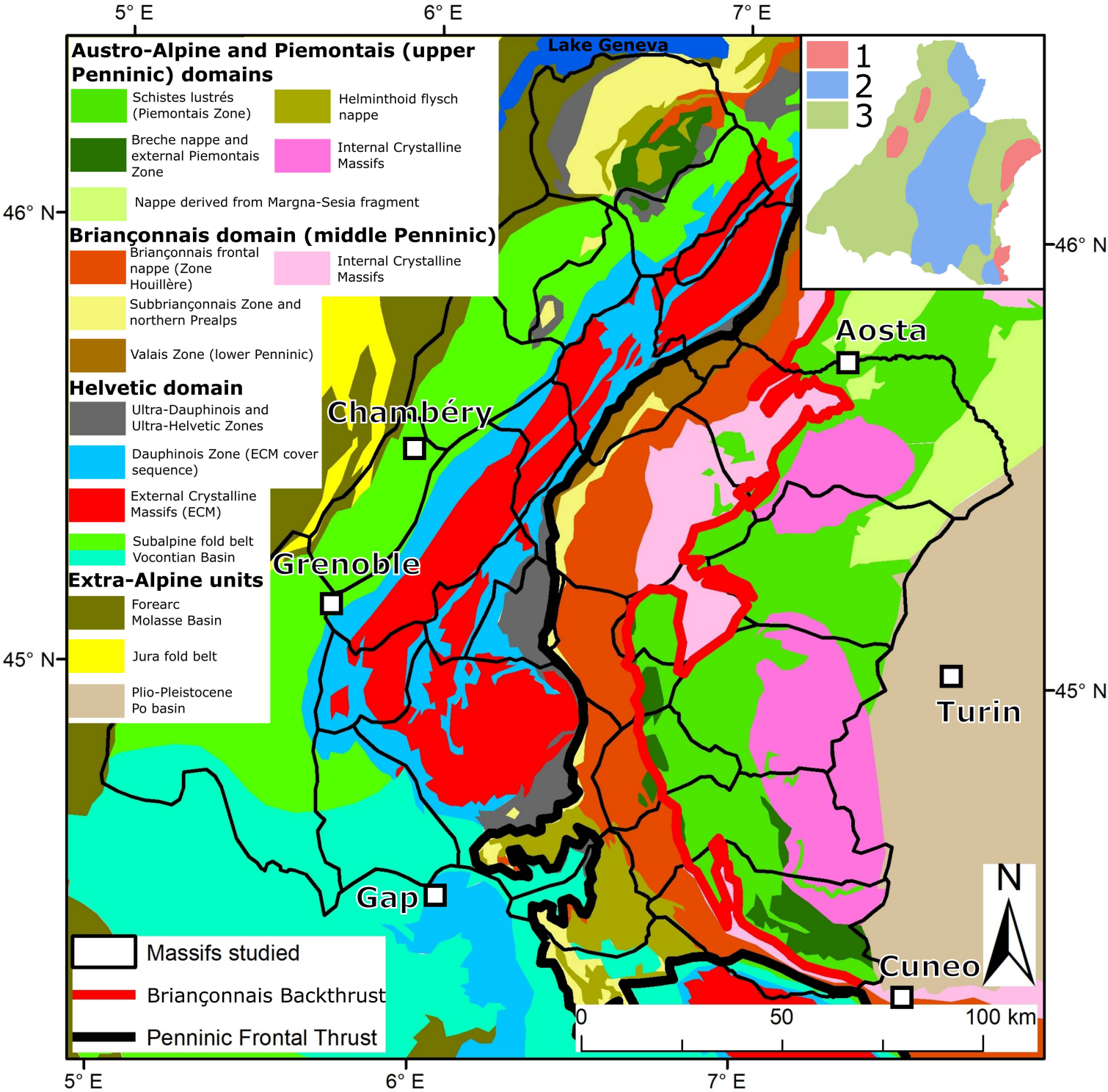
5° E
6° E
7° E
46° N
45° N
Lake Geneva
Austro-Alpine and Piemontais (upper Penninic) domains
Schistes lustrés (Piemontais Zone)
Helminthoid flysch nappe
Breche nappe and external Piemontais Zone
Internal Crystalline Massifs
Nappe derived from Margna-Sesia fragment
Briançonnais domain (middle Penninic)
Briançonnais frontal nappe (Zone Houillère)
Internal Crystalline Massifs
Subbriançonnais Zone and northern Prealps
Valais Zone (lower Penninic)
Helvetic domain
Ultra-Dauphinois and Ultra-Helvetic Zones
Dauphinois Zone (ECM cover sequence)
External Crystalline Massifs (ECM)
Subalpine fold belt Vocontian Basin
Extra-Alpine units
Forearc Molasse Basin
Jura fold belt
Plio-Pleistocene Po basin
1
2
3
Aosta
Chambéry
Grenoble
Turin
Gap
Cuneo
N
Massifs studied
Briançonnais Backthrust
Penninic Frontal Thrust
0
50
100 km

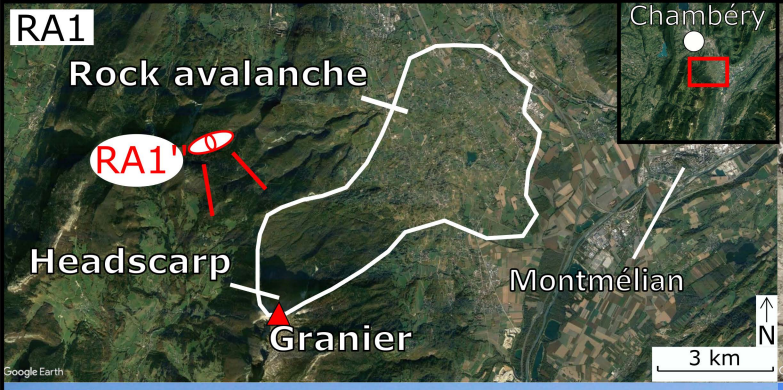

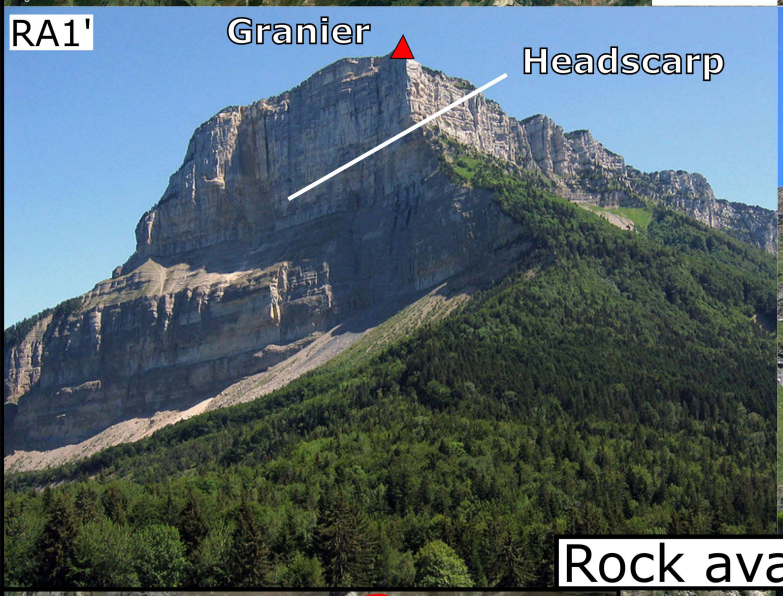

Rock avalanches

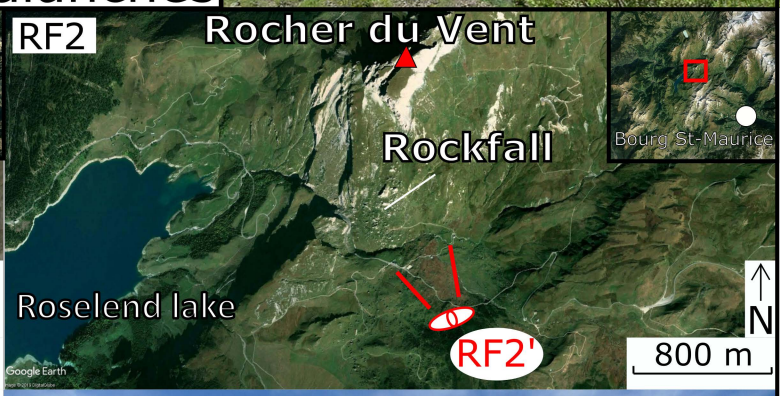

Rockfalls

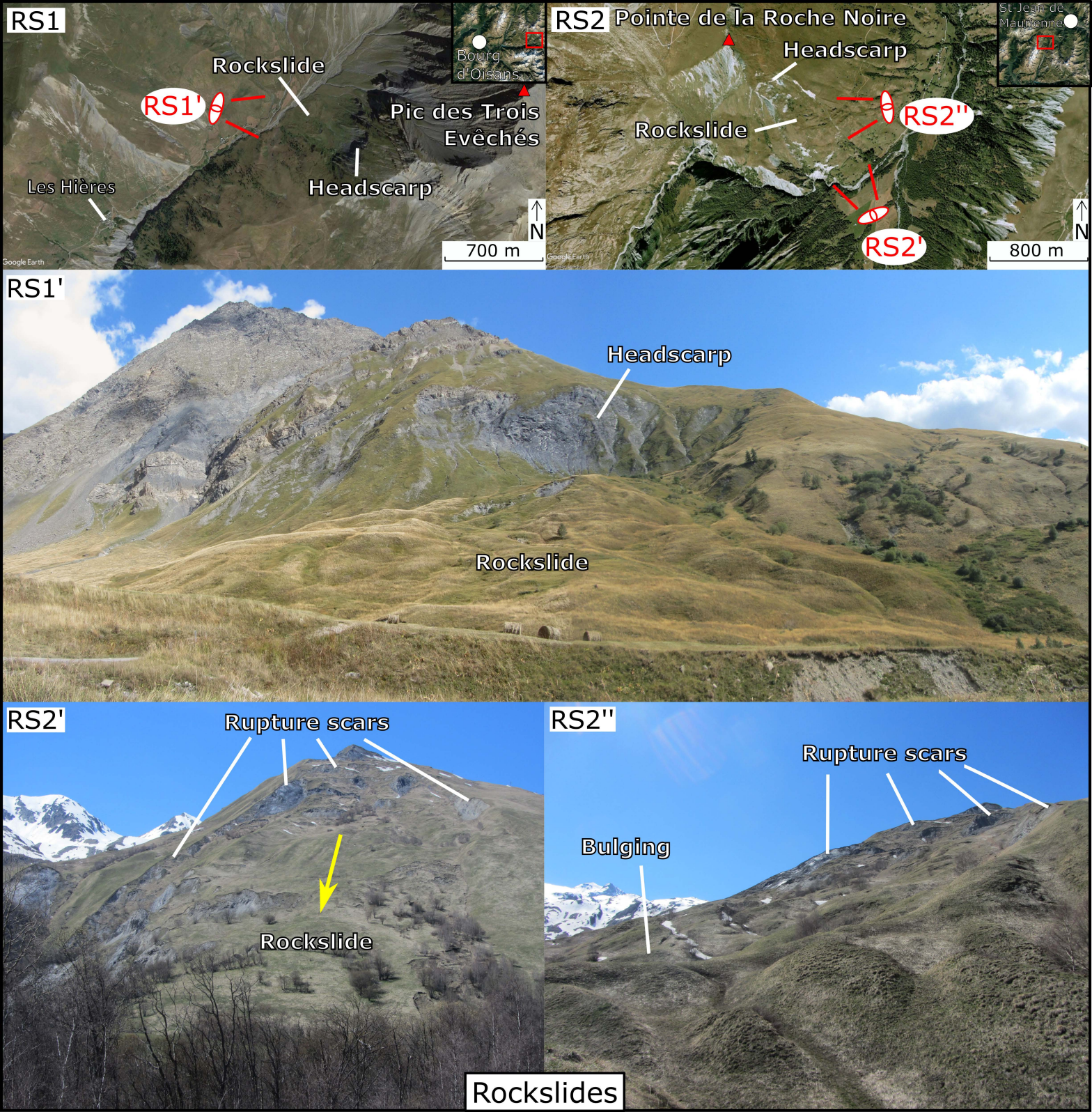
RS1
Rockslide
RS1'
Pic des Trois
Evêchés
Les Hières
Headscarp
Bourg
d'Oisans
N
700 m
Google Earth
RS2
Pointe de la Roche Noire
Headscarp
Rockslide
RS2''
RS2'
St-Jean de
Maurienne
N
800 m
Google Earth
RS1'
Headscarp
Rockslide
RS2'
Rupture scars
Rockslide
RS2''
Rupture scars
Bulging
Rockslides

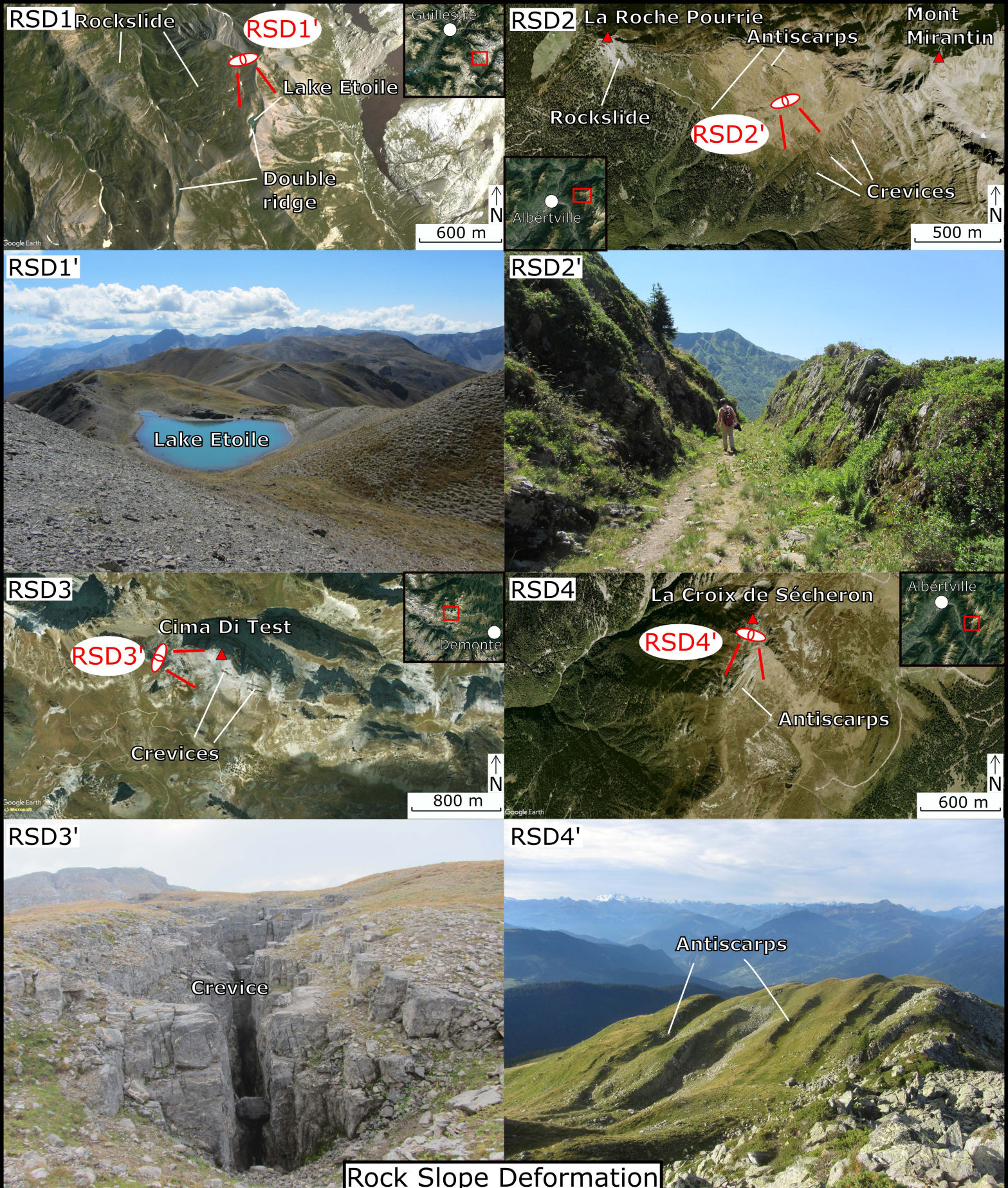
RSD1
Rockslide
RSD1'
Lake Etoile
Double ridge
Guillestre
N
600 m
Google Earth
RSD2
La Roche Pourrie
Antiscarps
Mont Mirantin
Rockslide
RSD2'
Crevices
Albertville
N
500 m
RSD1'
Lake Etoile
RSD2'
RSD3
Cima Di Test
RSD3'
Crevices
Demonte
N
800 m
Google Earth
RSD4
La Croix de Sécheron
RSD4'
Antiscarps
Albertville
N
600 m
Google Earth
RSD3'
Crevice
RSD4'
Antiscarps
Rock Slope Deformation

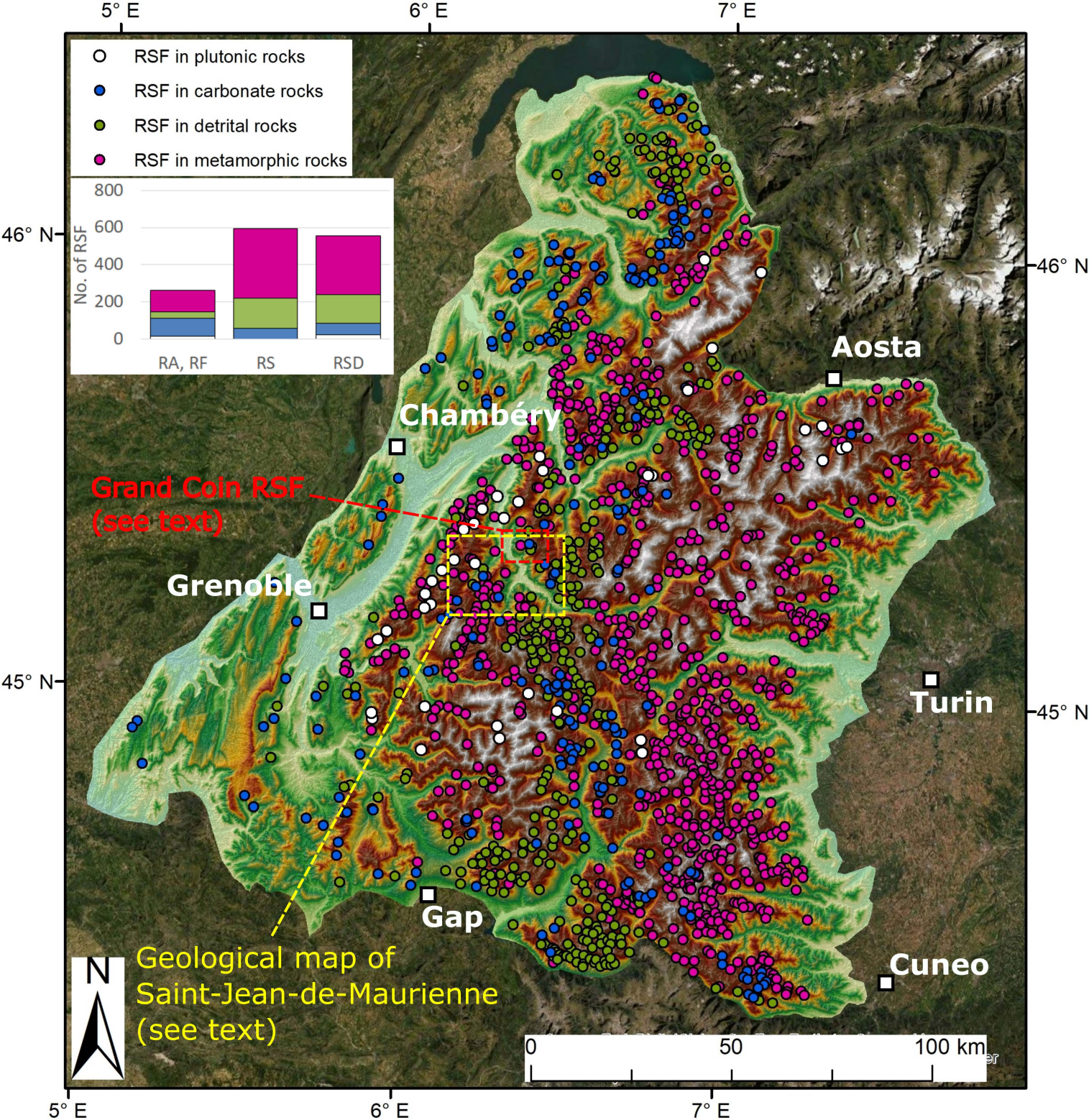
RSF in plutonic rocks
RSF in carbonate rocks
RSF in detrital rocks
RSF in metamorphic rocks
No. of RSF
800
600
400
200
0
RA, RF
RS
RSD
5° E
6° E
7° E
46° N
45° N
Aosta
Chambéry
Grand Coin RSF
(see text)
Grenoble
Turin
Gap
Cuneo
Geological map of
Saint-Jean-de-Maurienne
(see text)
N
0
50
100 km

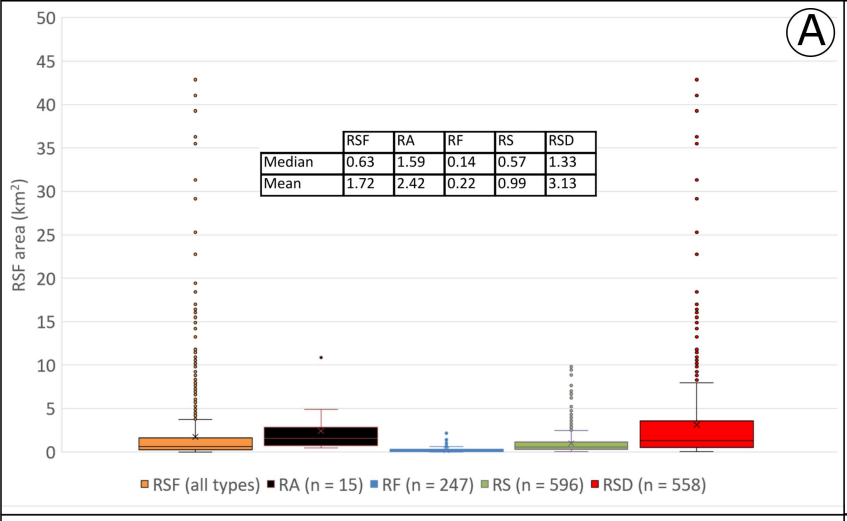

	RSF	RA	RF	RS	RSD
Median	0.63	1.59	0.14	0.57	1.33
Mean	1.72	2.42	0.22	0.99	3.13

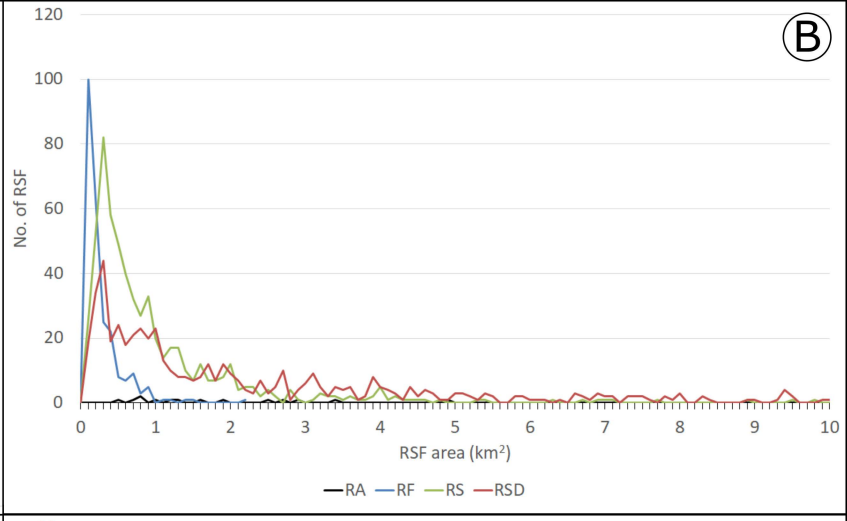

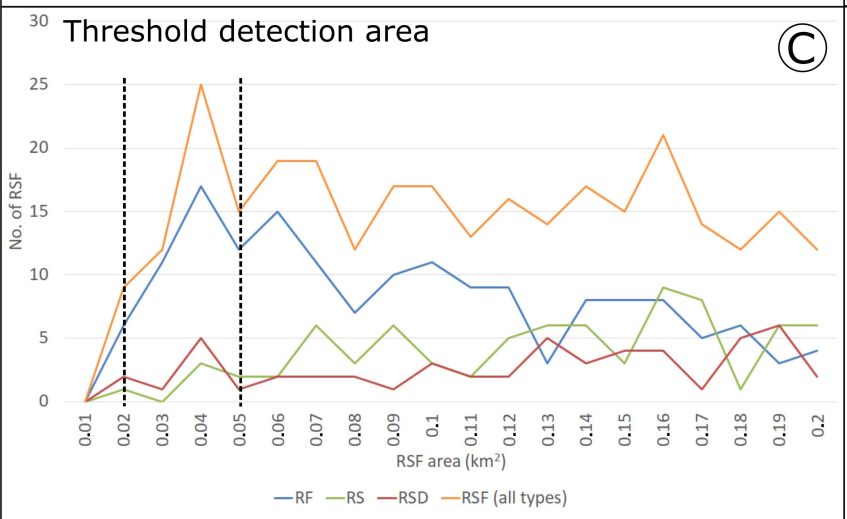

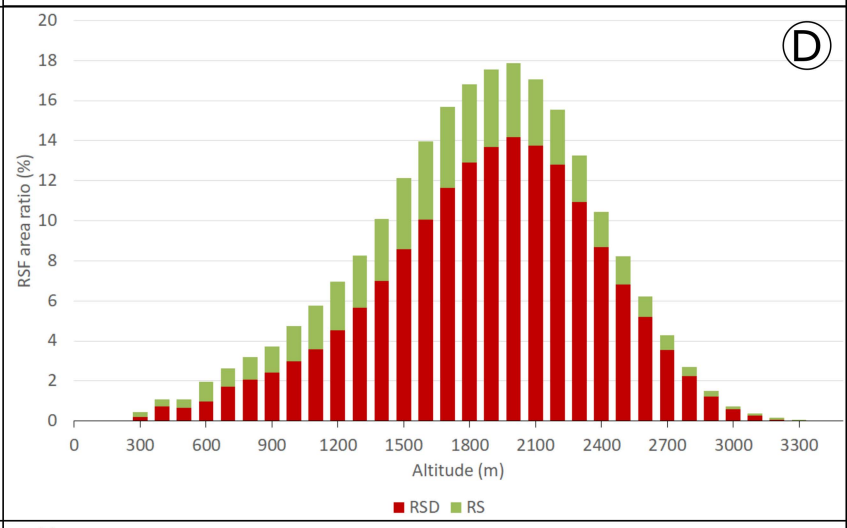

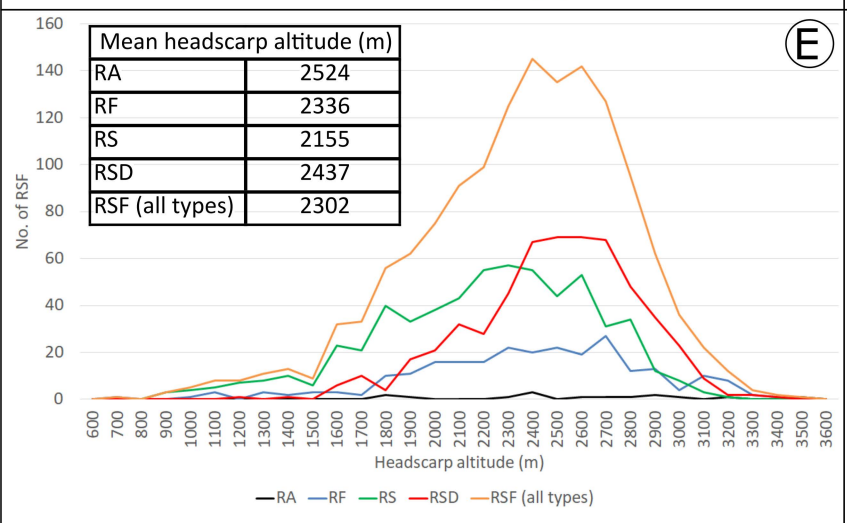

Mean headscarp altitude (m)	
RA	2524
RF	2336
RS	2155
RSD	2437
RSF (all types)	2302

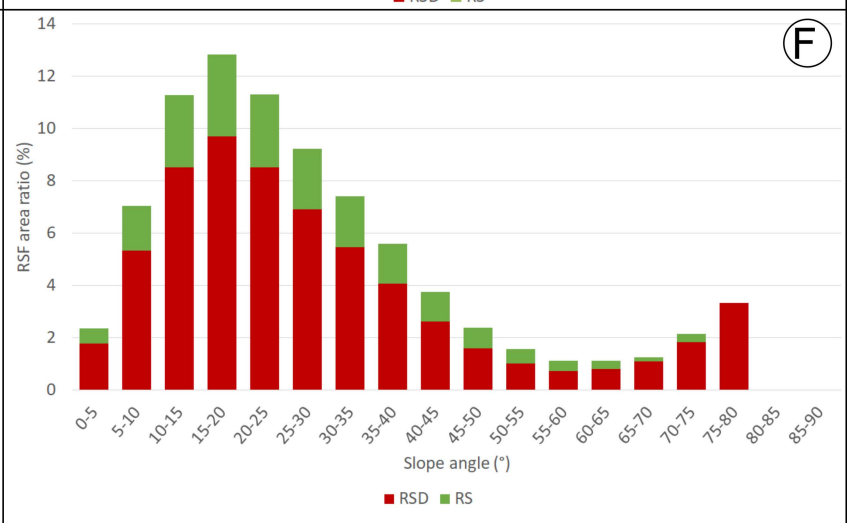

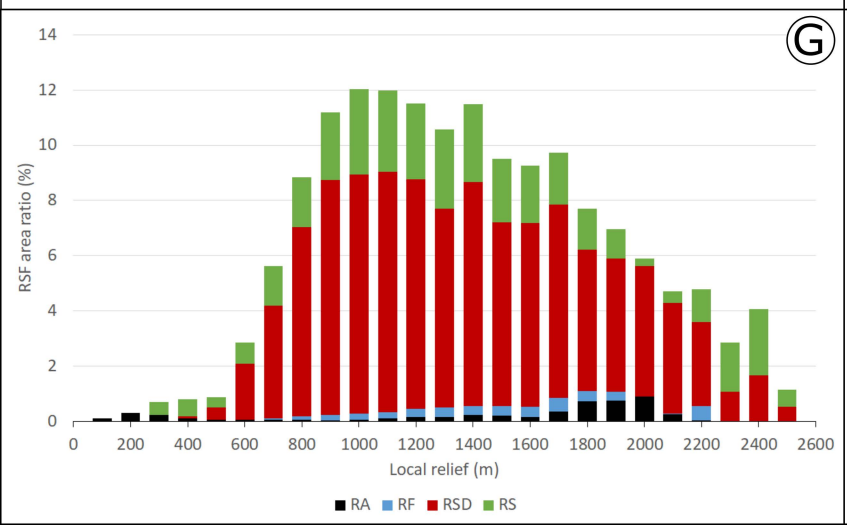

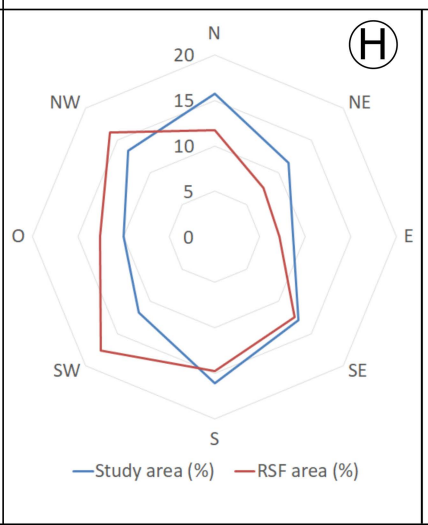

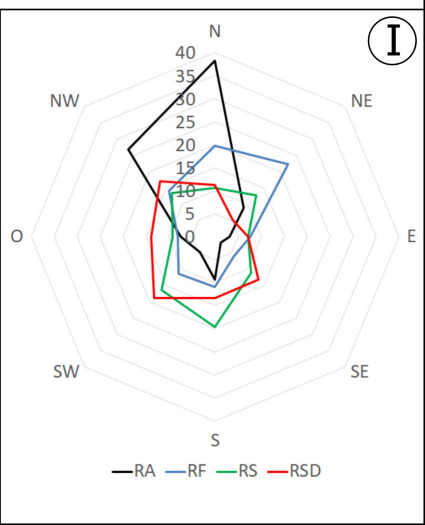

5° E
6° E
7° E
46° N
45° N
Granite, rhyolite, andesite
Gabbros, basalte, serpentine
Limestone
Dolomite
Evaporites
Arkose, sandstone, conglomerate, greywacke
Flysch
Claystone
Breccia
Marl
Quartzite
Meta-magmatic
Marble
Gneiss, migmatite
Schist
Water
Ice
Area relevant to Fig. 7B
Area relevant to Fig. 7A
Massifs studied
RSD > 8 km²
RS > 2.5 km²
RSF
N
0
50
100 km

A

France

Area (%)

50
40
30
20
10
0

Proportion of study area occupied by each lithological class
Percentage of lithological class affected by RSF by percentage of lithological class in region (by area)
Proportion of total RSF inventory area occurring in each lithological class

Schist
ASCG
Flysch
Gabbro, basalt, serpentine
Breccia
Dolomite
Meta-magmatic
Marble
Claystone
Gneiss, migmatite
Quartzite
Granite, rhyolite, andesite
Evaporites
Marl
Limestone

B

Italy (Piemonte region)

Area (%)

90
80
70
60
50
40
30
20
10
0

Proportion of study area occupied by each lithological class
Percentage of lithological class affected by RSF by percentage of lithological class in region (by area)
Proportion of total RSF inventory area occurring in each lithological class

Schist
ASCG
Quartzite
Marble
Gabbro, basalte, serpentine
Gneiss, migmatite
Meta-magmatic
Limestone
Dolomite

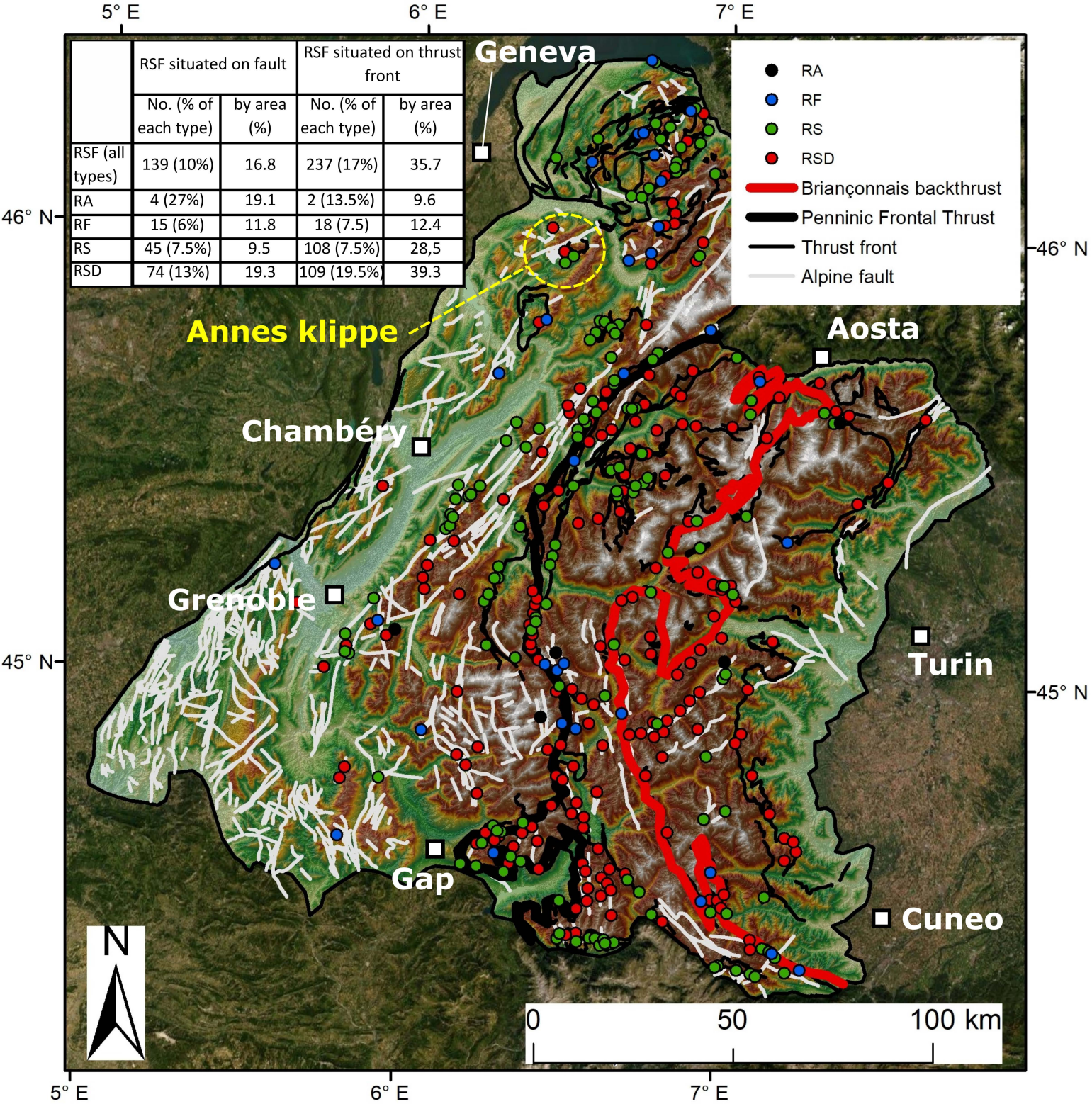

	RSF situated on fault		RSF situated on thrust front	
	No. (% of each type)	by area (%)	No. (% of each type)	by area (%)
RSF (all types)	139 (10%)	16.8	237 (17%)	35.7
RA	4 (27%)	19.1	2 (13.5%)	9.6
RF	15 (6%)	11.8	18 (7.5)	12.4
RS	45 (7.5%)	9.5	108 (7.5%)	28,5
RSD	74 (13%)	19.3	109 (19.5%)	39.3

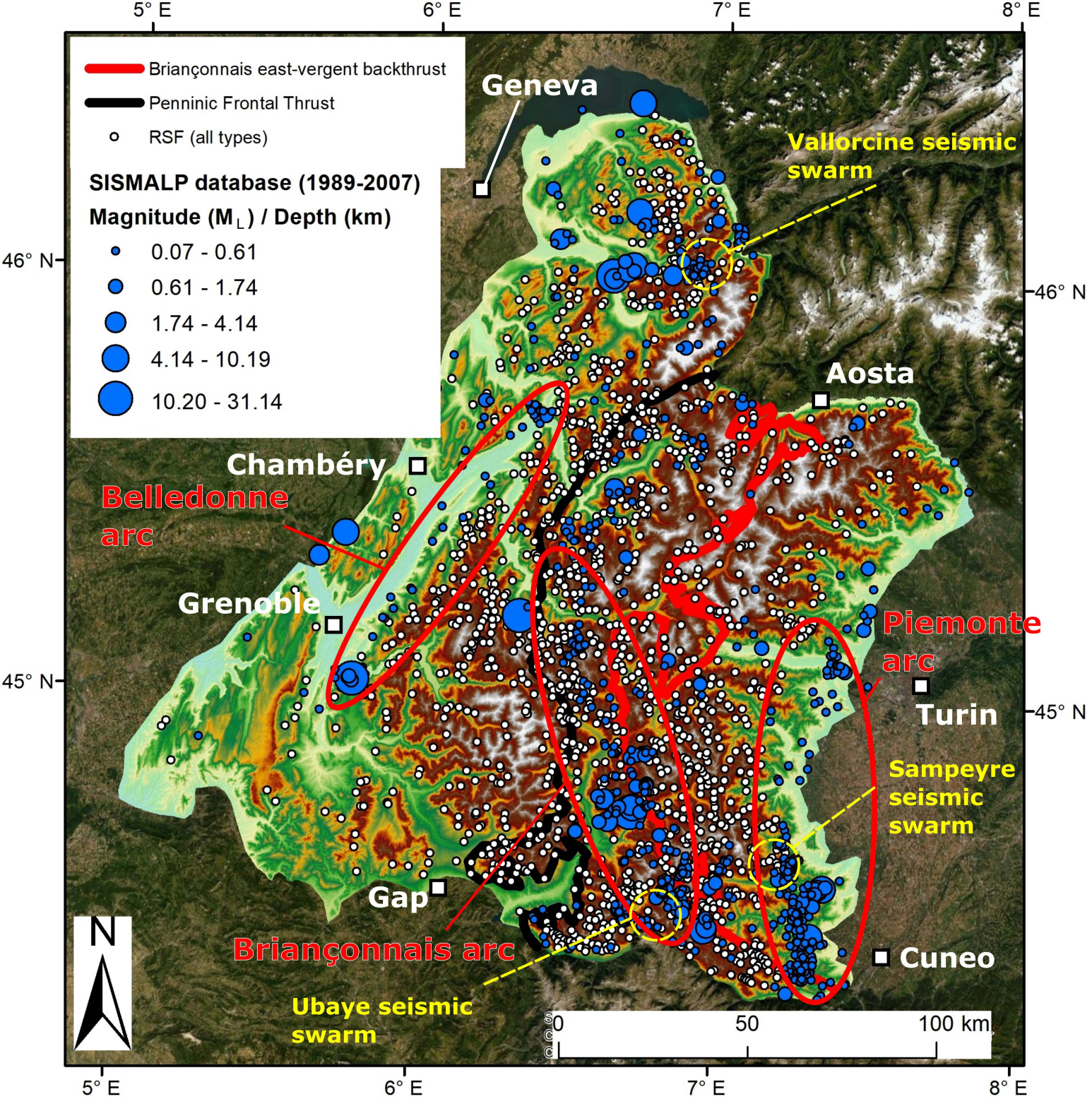
Briançonnais east-vergent backthrust
Penninic Frontal Thrust
RSF (all types)
SISMALP database (1989-2007)
Magnitude (M L) / Depth (km)
0.07 - 0.61
0.61 - 1.74
1.74 - 4.14
4.14 - 10.19
10.20 - 31.14
Geneva
Vallorcine seismic swarm
Aosta
Chambéry
Belledonne arc
Grenoble
Piemonte arc
Turin
Sampeyre seismic swarm
Gap
Briançonnais arc
Cuneo
Ubaye seismic swarm
N
0
50
100 km
5° E
6° E
7° E
8° E
46° N
45° N

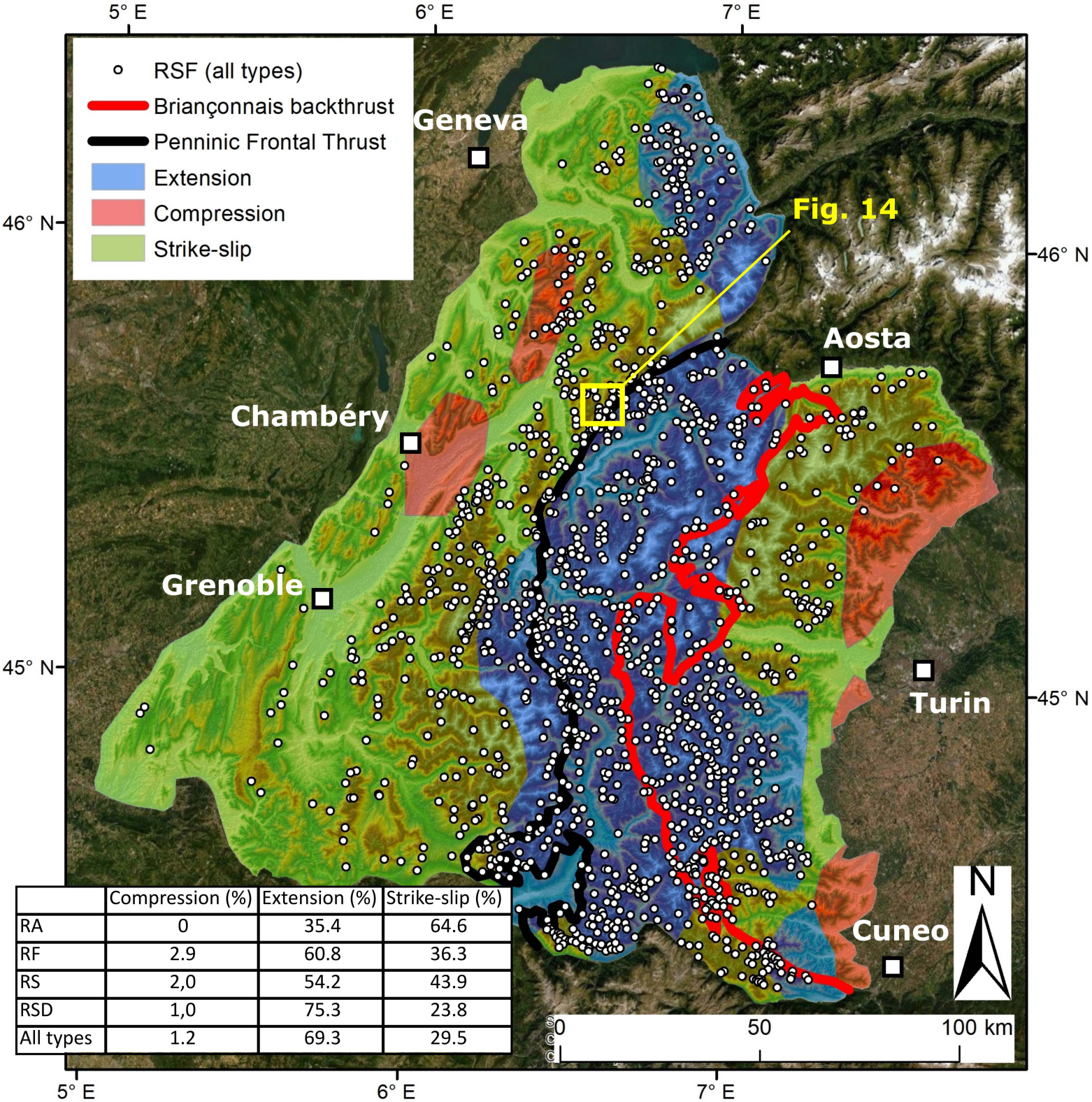

	Compression (%)	Extension (%)	Strike-slip (%)
RA	0	35.4	64.6
RF	2.9	60.8	36.3
RS	2,0	54.2	43.9
RSD	1,0	75.3	23.8
All types	1.2	69.3	29.5

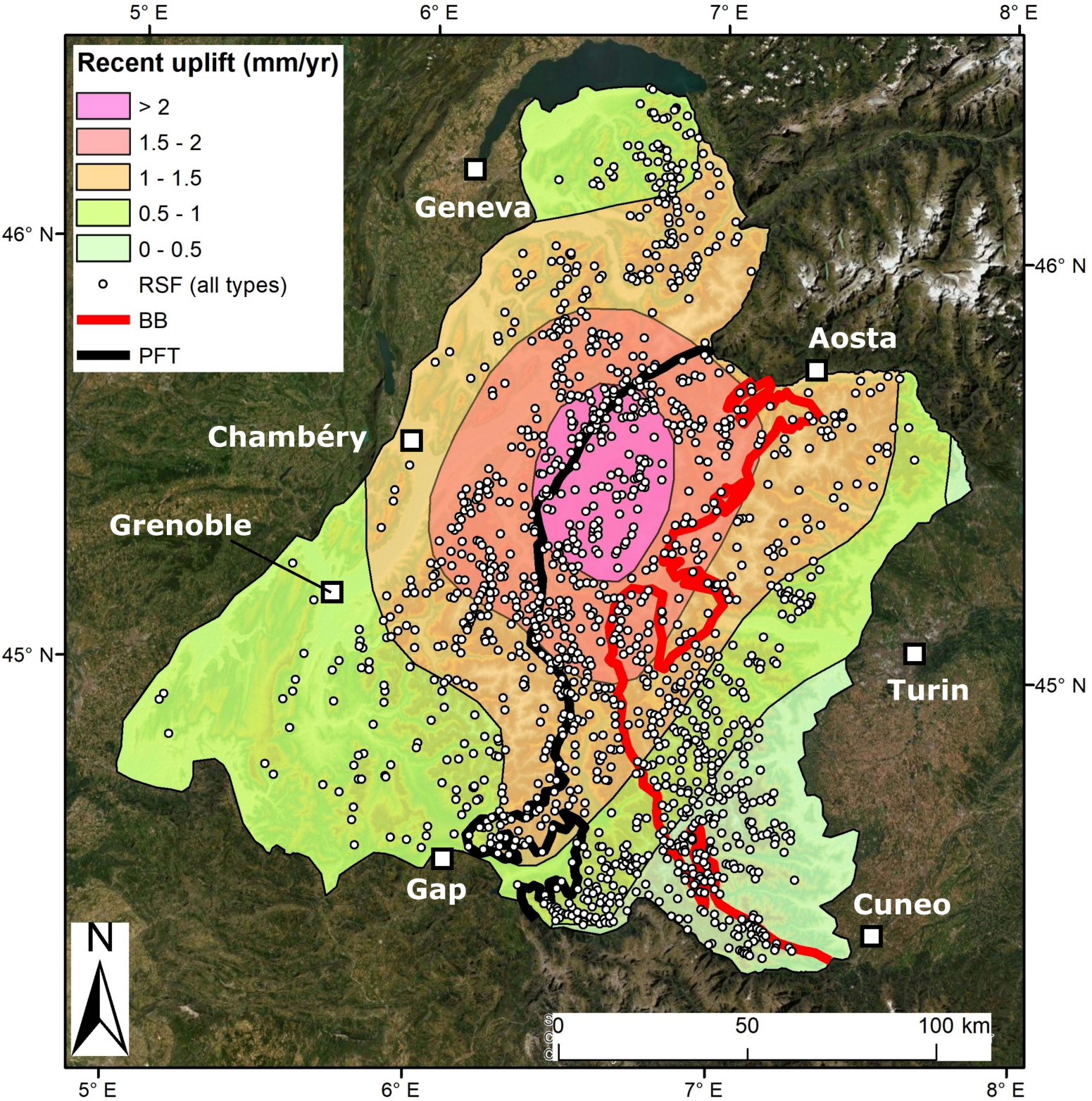
Recent uplift (mm/yr)
> 2
1.5 - 2
1 - 1.5
0.5 - 1
0 - 0.5
RSF (all types)
BB
PFT
Geneva
Aosta
Chambéry
Grenoble
Turin
Gap
Cuneo
5° E
6° E
7° E
8° E
46° N
45° N
N
0
50
100 km

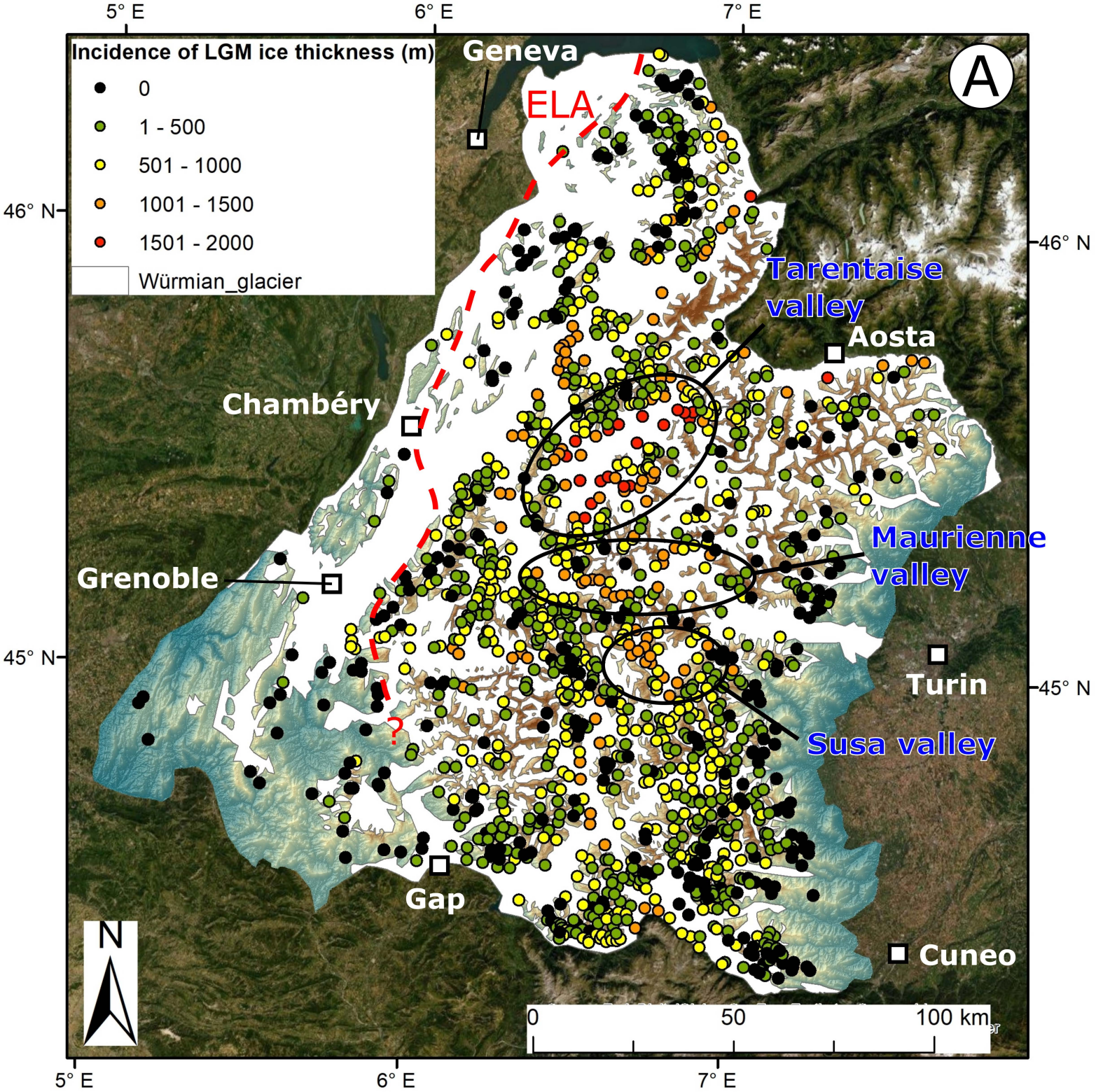
Incidence of LGM ice thickness (m)
0
1 - 500
501 - 1000
1001 - 1500
1501 - 2000
Würmian_glacier
A
Geneva
ELA
Tarentaise valley
Aosta
Chambéry
Maurienne valley
Grenoble
Turin
Susa valley
?
Gap
Cuneo
N
0
50
100 km
5° E
6° E
7° E
46° N
45° N

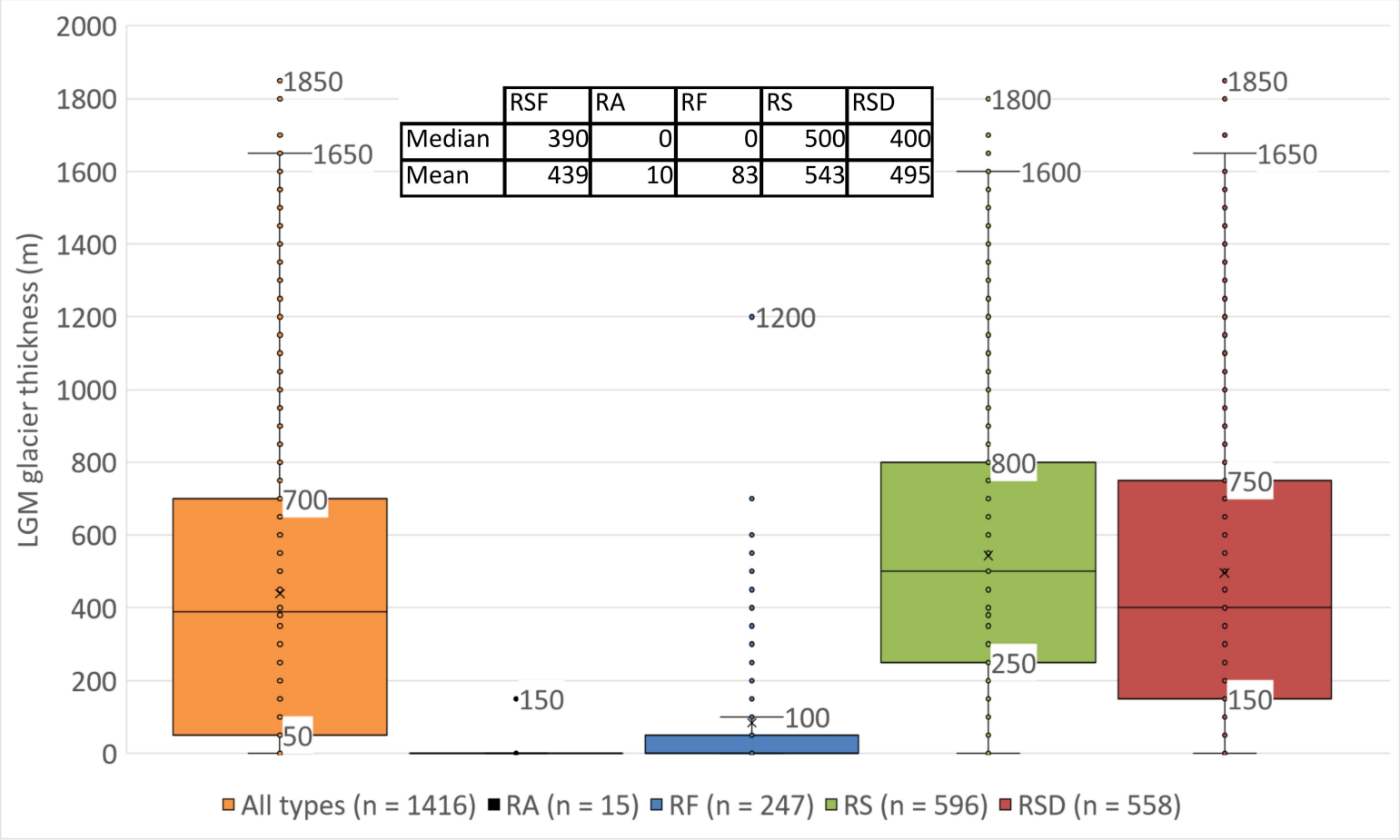

	RSF	RA	RF	RS	RSD
Median	390	0	0	500	400
Mean	439	10	83	543	495

A

Pic Ségure

Briançon

Guillestre

Pic Ségure

Split ridge

N

1 km

Alpine Permafrost Index Map

Blue: Permafrost in nearly all conditions

Purple: Permafrost mostly in cold conditions

Yellow: Permafrost only in very favorable conditions

Glacier

B

Pointe de la Sana

Headscarp

Bourg-St-Maurice

Modane

Rockslide

Femma mountain refuge

N

600 m

Google Earth

Image © 2017 DigitalGlobe

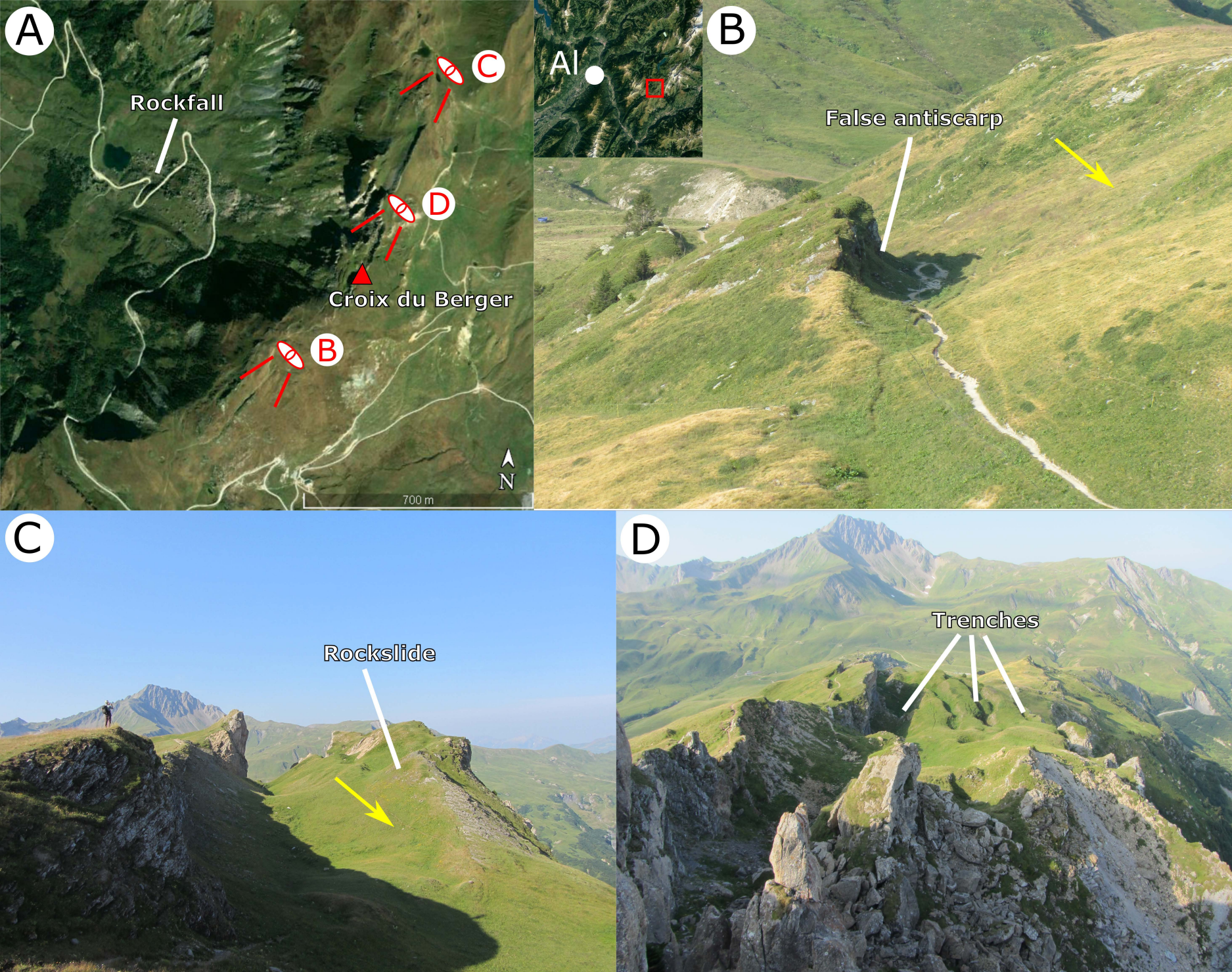
A
Rockfall
C
D
Croix du Berger
B
N
700 m
Al
B
False antiscarp
C
Rockslide
D
Trenches

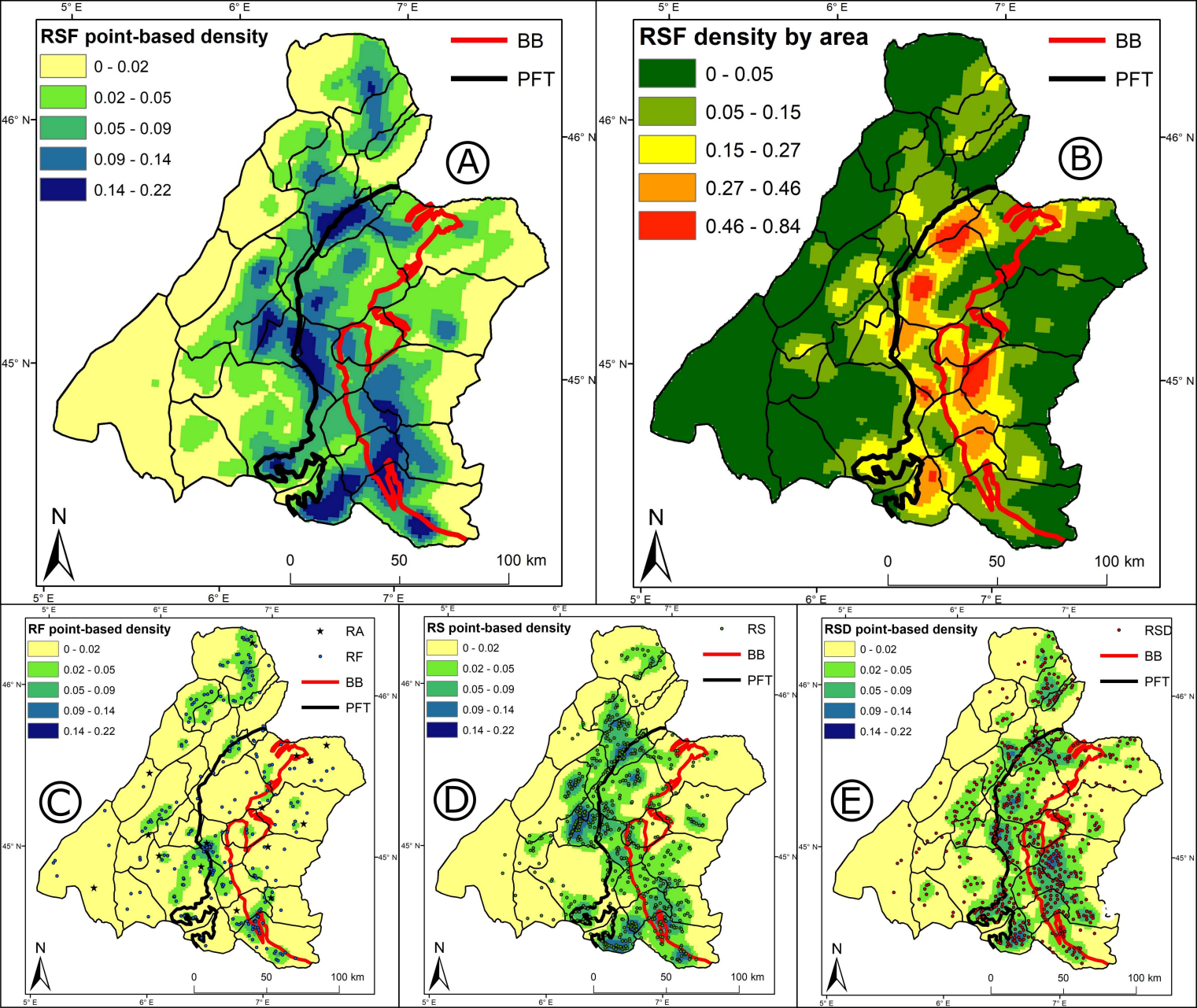
RSF point-based density
0 - 0.02
0.02 - 0.05
0.05 - 0.09
0.09 - 0.14
0.14 - 0.22
BB
PFT
A
RSF density by area
0 - 0.05
0.05 - 0.15
0.15 - 0.27
0.27 - 0.46
0.46 - 0.84
B
RF point-based density
RA
RF
C
RS point-based density
RS
D
RSD point-based density
RSD
E
N
0
50
100 km
5° E
6° E
7° E
46° N
45° N

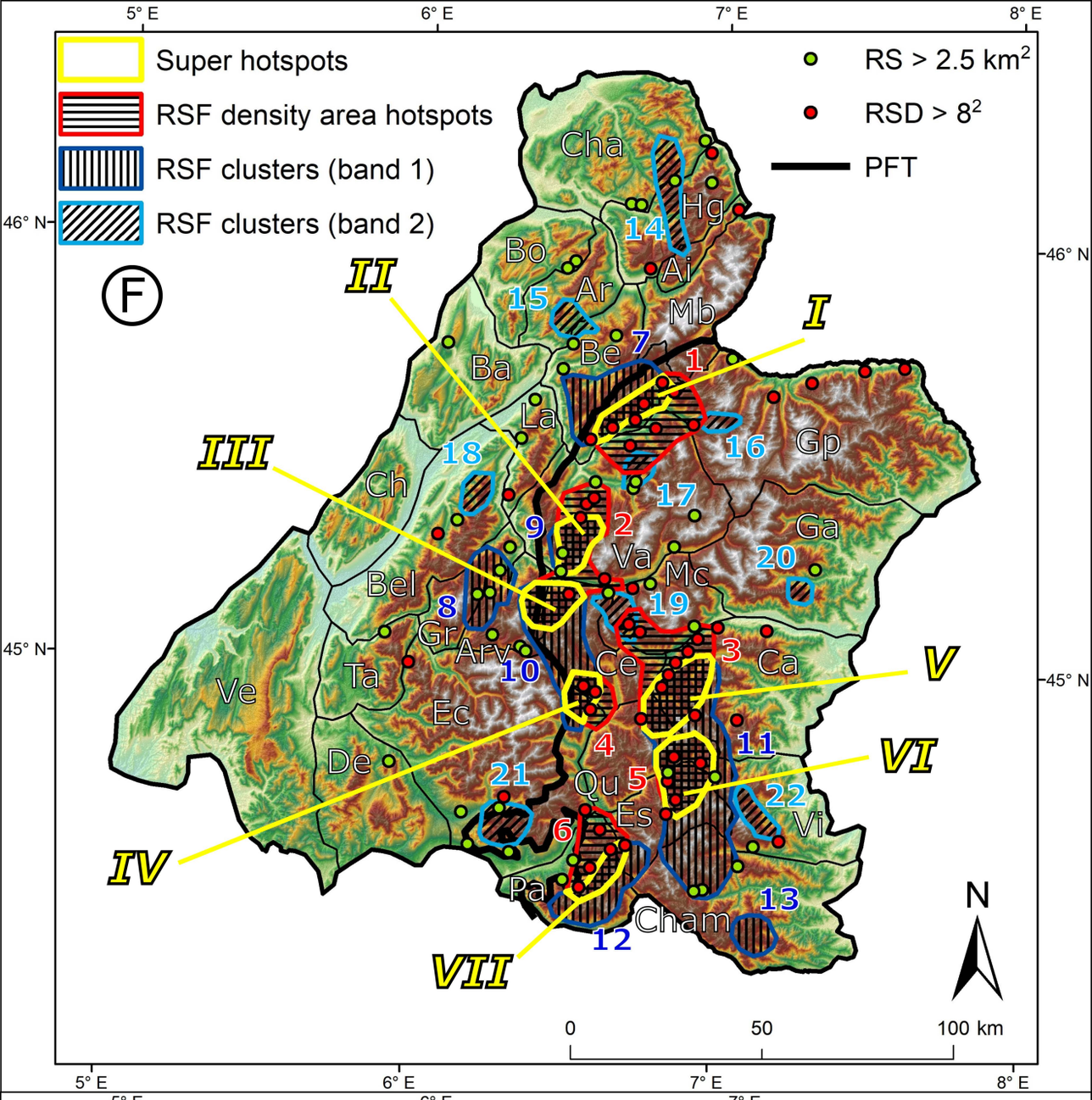
Super hotspots
RSF density area hotspots
RSF clusters (band 1)
RSF clusters (band 2)
RS > 2.5 km²
RSD > 8²
PFT
F
I
II
III
IV
V
VI
VII
Cha
Hg
Bo
Ai
Ar
Mb
Be
Ba
La
Gp
Ch
Ga
Va
Mc
Bel
Gr
Arv
Ce
Ca
Ta
Ve
Ec
De
Qu
Es
Vi
Pa
Cham
1
2
3
4
5
6
7
8
9
10
11
12
13
14
15
16
17
18
19
20
21
22
N
0
50
100 km
5° E
6° E
7° E
8° E
46° N
45° N

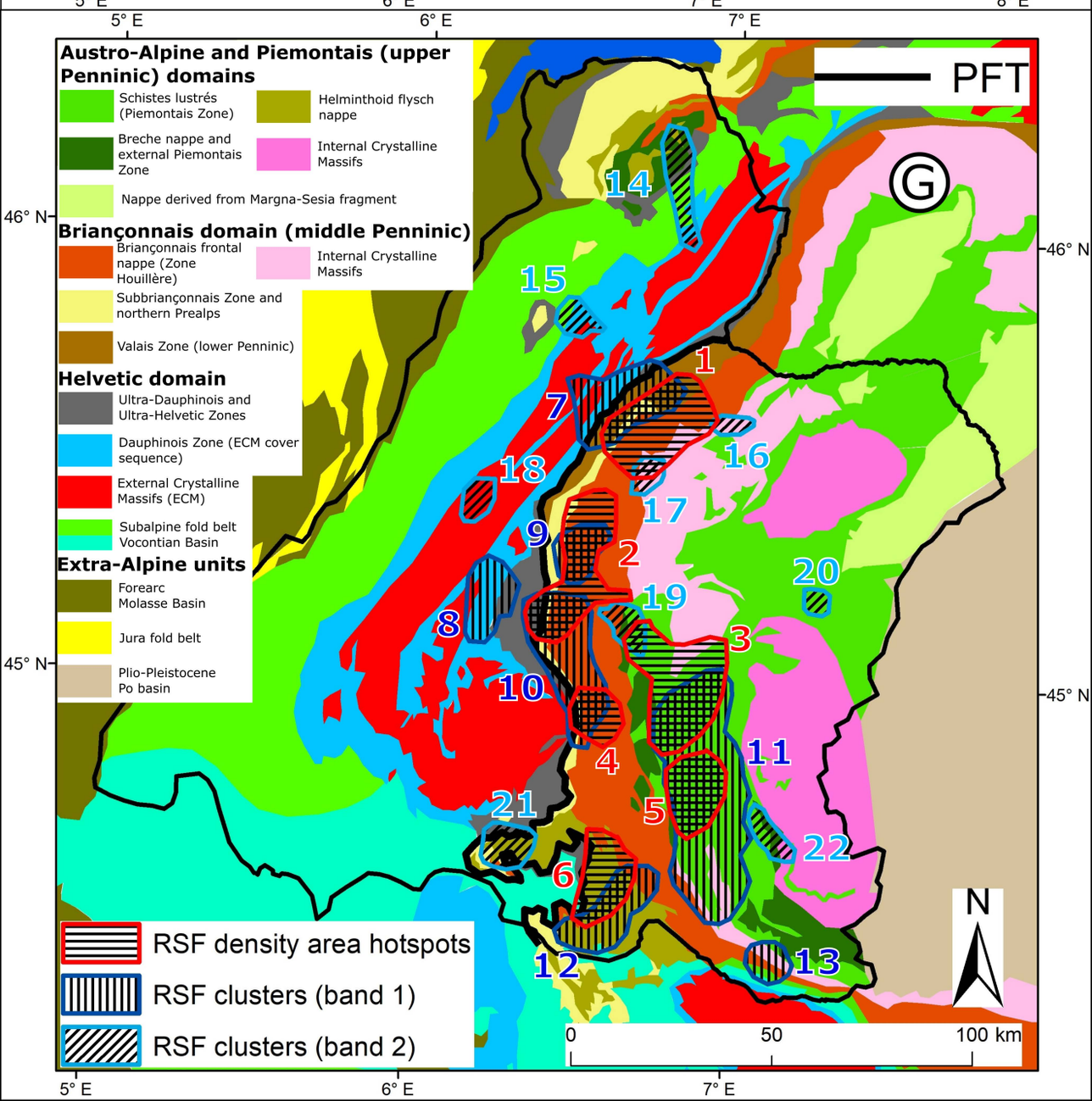
Austro-Alpine and Piemontais (upper Penninic) domains
Schistes lustrés (Piemontais Zone)
Helminthoid flysch nappe
Breche nappe and external Piemontais Zone
Internal Crystalline Massifs
Nappe derived from Margna-Sesia fragment
Briançonnais domain (middle Penninic)
Briançonnais frontal nappe (Zone Houillère)
Internal Crystalline Massifs
Subbriançonnais Zone and northern Prealps
Valais Zone (lower Penninic)
Helvetic domain
Ultra-Dauphinois and Ultra-Helvetic Zones
Dauphinois Zone (ECM cover sequence)
External Crystalline Massifs (ECM)
Subalpine fold belt Vocontian Basin
Extra-Alpine units
Forearc Molasse Basin
Jura fold belt
Plio-Pleistocene Po basin
PFT
G
RSF density area hotspots
RSF clusters (band 1)
RSF clusters (band 2)
1
2
3
4
5
6
7
8
9
10
11
12
13
14
15
16
17
18
19
20
21
22
N
0
50
100 km
5° E
6° E
7° E
46° N
45° N

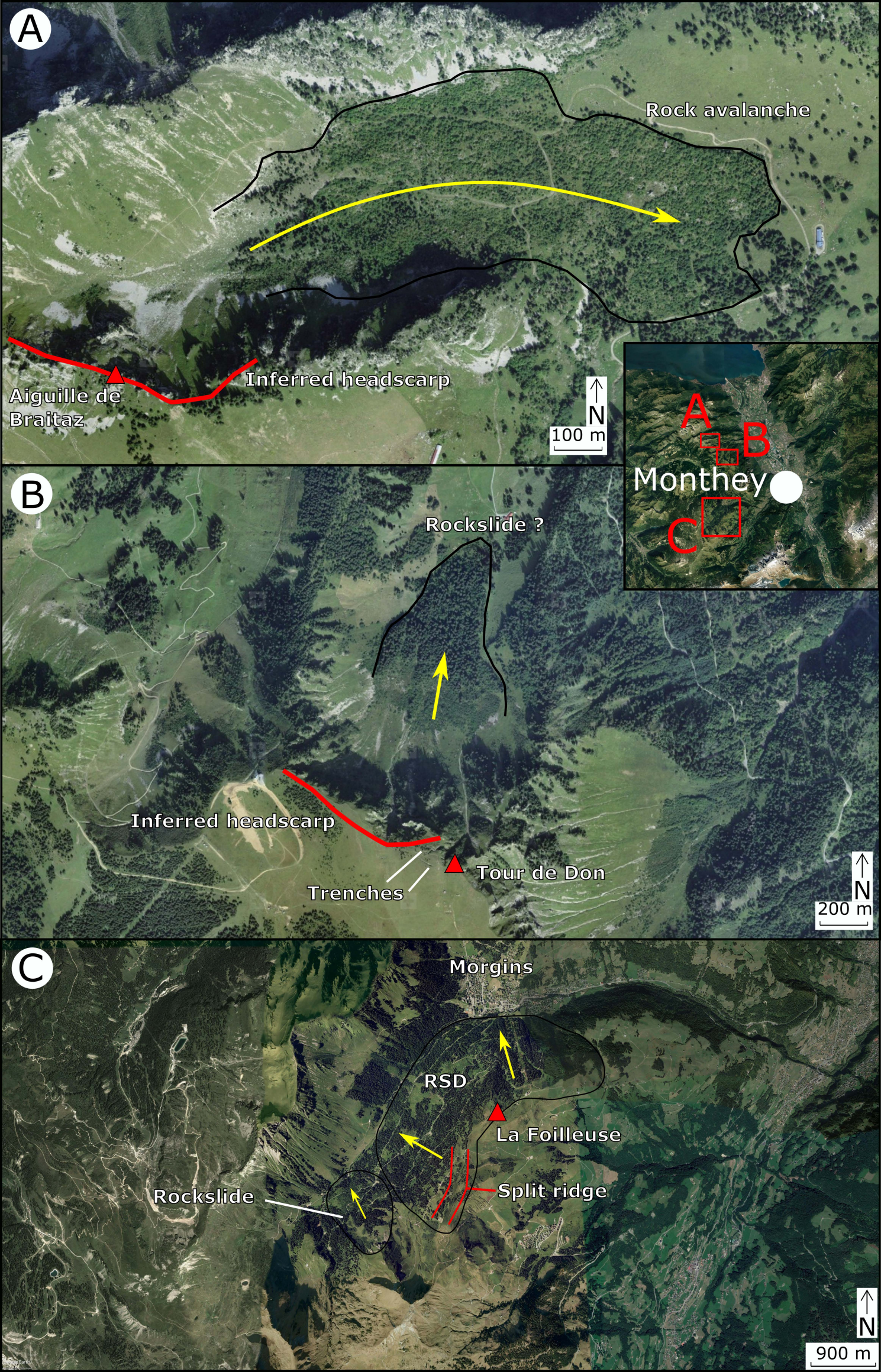
A
Rock avalanche
Aiguille de
Braitaz
Inferred headscarp
N
100 m
A
B
Monthey
C
B
Rockslide ?
Inferred headscarp
Tour de Don
Trenches
N
200 m
C
Morgins
RSD
La Foilleuse
Split ridge
Rockslide
N
900 m

Table 1. Aggregate RSF surface area by massif (ranked by decreasing order of RSF footprint size)

Massif name	Massif size	RSF surface area										Mean altitude of RSF headscarps	Massif area affected by RSF [1]
		Rock av.		Rockfall		Rockslide		RSD		All types			
	km²	km²	*n*	km²	*n*	km²	*n*	km²	*n*	km²	*n*	m	%
Parpaillon	618	0	0	0.9	2	37.3	40	103.8	29	142	71	2389	22.98
Beaufortain	919	0	0	1.9	10	50.9	61	151.8	36	204.6	107	2111	22.26
Escreins	531	0.7	1	1.7	8	23	36	88.6	21	114	66	2675	21.47
Cerces	628	0.7	1	5.3	17	28.4	31	91.1	24	125.4	73	2465	19.97
Queyras	590	0	0	0.4	7	14	20	100.9	28	115.3	55	2529	19.54
Aig. Rouges	150	0	0	0.4	3	0.7	1	28.4	12	29.2	16	2212	19.44
Vanoise	1704	0	0	4.5	10	66.7	59	244.5	53	315.7	122	2397	18.53
Arves	404	0	0	2	3	32.5	32	34.4	12	69	47	2375	17.08
Mont Cenis	556	0	0	1	5	17.4	15	71.8	14	90.2	34	2574	16.22
Cottian Alps	1420	3.33	1	1.4	8	14.1	23	204.8	46	223.7	78	2505	15.75
Gd. Rousses	365	0	0	0.4	2	29.7	28	14	10	44.2	40	2124	12.11
Lauzière	345	0	0	0.1	1	16.6	8	21.2	7	37.9	16	1991	10.99
Ecrins	2456	2.1	2	6.4	33	49.6	41	170.3	54	228.5	130	2299	9.30
Haut-Giffre	630	0	0	5.3	13	10.2	5	41.9	21	57.3	39	2181	9.10
Viso	737	1.6	1	0.5	3	16.9	16	44.4	24	63.4	44	2309	8.60
Gd. Paradis	2367	7.9	3	5.7	16	22	18	152.2	45	187.8	82	2516	7.93
Chambeyron	1401	0	0	6.3	28	42.6	58	41.3	28	90.2	114	2502	6.44
Belledonne	1206	0	0	1.6	11	24.3	26	47.9	19	73.8	56	1920	6.12
Aravis	453	0	0	1.1	7	9.6	14	8.8	5	19.5	26	1852	4.30
Taillefer	486	1.9	1	0.5	2	11.2	10	5	3	18.6	16	1798	3.83
Graian Alps	1539	6.14	1	2.3	10	14.2	17	35.3	21	57.9	50	2323	3.76
Bornes	611	0	0	1.1	12	12.9	5	5.3	3	19.2	20	1794	3.14
Mont Blanc	715	0	0	0.9	4	1	1	19.3	12	21.3	17	2470	2.98
Chablais	1456	0.6	1	2.1	19	26.9	20	13.2	16	42.9	56	1819	2.95
Dévoluy	938	0	0	0.4	4	9	5	11.3	9	20.7	18	1928	2.21
Chartreuse	727	10.7	1	0.2	1	0	0	2	2	13	4	1723	1.79
Bauges	913	0	0	0.2	3	7.1	4	0	0	7.2	7	1656	0.79
Vercors	2799	0.4	1	0.4	5	1.9	2	6	4	8.8	12	1379	0.31
Total	27664	36.33	15	55.1	247	590.8	596	1759.6	558	2441	1416	2300	8.82

Notes. [1] When adding to this inventory reports by Eisbacher and Clague (1984), the CEREMA, and Crosta et al. (2013), which each mention RSFs not included in this database because they were not detectable from the imagery (see discussion in section 5.1), massif areas affected by RSF change thus: Arves, 17.2%; Cottian Alps, 17.48%; Ecrins, 9.42%; Haut-Giffre, 9.40%; Viso, 10.65%; Grand Paradis, 8.72%; Chambeyron, 6.75%; Taillefer, 3.95%; Graian Alps, 4.26%; Mont Blanc, 3.01%; Chablais, 3.04%. Other values are unchanged. Augmented thus, the inventory brings the regional total footprint of RSF to 9.1% of the study area, i.e. 1446 RSFs covering a total area of 2526 km^2.

Table 2. Relative areal concentration of RSFs relative to the Penninic Frontal Thrust (PFT)

Location relative to PFT	All RSF types				RSD		
	1	2	3	4	5	6	7
	Total area (km^2)	No. of RSFs	Area (km^2)	Proportion of total land area impacted by RSF (col. 3 ÷ col. 1) (%)	No. of RSDs	Area (km^2)	Proportion of total land area impacted by RSD (col. 6 ÷ col. 1) (%)
West of PFT	14958	546	691	4.6	180	364	2.4
East of PFT	12706	870	1750	13.7	379	1393	10.9

Table 3. RSF super-hotspots in the Western Alps

	Attribute	Super-hotspot (code name in Roman numerals: *refer to Figure 15F for location*)						
		I	*II*	*III*	*IV*	*V*	*VI*	*VII*
Location	Cluster–Hotspot intersection (*refer to Figs. 15F and 15G*)	Cluster 7 and Hotspot 1	Cluster 9 and Hotspot 2	Cluster 10 and Hotspot 2	Cluster 10 and Hotspsot 4	Cluster 11 and Hotspot 3	Cluster 11 and Hotspot 5	Cluster 12 and Hotspot 6
	Massif name	S. Beaufortain	SW Vanoise	NE Arves, NE Grandes Rousses	E. Ecrins, SW Cerces	Triple junction between W Cottian Alps, NE Queyras, and SE Cerces (Alpine drainage divide)	Queyras, Escreins	Central Parpaillon (massif core)
	Bisecting or bounding valley	North flank of middle Isère (Tarentaise)	South flank of middle Arc (Maurienne)	North flank of middle Arc (Maurienne)	Guisane	Upper Dora Riparia and upper Chisone (east)-flowing); upper Durance and Cerveyrette (west-flowing)	Upper Guil	None
Topography	Maximum altitude (m)	2600	3000	2900	2600	3200	3100	2900
	Minimum altitude (m)	600	550	1000	1100	1300	1400	1600
	Maximum relief (m)	2000	2450	1900	1500	1900	1700	1300
Predisposition (preconditions)	Tectonic Domain (*refer to Figs. 2, 15G*)	Middle and Lower Penninic	Middle Penninic	Middle and Lower Penninic, Helvetic		Upper Penninic		
	Tectonic Zone (*refer to Figs. 2, 15G*)	Valais, Sub-Briançonnais, Zone Houillère	Sub-Briançonnais, Zone Houillère	Valais, Sub-Briançonnais, Zone Houillère, Ultra-Dauphinois, Ultra-Helvetic		Piémontais		Helminthoid flysch nappe, Zone Houillère
	Presence of major tectonic 'Zone' boundary (e.g. thrust front) or Alpine fault (*refer to Fig. 8*)	Lower and Middle Penninic thrusts and their thrust fronts	Middle Penninic internal thrusts	PFT, Middle Penninic internal thrusts, Ultra-Dauphinois thrust	PFT, some faults	BB (here striking NE–SW), and one NE–SW fault, both focusing large RSD	None of note	Briançonnais (i.e. Zone Houillère) thrust front, a few N–S faults
	Dominant lithology (*refer to Fig. 6*)	Detrital sedimentary (semischist fabric), flysch, evaporites	Detrital sedimentary (semischist fabric), flysch, marl, evaporites		Detrital sedimentary (semischist fabric), flysch, schist, some limestone	Schistes lustrés, gabbro, basalt, serpentinite		Flysch, marl, schist, evaporites
Possible drivers	Antiquity of syn-orogenic denudation paroxysm (*refer to Section 2.2.3*)	Substantial (> 20 Ma)						
	Late Neogene / Quaternary crustal stress regime (*refer to Fig. 10*)	Extensional						
	Relative residence time above successive Quaternary ELAs	Long						
Possible	Reconstructed LGM ice thickness (m)	1500–2000	1–1000 (a few exceptions up to 1500)	1–1000 (a few exceptions up to 1500)	1–1000 (a few exceptions up to 1500)	1–1000 (a few exceptions up to 1500 on Dora Baltea trough flank)	0–1000	< 500

(*refer to Fig. 12*)							
Recent surface uplift rate (mm/yr) (*refer to Fig. 11*)	> 2	> 2	1.5–2	1–1.5	~1	0.5–1	0.5–1
Modern seismicity (*refer to Fig. 9*)	None of note		Briançonnais Seismic Arc			None of note	

Table 4. Spatial incidence of RSF in mountain ranges documented by systematic mapping

Mountain range	Proportion of study area affected by RSF (%)	Size of study area (km^2)	Data source
Western Alps (France, Italy, Switzerland)	9.1	27,500	This study
South Carpathians (Romania)	1.1	20,000	Blondeau (unpubl.)
Southern Alps, central area (New Zealand)	2.0	21,000	Allen et al. (2011)
Highlands (Scotland)	0.8	21,000	Jarman and Harrison (2019)
Eastern Pyrenees (France, Spain)	1.8	3,000	Jarman et al. (2014)